Metals and Ceramics Division

Heavy Vehicle Propulsion Materials Program
Quarterly Progress Report for
October through December 2001

D. R. Johnson
Technical Project Manager

Prepared for
U.S. Department of Energy
Assistant Secretary for Energy Efficiency and Renewable Energy
Office of Transportation Technologies
EE 07 01 00 0

Prepared by the
OAK RIDGE NATIONAL LABORATORY
Oak Ridge, Tennessee 37831-6066
Managed by
UT-Battelle, LLC
for the Department of Energy
Under contract DE-AC05-00OR22725

CONTENTS

Cost Effective High Performance Materials and Processing

Development of Low Cost Austenitic Stainless Diesel Engine Components with Enhanced High-Temperature Reliability (ORNL and Caterpillar, Inc.)

Cost-Effective Smart Materials for Diesel Engine Applications (ORNL)

Low-Cost Manufacturing Processes for Ceramic and Cermet Diesel Engine Components (SIU-C)

Low Cost High Toughness Ceramics (ORNL)

Utilization of Thermally Conductive Graphite Foam for Cooling Diesel Engine Blocks (ORNL)

Advanced Manufacturing Technology

Intermetallic-Bonded Cermets (ORNL)

Low-Cost Manufacturing of Precision Diesel Engine Components (ORNL)

Cylindrical Wire Electrical Discharge Machining (EDM) and Temperature Measurement (North Carolina State University)

Testing and Characterization

NDE Development for Ceramic Valves for Diesel Engines (Argonne National Laboratory)

Processing and Characterization of Structural and Functional Materials for Heavy Vehicle Applications (North Carolina A&T State University)

Life Prediction of Diesel Engine Components (ORNL)

Field Emission Analytical Electron Microscopy for Characterization of Catalyst Microstructures (ORNL)

Durability of Diesel Engine Component Materials (ORNL)

Materials and Testing Standards

Implementing Agreement for a Programme of Research and Development on Advanced Materials for Transportation Applications (ORNL)

Standards for Reliability Testing of Heavy Vehicle Propulsion Materials (NIST)

Mechanical Property Testing and Standards Development (NIST)

Development Of Low-Cost Austenitic Stainless Diesel Engine Components With Enhanced High-Temperature Reliability

P.J. Maziasz and R.W. Swindeman
Oak Ridge National Laboratory
and
M.E. Frary
Caterpillar, Inc.

Objective/Scope

The objective of this work is to evaluate cast austenitic stainless steels as high-performance alternatives to SiMo ductile cast iron, which is currently the standard material used in most diesel engines for exhaust manifold and turbocharger housing components. The new material must be able to withstand prolonged exposure at temperatures of 750°C or above, as well as to survive the severe thermal cycling from near room-temperature to such high-temperatures without developing cracks. This project has tested commercially available cast alloys, as well as developed new, modified cast alloys with significantly enhanced performance. The ultimate project goal is to provide high-performance, reliable materials that are also cost-effective for such applications. This advanced diesel engine work is part of a broader CRADA (Cooperative Research and Development Agreement) project (ORNL99-0533) that began July 21,1999,and was scheduled to end July 22, 2001, but has been extended for 6 more months. Any more detailed information on this project must be requested directly from Caterpillar, Inc.

Technical Highlights, 1st Quarter, FY2002

Background

Advanced large diesel engine require higher fuel efficiency as well as reduced exhaust emissions, without sacrificing durability and reliability. Therefore, exhaust manifold and turbocharger-housing materials must withstand temperatures ranging from 70 to 750°C or higher in a normal duty cycle that includes prolonged, steady high-temperature exposure as well as more rapid and severe thermal cycling. New technology to reduce emissions and heavier duty cycles will push temperatures in these critical components even higher. Current exhaust components are made from SiMo ductile cast iron, and higher engine temperatures would push such materials beyond their current strength and corrosion limits. Therefore, the goals of this project were to generate new data on alternate higher performance materials like cast austenitic stainless steels to enable materials selection and component lifing. There is limited industrial experience on cast austenitic stainless steels like CN12, especially for diesel engine applications, and little high-temperature mechanical properties data available, particularly creep and fatigue. The main purpose of this project is to produce data comparing cast CN12 and SiMo cast iron for such diesel exhaust component applications. Another component of this project was a parallel alloy development effort to further optimize the cost-effective performance of such cast austenitic stainless steels.

Approach

Commercial cast CN12 austenitic stainless steel (Fe-25Cr-13Ni-1.8Nb, C, N, S) was chosen as the baseline alloy for evaluation relative to SiMo ductile cast iron. Materials were evaluated in the as-cast condition as well as after appropriate thermal aging at temperatures up to 850°C. Tensile and isothermal cyclic fatigue properties were evaluated selectively from room temperature up to 900°C, together with some high-temperature creep-rupture and oxidation/corrosion testing. Microstructure analysis was performed on some of the specimens to better understand mechanisms associated with the properties changes. In a parallel effort, new alloying element modifications were made to CN12 and studied to further enhance the high-temperature performance.

Technical Progress

Previously, the commercial cast iron and baseline CN12 materials were obtained, all mechanical properties specimens machined and all tensile and creep testing of unaged and aged specimens have been done. High-cycle isothermal fatigue testing at 700°C and 850°C at ORNL has been completed, and thermal fatigue testing over this temperature range continued at Caterpillar. Microstructural analyses of selected specimens of as-cast or as-cast and aged materials have been completed to better understand the properties behavior and to establish the effects of aging on the baseline CN12 material. CN12 has a clear tensile strength advantage and an overwhelming creep-strength advantage (Fig.1) over SiMo cast iron above 550-600°C. A summary of the isothermal fatigue data at room temperature and at 700°C also shows an enormous fatigue life advantage of CN12 over the SiMo cast iron (Fig. 2).

To date, eight smaller heats (15 lbs each) of modified CN12 austenitic stainless steels have been produced at ORNL and have been evaluated. Initial screening of as-cast or cast and aged material with tensile testing, and of as-cast material with creep-rupture testing at 850°C indicates that significant improvements have been achieved in high-temperature strength and aging resistance. The improvement of the best modified CN-12 alloys is five to ten times better relative to the standard commercial CN-12 alloy for creep-rupture testing at 850°C and 110 MPa.

In addition to the modified CN12 austenitic stainless steels, similar efforts were made to modify a less costly and more castable CF8C (Fe-19Cr-12Ni-Nb, C) austenitic stainless steel that has previously been considered as a candidate for diesel exhaust applications (but dismissed for lack of high-temperature strength), and which also finds use in some gas-turbine exhaust components at 650°C or below. Three smaller heats of modified CF8C were made at ORNL (one baseline unmodified alloy and two modified alloys) and screened using tensile tests and creep-rupture testing at 850°C. The dramatic improvement in creep-resistance of the best modified CF8C steel at 850°C relative to commercial material is shown in Fig. 3. Both modified CF8C steels are several orders of magnitude better than the standard commercial CF8C steel. One modified CF8C steel ruptures after almost 13,000 h this quarter, while the other modified CF8C steel has not ruptured after more than 16,000 h of creep-testing. Additional creep-test of standard, commercial CN12 steel began previously for comparison with the best modified CF8C steel at the same creep conditions (Fig. 3), and that test has exceeded 6,000 h. These remaining creep-tests of the modified CF8C and standard CN12 steels will continue next quarter.

Communications/Visits/Travel

Team communications between ORNL and Caterpillar occur in detail at least several times a week. Discussions began this quarter and agreement was reached to extend this current CRADA another 6 months, and to being a new CRADA focused on commercial scale-up of the best modified CF8C and CN12 steels to obtain more mechanical properties data on these new steels, including fatigue and thermal fatigue data. Production and evaluation of prototype components with the new alloys will also be included in this new project

An invention disclosure and patent application on cast austenitic stainless alloys with improved performance were completed by Caterpillar and filed with the U.S. Patent Office in December 2000. It is entitled "Heat and Corrosion Resistant Cast Stainless Steels With Improved High Temperature Strength and Ductility," by P.J. Maziasz (ORNL), T. McGreevy (U. of Bradley/CAT), M.J. Pollard (CAT), C.W. Siebenaler (CAT), and R.W. Swindeman (ORNL).

Status of Milestones

Formal milestones are imbedded in the CRADA and are not part of the HVPM Program FWP. However, all milestones have achieved on or significantly ahead of schedule.

Publications

There have been several detailed internal reports on this project at Caterpillar Technical Center.

Several highlights for this project have been produced for the DOE HVPM program, and a highlight entitled "Cast Stainless Steels are Stronger at Higher Temperatures," was submitted in December 2001 to ASM-International for publication in Advanced Materials and Processes in January 2002.

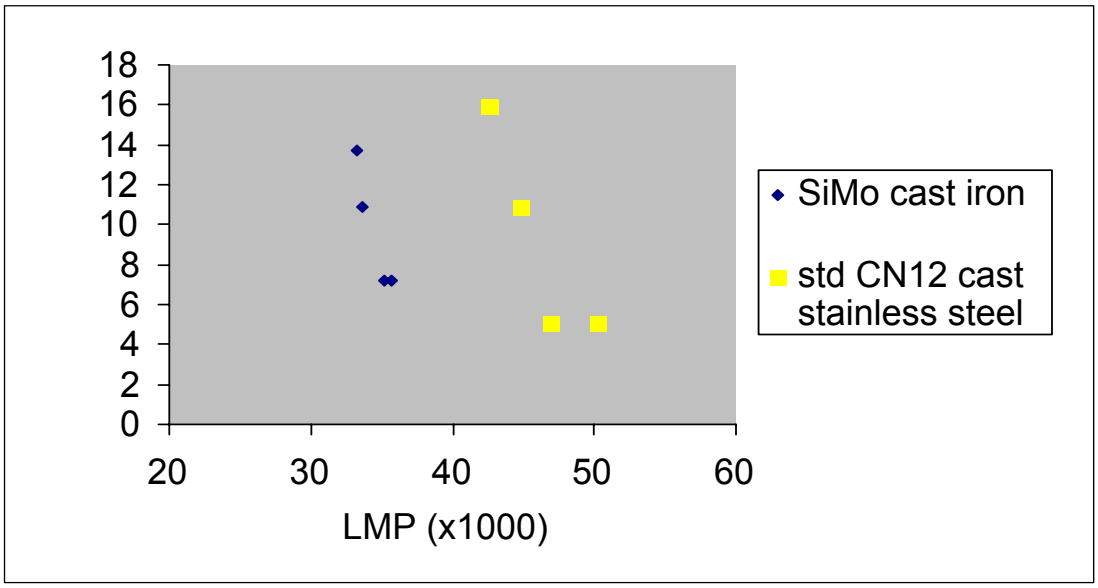

Fig. 1. Plot of Larson-Miller Parameter (LMP, = (T+ 460)(20+log t_r), where T is creep test temperature in ^oF and t_r is the time to rupture in hours) versus creep-rupture stress (vertical axis in ksi) for various creep tests run on SiMo cast iron (550-650^oC) and commercial CN-12 cast austenitic stainless steel (750-900^oC). Cast CN-12 austenitic stainless steel has an overwhelming advantage in creep strength.

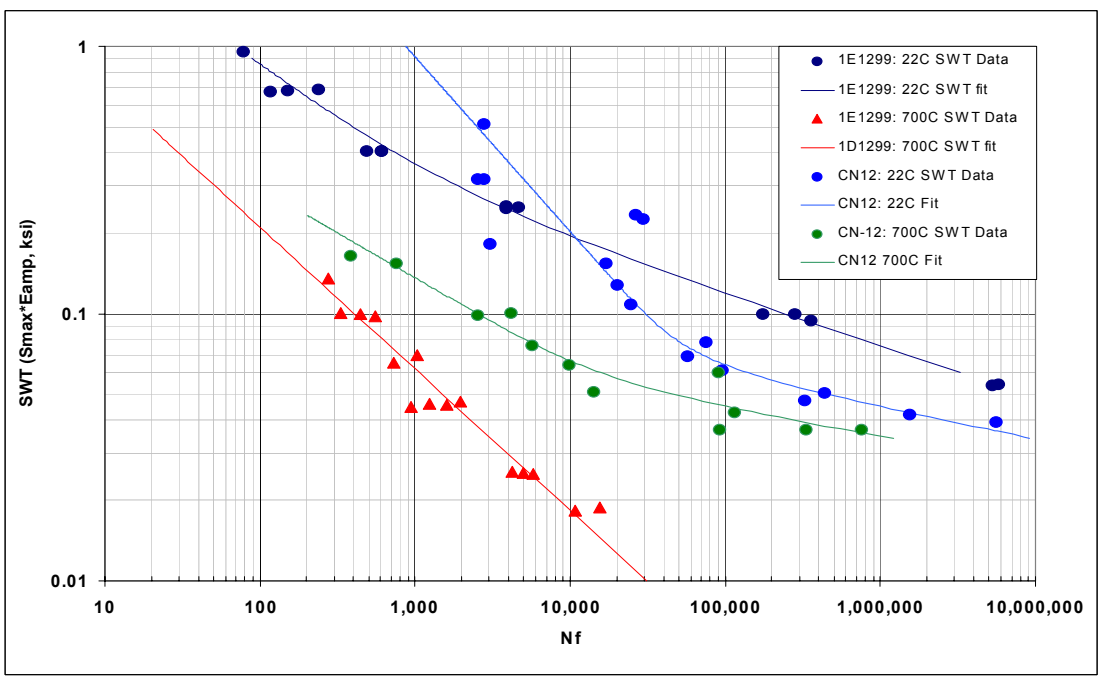

Fig. 2. A plot of the Smith-Watson-Topper (SWT) parameter (maximum stress x strain amplitude of the fatigue stress-strain loop) versus number of cycles to fracture for fatigue tests of SiMo cast iron and CN12 cast austenitic stainless steel isothermally fatigue tested at room temperature and at 700^oC in air. At 700^oC, the CN12 is approaching an endurance limit, and is significantly more resistant to fatigue than SiMo cast iron.

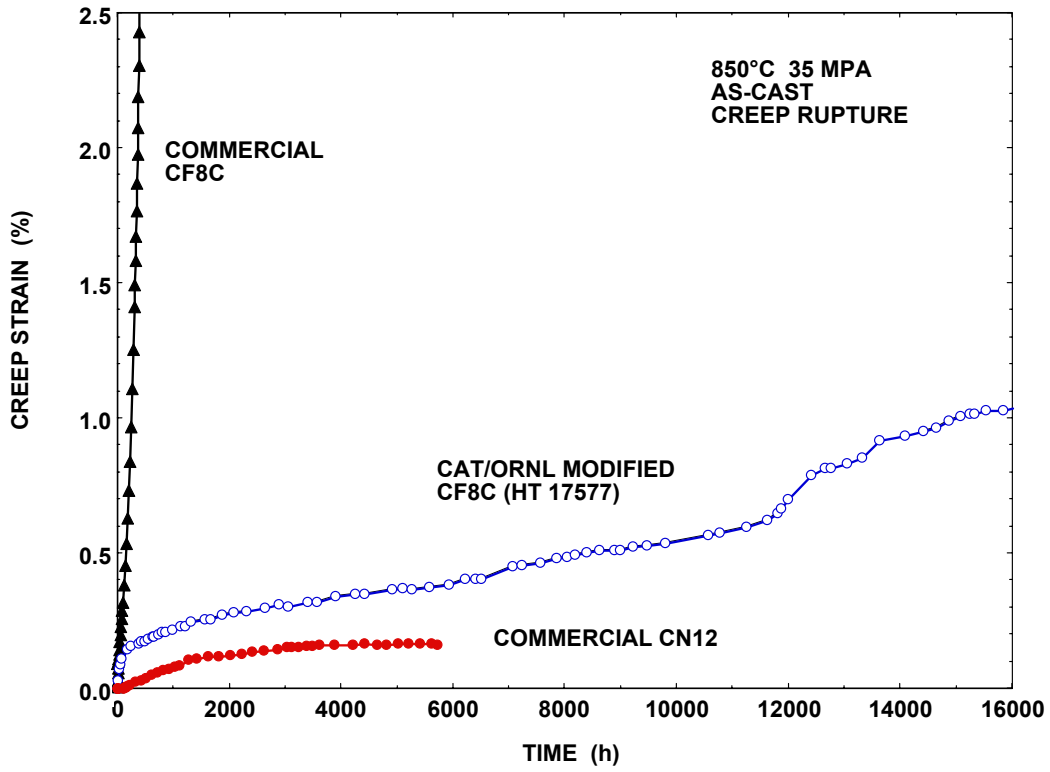

Fig. 3 - Creep-rupture curves of creep-strain versus rupture time for a commercial standard CF8C cast austenitic stainless steel and the best laboratory heat of modified CF8C cast austenitic stainless steel developed by ORNL and Caterpillar. Similar creep-rupture testing of standard commercial CN12 shows that best modified CF8C steel has comparable creep-resistance at this point, and both tests will continue next quarter.

Cost-Effective Smart Materials for Diesel Engine Applications

J. O. Kiggans, Jr., F. C. Montgomery, T. N. Tiegs,
L. C. Maxey, Hsin Wang, and A. Steffens
Oak Ridge National Laboratory

Objective / Scope

There are two objectives for this project. The first is to evaluate the cost-effectiveness and maturity of various "Smart Materials Technologies," which are under consideration for diesel engine applications, such as fuel injection systems. The second is to develop "Smart Materials" to be incorporated into working actuators and sensors.

Task 1 - Multilayer Electroded Laminates

The purpose of this task is to find satisfactory methods to prepare PZT laminates with internal electrodes from tape cast materials and cost effective electrode materials. This report contains light and SEM analyses of a commercial TRS Inc. stack and a PZT stack, which was fabricated at ORNL. This study was made to compare the progress at ORNL in fabricating multi-layer PZT stack with products commercially. Future ORNL stacks are planned which use less expensive internal electrode materials.

The TRS PZT stack actuator is a 5 mm cube. This PZT stack has 42 layers that are 100 microns in thickness and are separated by platinum electrodes. The composition of the TRS material is unknown. The stack was polished on a side perpendicular to the electrode layers using standard procedures used for PZT materials. A small section on the polished surface was etched at room temperature for 15 sec with a solution containing 2.3 wt. % hydrochloric acid and 0.12 wt. % hydrofluoric acid.

An ORNL PZT stack was made using a combination of procedures discussed in previous reports. Approximately 0.015 cm thick ceramic tapes were cast using PZT-4 powders purchased from APC Ceramics Inc. A custom electrode pattern (70 silver – 30 palladium composition with a bonding glass, product EL44-013, manufactured by Ferro Inc.) was screen printed onto the ceramic tapes using an Affiliated Manufacturers Inc. screen printer. . 2.7 cm diameter individual discs, which include the printed pattern, were punched from the tapes. 10-15 layers of the discs were stacked in a 2.85 cm diameter Carver die, and they were hot laminated with the application of 13.8 MPa pressure for 15 min at 80 °C. The binder was removed by heating at 1 °C to 600 °C, and the laminates were sintered at 1125 °C for 24 hour in covered alumina crucibles with a 10 wt. % ZrO_2 – 90 wt. % $PbZrO_3$ packing powder. One side of each sample was polished using previously discussed methods, and etched using the same procedure as the TRS stack.

Both the TRS and ORNL stacks were examined using a Nikon Epiphot –TME inverted microscope. Samples were then coated with carbon, and examined with a Philips XL30 Scanning Electron Microscope.

Figures 1a and 1b show photos from the light microscope of the ORNL and TRS parts. Both the ceramic and electrode thickness of both multilayer types are of the same relative dimensions. Figures 2a and b show SEM photos of the ORNL and TRS parts. Once again the relative sizes of the ceramic and electrode structures are of similar dimensions. Figure 3a shows the etched microstructure of the ORNL material. The grains range from to 1 to 3 μm in diameter. A few pull-outs from polishing are apparent in the photo. Figure 3b shows the etched microstructure of the TRS material. The microstructure is very uniform, but the many holes apparent within individual grains. The average grains are from 1 to 2 μm in diameter.

Task 2. Static and dynamic testing of flexure amplified piezo stack actuator

A commercially constructed compact piezo stack actuator (EDO E100P-4) was tested in combination with an ORNL-designed flexure amplifier to evaluate its displacement characteristics. Displacements were measured at various drive voltages up to the maximum rated voltage for the actuator (800 volts dc). Static measurements were conducted by applying dc voltages and dynamic measurements were conducted by applying pulsed dc voltages at 10 and 100 Hz.

The apparatus shown in Figure 4 was used to perform the tests. The load spring was used to establish a preload of 4.5 kgf force on the amplifier, as monitored using the load cell (Transducer Techniques THC-3K-T). The gain of the mechanical amplifier was calculated to be 5.07, resulting in a preload on the actuator of 23.0 kgf. A fiber optic displacement sensor (Philtek D-20) was used to monitor the movement of the actuator via a displacement transfer rod in contact with the top of the amplifier.

<u>Static Tests</u>
The static test results (Figure 5) showed good agreement with the predicted displacements based on the manufacturer's data and the amplifier characteristics. The measured displacements exceed the calculated displacements by about 5%, which may be attributable to the fact that the manufacturer's data was based on a 45.4 kgf preload and the unit was tested at 22.7 kgf. For the initial tests of the mechanical amplifier, we chose to limit the preload to a conservative level. A small (~1-2%), inherent non-linearity in the fiber optic displacement probe can be observed in the plot of the measured data. The measured displacements in microns for each input voltage level are indicated on the plot.

<u>Dynamic Tests</u>
The dynamic test data were obtained at 200, 400, 600, and 800 volt pulsed dc levels. The low frequency displacement data for each of these signal levels are shown in Figures 6 through 9. The average displacements obtained in the dynamic tests for each voltage level are ~5% lower than the static displacements measured at the same voltage levels.

Significant mechanical resonance contributed to the noise observed in the displacement signals. The noise made it extremely difficult to obtain useful waveforms at higher frequencies (e.g. 100 Hz). Much of this resonance was attributed to the load spring, which was later damped by wrapping it with a thin rubber sheet. This damping significantly improved the displacement signals, as shown in Figures 10 and 11. One displacement waveform was recorded at 100 Hz

and 200 volts after adding the damping. Although significantly improved over previous attempts to make measurements at 100 Hz, the data are still significantly affected by mechanical resonance. Additional damping improvements will be evaluated.

Discussion

The results indicate that the combination of piezo stack and mechanical amplifier are viable for obtaining larger displacements capable of driving useful loads. System designs will have to account for and limit the effects of mechanical resonance. This simple flexure amplifier is a useful breadboard for evaluating dynamic effects but is limited in its range of practical applications. Alternate mechanical amplifier configurations will be considered for their applicability to the program goals.

Task 3. Infrared Imaging of Piezoelectric Stacks During Operation (Hsin Wang)

We performed IR imaging of piezoelectric stacks under low voltage condition. The IR camera was used to obtain surface temperature maps in a non-contact mode. The objective of this test was to evaluate the possibility of using IR imaging in piezoelectric material studies. The temperature change depends on the Q factor, the test frequency and the voltage. We are interested in the temperature change in the piezoelectric stack as well as the "neck" sections of the mechanical amplifier.

Experiment:

A Raytheon, Radiance HS®, camera was used in this study. Three camera clock modes are available in this camera 1) video, 2) internal clock from computer and 3) external synchronization signals (normally 3-5 volts square waves or pulses). The software allows the user to chose the image acquisition to start at the rising or trailing edge of the external sync signal. The maximum frame speed of the camera is 141 Hz at 256 x 256 pixel format. The integration time can vary from 2 μs to 12 ms. The temperature resolution at ambient is 0.015 K.

During the tests, a background image was taken before energizing the piezoelectric stack. After running the stack at a certain condition for 5-10 minutes, an IR image was taken. The temperature difference between the energized stack and the background was digitally processed.

Results:

The preliminary test results are shown in Figure 12. The estimated temperature increase at 10 Hz, 100V was less than 1 degree C. The bright spots in the stack are the electrical connectors which are highly reflective It is very obvious that the stack and the mechanical amplifier both heated. The "neck" areas also heated. A better way to look at the temperature change is through the temperature differences. In Figure 13, the temperature differences between energized states and the background are shown. There is a slight temperature increase at 10Hz, 100V. The temperature increase at 10Hz, 200 V was very significant.

In Figure 14, IR images were taken with a 50 mm lens and an extension ring. Only the piezoelectric stack was imaged. Using the same display scale the heating of the stack is clearly

shown. Further temperature increase was observed at 10Hz, 400V, when the waiting time was longer, indicating it takes longer to reach steady temperature when the input energy is high.

Summary:
We have shown in the preliminary tests that the IR imaging technique can be used to monitor piezoelectric stacks during operation. Small temperature increase was observed during low-voltage mode. The IR camera is sensitive enough to pick up the temperature changes. We expect this technique can be used to locate hot spots in the stack when defects are present.

Status of Milestones
1) Evaluate and characterize commercially available PZT materials. Seek methods to improve the properties of these materials through alternative processing and forming methods. Fabricate new PZT compositions that allow sintering of the PZT materials at lower temperatures.
Status: The evaluation of new commercial materials and low temperature PZT materials are in progress.
2) Fabricate new PZT compositions to seek improvement in the electrical and mechanical properties. More specifically, research work will center on dopants that increase toughness of PZT materials.
Status: Work has not begun.
3) Use ORNL expertise in motion amplifier devices to design and fabricate motion-amplifying fixtures for fuel injector assemblies. A paper study will be conducted to compare the advantages of fluid-mediated diaphragm amplifiers versus machined, bending structures.
Status: Discussions underway with ORNL specialists who will conduct this study.

Communications/Travel/Visits
None

Publications
None

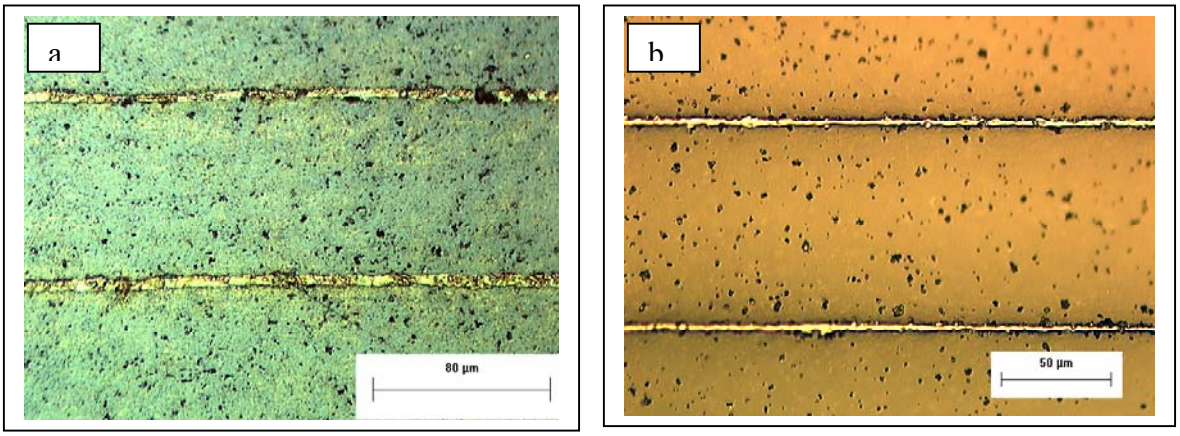

Figure 1. Light microscope images of the ceramic and electrode layers within ORNL (a) and (b) TRS Inc. multilayer parts.

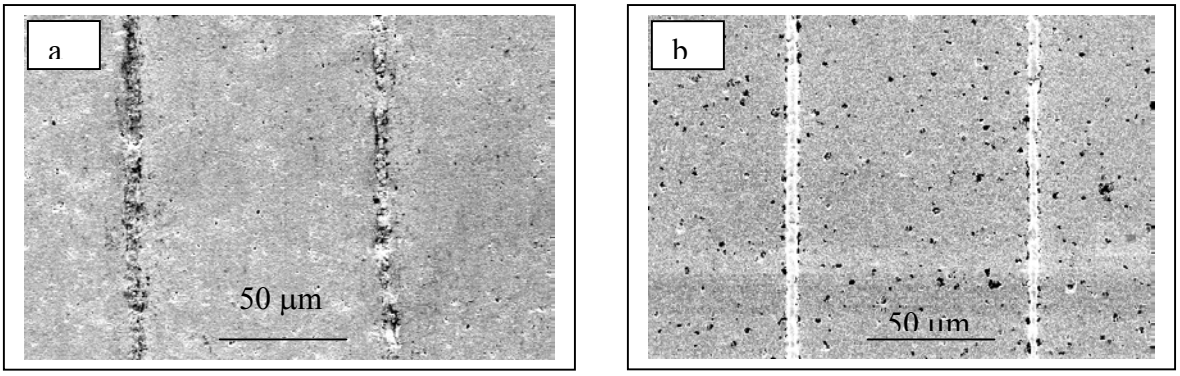

Figure 2. SEM images of the ceramic and electrode layers within ORNL (a) and (b) TRS Inc. multilayer parts.

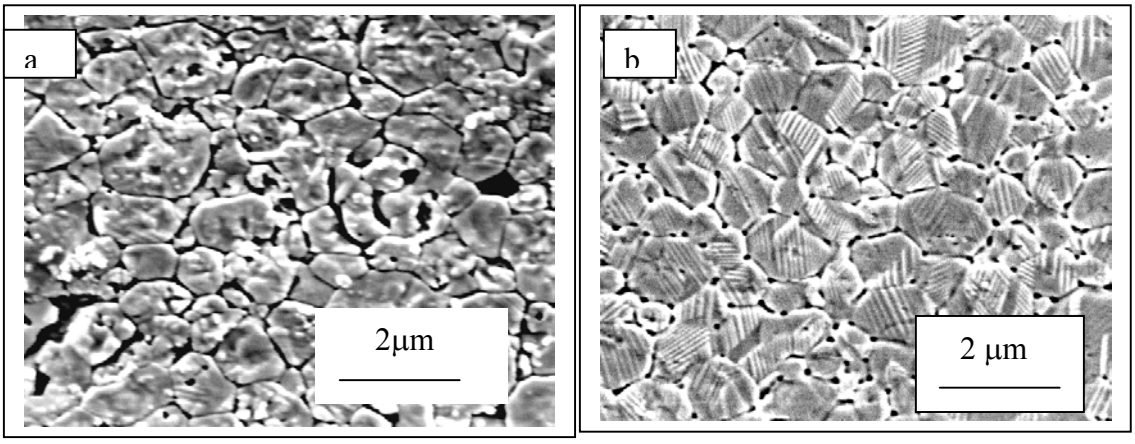

Figure 3. SEM images of PZT grains within ORNL (a) and (b) TRS Inc. multilayer parts.

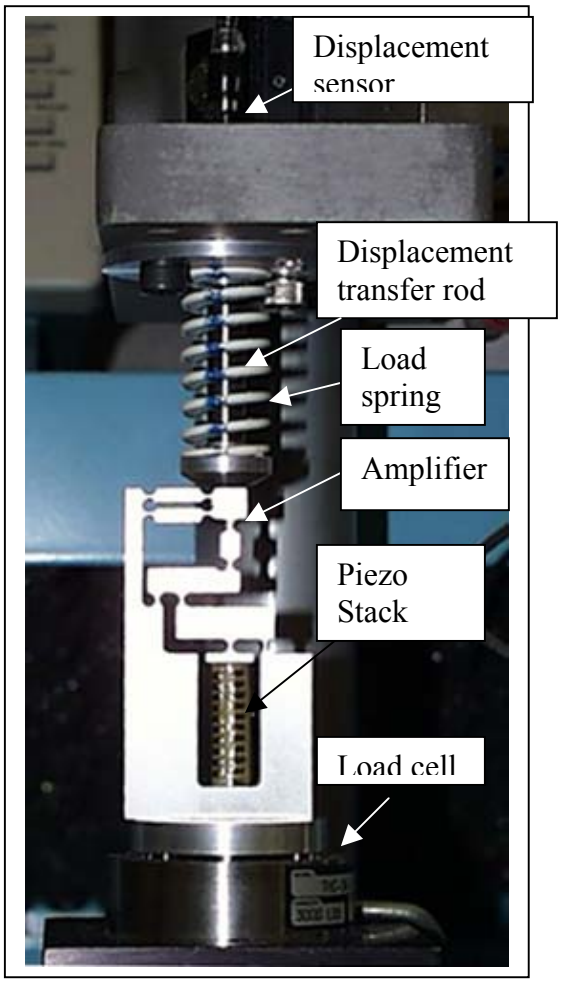

Figure 4. Text fixture for EDO stack and ORNL amplifier device.

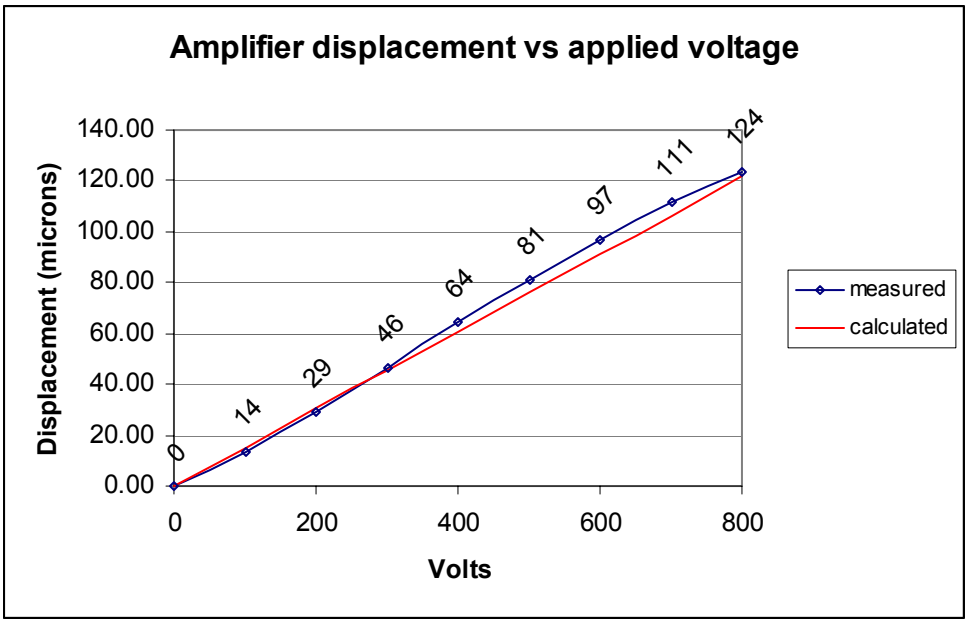

Figure 5 – Static displacement measurements

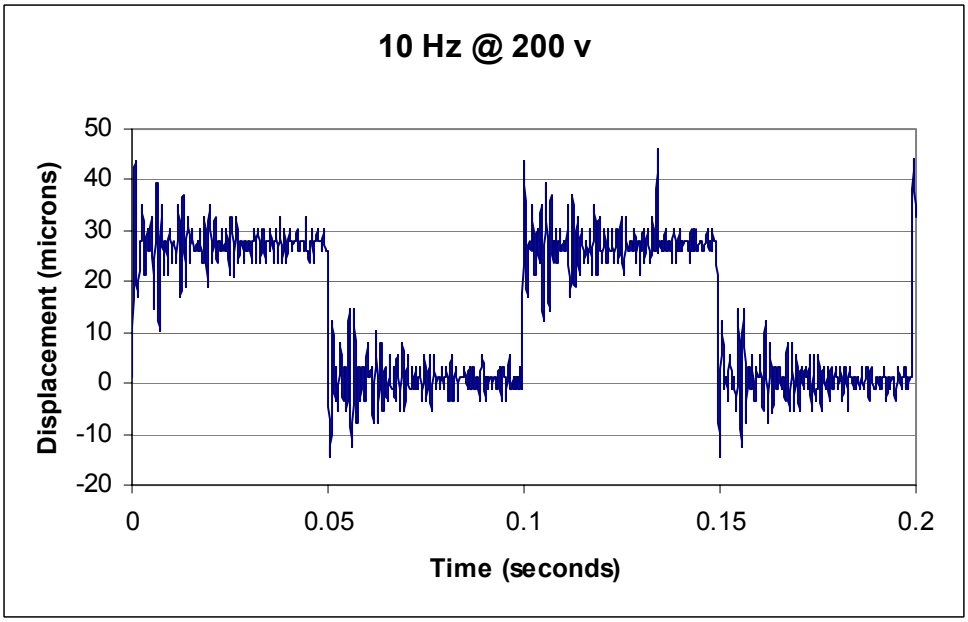

Figure 6 – Low frequency 200v displacement data, 27 microns

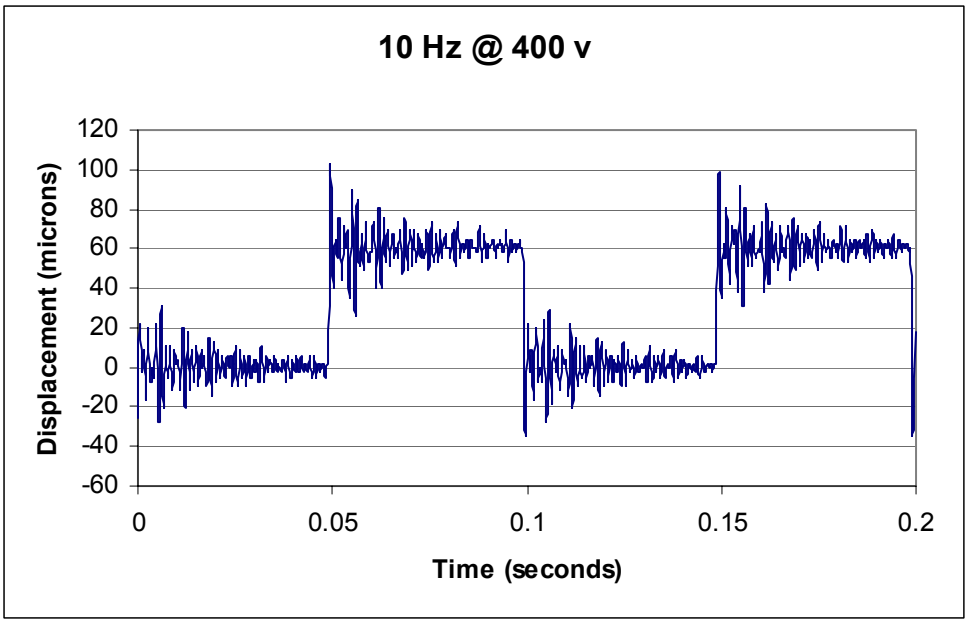

Figure 7 – Low frequency 400v displacement data, 62 microns

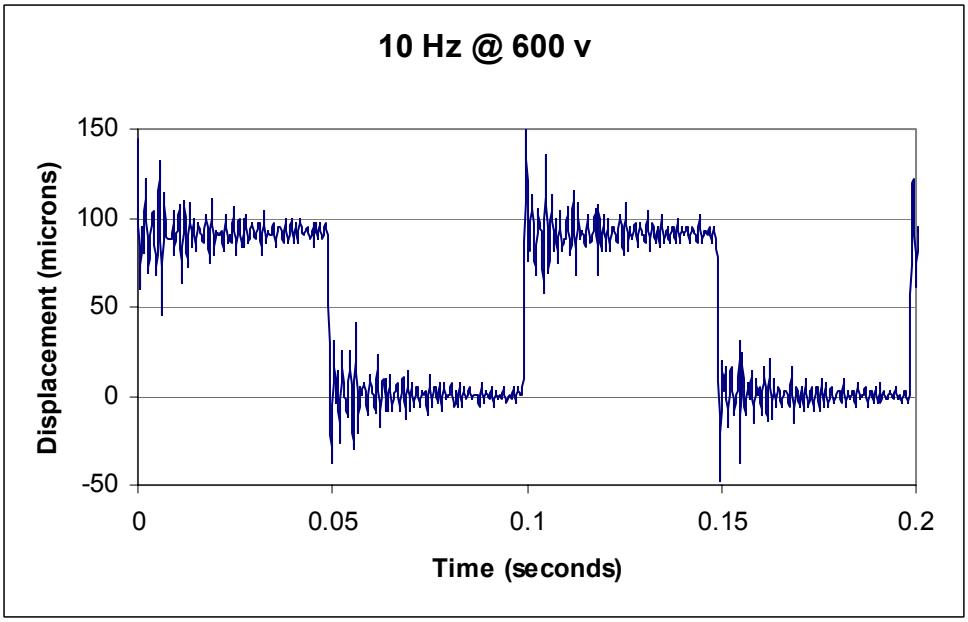

Figure 8 – Low frequency 600v displacement data, 92 microns

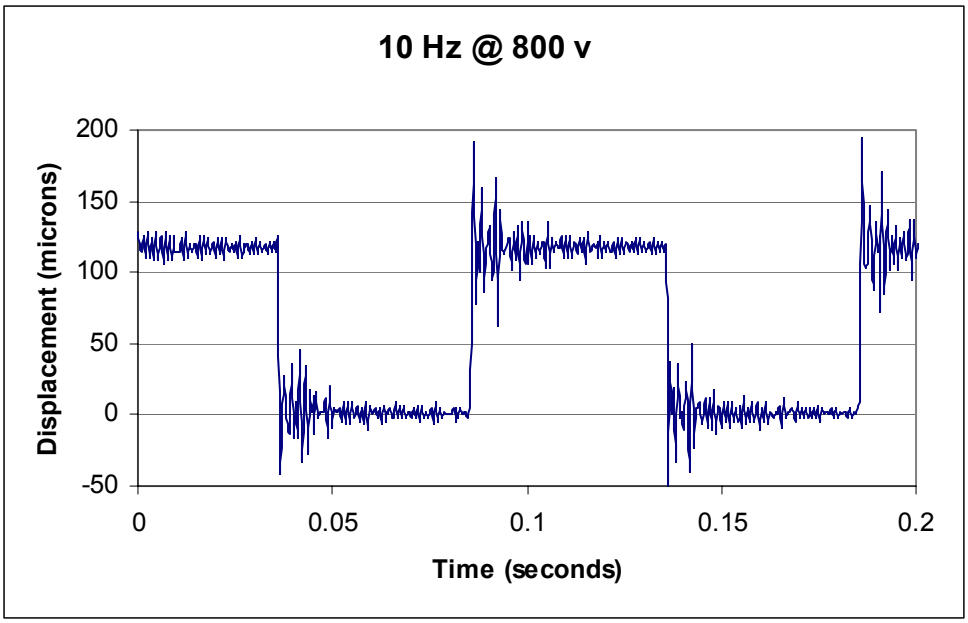

Figure 9 – Low frequency 800v displacement data, 117 microns

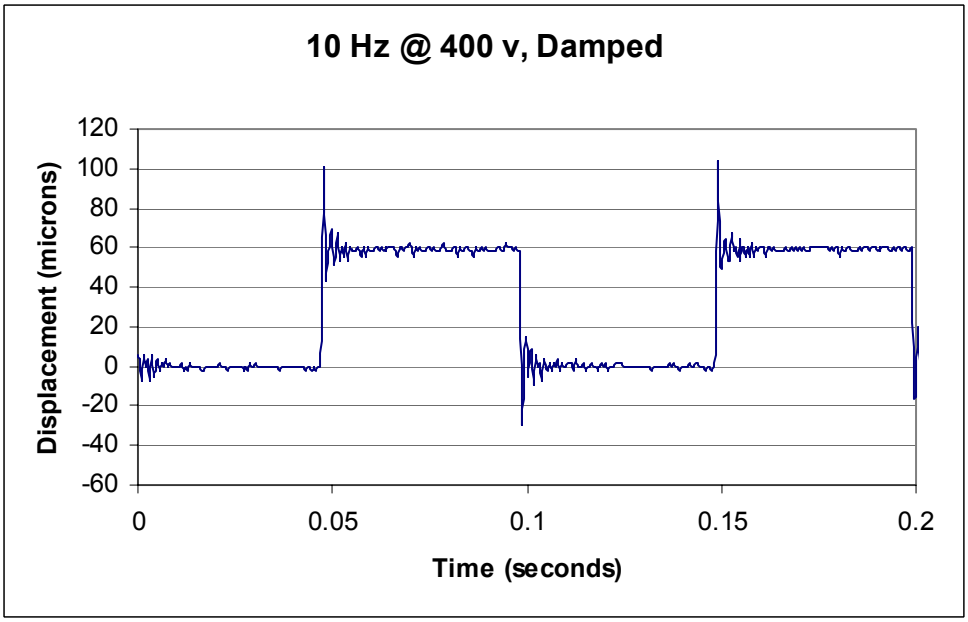

Figure 10 – Improved low-frequency data obtained by adding damping

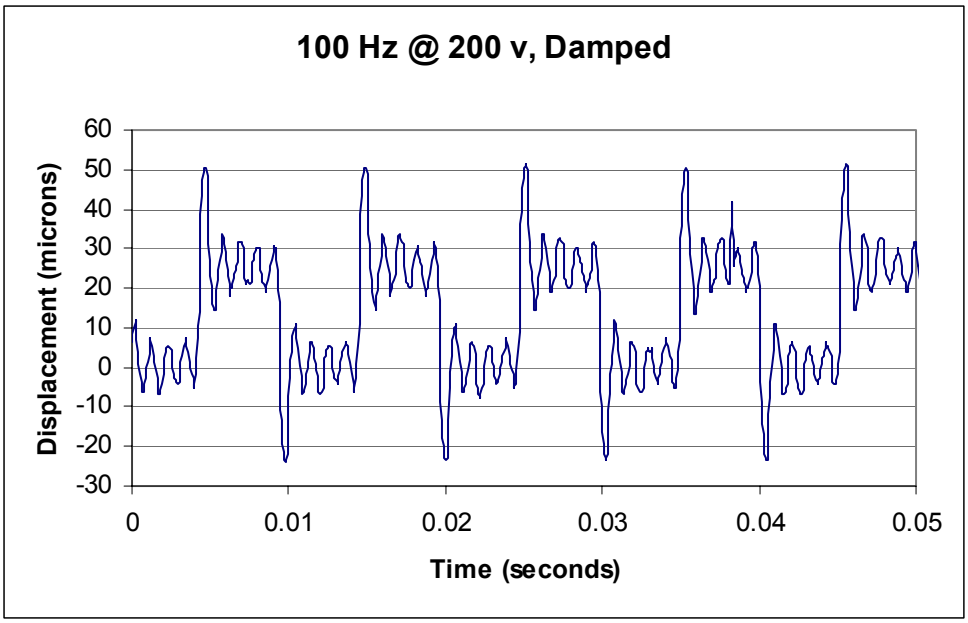

Figure 11 – High frequency 200v data obtained with damping

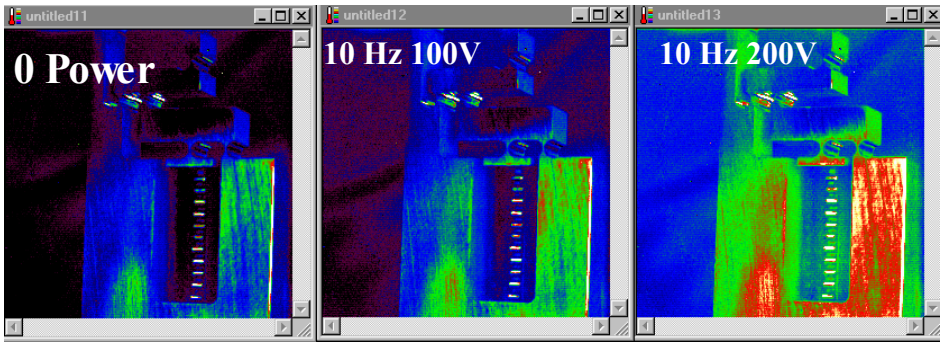

Figure 12. Heating of the piezoelectric stack and test apparatus (IR Intensity displace range: 1800 – 1900 Rainbow color scale: red-white = warm)

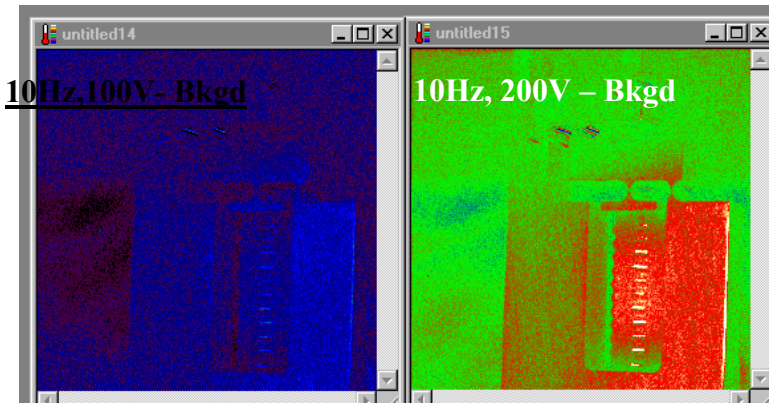

Figure 13. Temperature changes after background subtraction.

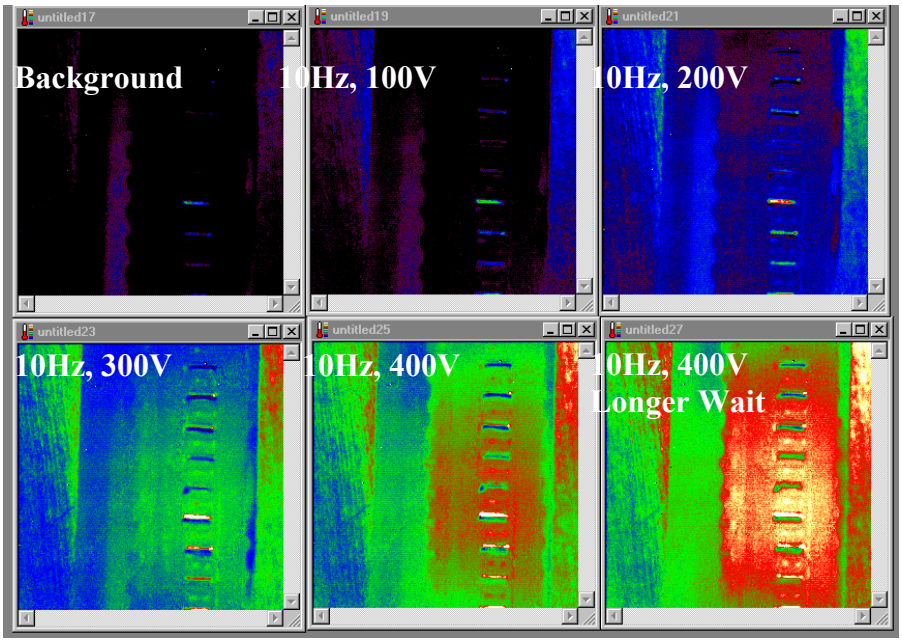

Figure 14. Close-up images using 50 mm lens with extension ring.

Low-Cost Manufacturing Processes for Ceramic and Cermet Diesel Engine Components

D. E. Wittmer
Southern Illinois University

Objective/Scope

The purpose of this work is to investigate the potential of low-cost manufacturing processes for ceramic and cermet diesel engine components. The primary task is to develop cost effective processing, forming and sintering methodologies for cermet and ceramic formulations, used by industrial diesel engine manufacturers.

Technical Highlights

Task 1. Collaboration with industrial partner(s).

This task involves the collaboration with industrial partners to assist them in processing and sintering of their diesel engine components. Our goal is provide assistance in processing and sintering which may result in a reduction in surface reactions and part warping. Moreover, this may also provide an alternative sintering process that will allow improved throughput efficiency and manufacturing economy. Due to the proprietary nature of this task, any research data generated from this task is normally controlled by the terms of each specific confidentiality agreement. The reporting of this data and any results are the responsibility of the industrial partner(s).

Task 2. Cost Effective Processing and Sintering

During this reporting period, we have continued to work on intermetallic bonded TiC with the primary objectives of comparing isopressing to not isopressing, pre-alloying to reaction sintering, and pre-sintering to no pre-sintering. Both batch sintering, with a vacuum-low pressure cycle, at ORNL, and continuous sintering at SIUC were used for sintering comparisons. The formulations were all 40 vol. % intermetallic with 60 vol. % TiC. Two TiC powder sources were used, ultrafine grade from H.C. Starck and T2000 grade from Kennametal. Pellets were formed by uni-axial pressing and rods were formed by injection molding. The binder used for uni-axial dry pressing was PVP. For injection molding, the binder ratio was 55:44:1 (petroleum jelly:parafin wax:stearic acid) and the injection molding temperature was 160EF at a pressure of 60 psi. In the previous reporting period the densities were measured and reported. During this reporting period, the hardness values were determined for all of the injection molded rods where the density was at least 96% of the theoretical value. These results are reported in Tables 1.

Isopressing vs. Not Isopressing

In previous work, isopressing was found to have negative effects on densification for milled formulations. This negative effect was aggravated by using finer starting materials. It was thought that bridging created more open structures during sintering. For these results, in general, isopressing had little effect or did not improve the density of uni-axial pressed disks for any intermetallic-TiC formulation, regardless of TiC source or sintering method. The only situations where isopressing appeared to have a marginal positive effect on sintered density were for uni-axial pressed pellets and injection molded rods that were continuously sintered.

Pre-sintering

Pre-sintering was only explored for specimens that were to be continuously sintered. Pre-sintering was performed at ORNL using the same V-LHIP cycle, however the specimens were only taken to 1200EC for 30 minutes. It was hoped that pre-sintering would remove some of the surface oxygen and react some of the constituents to form a machinable body with better sintering behavior. Pre-sintered bodies would be easier to machine into near-net shape forms, prior to final densification. Pre-sintering was found to have a slight negative effect or no observable effect on the density. Hardness does not appear to have been affected by pre-sintering. The microstructural results will help determine the future of this task.

Pre-alloying vs. Reaction Sintering

In general, higher densities were obtained for pre-alloyed intermetallic-TiC cermets, compared with the same formulations prepared by reaction sintering, regardless of the other parameters investigated. Only in isolated cases, the reaction sintered formulations that were continuously sintered reached higher density than the pre-alloyed formulations. This was observed more for the injection-molded rods than for the uni-axially pressed pellets. The highest densities were obtained for the NiCrFe-TiC and NiAlFe-TiC formulations.

Stark TiC vs. Kennametal TiC

This study is incomplete because we are still waiting to receive the lot of Kennametal TiC that was recently ordered. We still need to process the same formulations and injection mold rods to complete the comparison. For the pellets, it appears that for some those formulations sintered by V-LHIP, marginally higher or the same density was obtained for the H.C. Starck TiC. For some formulations that were continuously sintered, only marginally higher density was obtained using the Kennametal TiC, while for others higher density was produced using the Starck TiC.

Continuous Sintering vs. V-LHIP

It would appear from this limited data that for some NiCr-TiC and NiCrFe-TiC formulations that higher or equivalent density was obtained for both pellets and injection-

molded rods, compared with the same formulations sintered by the V-LHIP method. More testing is required to statistically confirm these observations; however, these results indicate a window of potential opportunity for specific cermet formulations.

Low Pressure Injection Molding

Work is continuing to try to optimize low-pressure injection molding for processing simple shapes. Minimizing internal defects of injection-molded rods has be a goal from the start of this task. We have made significant improvements in elimination of voids that form near the centerline of the injection-molded rods. The temperature control of the mix and the mold appear to be the controlling factors. During this reporting period an in-line heater was installed to better control the hot water flow to both the injection molder mixer and the mold. It would appear that this addition has improved our ability to control the flow properties.

Also, during this reporting period, two batches of NiCr-TiC (Starck TiC) were prepared in the reaction-sintered formulation. However, the Ni was added as mixture of either Novamet T123 (~3.6 micron) and Alpha 10581 (-300 micron spherical) or Novamet T123 and Novamet HDNP (-325 micron spherical) powders. The reason was to decrease the surface area of the Ni powders to try to eliminate some of the flow problems in the injection molder. Both of these formulations injected well but were much "wetter" than previous batches containing all fine Ni powder. The binder content in both formulations was kept at 37 vol. % which was the previous standard. During the next reporting period the binder volume will be reduced to see if the good injection flow can be maintained with less binder. This should help eliminate flow defects and improve green density.

Extrusion

During this reporting period the power and water facilities required for the twin-screw extruder were installed. The die set for extruding a cylinder had been designed and is currently being machined. Preliminary test are scheduled to be run during the first quarter of the year.

Table 1. Hardness Results for Injection Molded Rods Using H.C Starck TiC

Formulation	Process	V-LPHIP (ORNL)		Continuous (SIUC)	
		Density %TD	Hardness (kg/mm^2)	Density %TD	Hardness (kg/mm^2)
NiCr-TiC (RS)	Isopressed	83.1	---	96.6	720
	Not Isopressed	97.4	737	97.1	718
	Isopressed-Pre-S	----	---	97.3	708
	Pre-S	----	---	96.8	729
NiCrFe-TiC (PA)	Isopressed	99.2	722	98.2	694
	Not Isopressed	99.3	743	97.2	729
	Isopressed-Pre-S	----	---	98.1	662
	Pre-S	----	---	95.3	---
NiCrFe-TiC (RS)	Isopressed	80.6	---	----	---
	Not Isopressed	97.6	784	96.9	672
	Isopressed-Pre-S	----	---	97.4	698
	Pre-S	----	---	97.5	695
NiAlFe-TiC (RS)	Isopressed	99.5	803	94.7	---
	Not Isopressed	99.2	783	90.9	---
	Isopressed-Pre-S	----		94.5	---
	Pre-S	----		90.9	---
NiAlFe-TiC (PA)	Isopressed	99.5	783	97.5	694
	Not Isopressed	99.2	720	96.1	729
	Isopressed-Pre-S	----		98.6	662
	Pre-S	----		93.8	---

PA = Pre-alloyed RS = Reaction Sintered Pre-S = Pre-Sintered

Status of Milestones

1.	Collaboration with Industrial Partners	On Schedule
2.	Cost Effective Processing and Sintering	On Schedule

Communications/Visits/Travel

D. E. Wittmer to ORNL to participate in meeting with Cummins and CoorsTek.

Problems Encountered

None

Publications and Presentations

None

Low Cost-High Toughness Ceramics

T. N. Tiegs, F. C. Montgomery, and P. A. Menchhofer
Oak Ridge National Laboratory

Objective/Scope

Significant improvement in the reliability of structural ceramics for advanced diesel engine applications could be attained if the critical fracture toughness (K_{Ic}) were increased without strength degradation. Currently, the project is examining toughening of ceramics by incorporation of ductile intermetallic phases.

Technical Highlights

Previous studies have shown that the properties of the aluminide-bonded ceramics are attractive for diesel engine applications and consequently, development of these materials was started. At the present time, TiC-based composites with 40-60 vol. % Ni_3Al are being developed because they have expansion characteristics very close to those for steel. Preliminary wear testing indicated that improved wear resistance could be achieved by decreasing the grain size of the TiC. Achieving fine grain size with the high binder contents is difficult because of the large inter-grain distances. In addition, it was thought that changing the TiC grain shape from a highly faceted one to a more rounded equiaxed grain would reduce localized stress at sharp corners. This, in turn, would improve abrasion resistance from any wear debris. Consequently, grain size refinement is presently being studied. Several approaches can be used to control the final TiC grain size. The methods studied in the present report include: (1) use of additives to change the interface behavior of the growing TiC grains, and (2) reduction of the initial TiC particle size. The development effort is being done in collaboration with CoorsTek, Inc.

Large Batch Processing of TiC-Ni_3Al Composites - The series of large batches (≥2 kg) discussed in the previous progress report to investigate batch-to-batch variations, milling conditions, use of alternate binders/dispersants, and addition of grain growth inhibitors was continued. The test samples and conditions for all the samples examined to date are shown in Table 1.

Multiple billets of the powder mixtures from #9A through #13 were uniaxially pressed and then sintered. The sintering schedule was the standard cycle at ORNL using vacuum and low pressure HIP at 1400-1425°C. Because of the high liquid phase contents, densities achieved in all cases were >99% T. D. The effect of the processing conditions on the flexural strength is also shown in Table 1.

The previous work had shown that grain growth in TiC-Ni_3Al composites can be manipulated by use of additives. The various additives can be categorized into three basic types: strong carbide formers, moderate carbide formers, and additions that do not alloy with TiC. Strong carbide formers include Ta, V, and W which form stable carbides that have complete solid solubility with TiC. These materials are incorporated into the TiC during reprecipitation and no change in the grain shape occurs with these additions. The moderate carbide formers include Mo and Cr

and these have limited solubility in TiC. These types are also incorporated into the TiC during grain growth, but change the grain shape to less faceted grains and reduce the grain size. Additions that do not alloy with TiC in the Ni_3Al system include elements such as Fe, Si, and Co. These remain in the Ni_3Al phase and result in smaller less faceted TiC grains.

The recent results indicate that very short milling times are not beneficial to the composite flexural strength. Evidently, some milling is needed to refine the TiC grain size while not adding too much oxygen into the system. In addition, it was shown that higher additions are Mo (4%) do not increase the flexural strength above that attained by the 2% addition.

Grain Refinement by Multiple Additives - Based on the previous results which showed the effects of individual additives, a new series of samples is being fabricated that will examine the behavior of multiple additives. The initial compositions are shown in Table 2. The Mo addition is used to refine the grain size, round the grains, and to improve the strength. The TaC additions are being examined to increase the hardness. The Fe addition has been shown to be very effective at grain rounding and to improve the room temperature strength.

Status of Milestones

On schedule.

Communications/Visits/Travel

Travel by T. N. Tiegs to Orlando, FL, Nov. 16-17, 1999 to attend a Program Coordination Meeting for the Metal Powder Industries Federation 2000 International Conference on Powder Metallurgy and Particulate Materials.

Problems Encountered

None.

Publications

T. N. Tiegs, F. C. Montgomery, P. A. Menchhofer, and P. F. Becher, "Effect of Additives on Grain Size and Shape in TiC-Ni_3Al Composites," to be published in Ceram. Sci. Proc., Am. Ceram. Soc., Westerville, OH (2002).

Table 1. Summary of large batch processing variables for different TiC- Ni_3Al composites.

Batch No.	Ni_3Al Content (vol. %)	Grain Growth Inhibitor (wt. %)*	Dispersant Addition (wt. %)	TiC Milling Time (min.)	Metal Milling Time (min.)	Flexural Strength (MPa)
#1	40	2% Mo	---	180	60	700±261
#2	40	---	---	60	10	930±207
#2A	40	---	---	60	10	1181±135
#3	40	1% Mo	---	60	20	892±108
#4	40	1% Mo	---	60	20	1111±186
#5	40	1% Mo	1% PVP	60	20	791±46
#6	40	1% Mo	1% PVP, 1% Ox.Acid†	120	60	885±78
#7	40	2% Cr_3C_2	1% PVP, 1% Ox.Acid†	---	180	641±57
#8	50	2% Cr_3C_2	---	60	60	941±104
#9	50	1% Mo	---	90	30	1153±287
#9A	50	1% Mo	---	90	30	1199±169
#10	50	2% Mo	---	90	30	1247±104
#11	60	2% Mo	---	90	30	N. D.[a]
#12	50	2% Mo	---	10	10	1001±178
#13	50	4% Mo	---	90	30	1164±95

* Percent based on TiC content.
† Polyvinylpyrrolidone; Oxalic acid.
Specimens did not attain full density, but slumped excessively during sintering.

Table 2. Summary of processing variables for different TiC- Ni_3Al composites that will examine the effects of multiple additives.

Batch No.	Ni_3Al Content (vol. %)	Additives (wt. %)*	TiC Milling Time (min.)	Metal Milling Time (min.)
2001-1	50	2 Mo, 2 TaC	60	20
2002-2	50	2 Mo, 2 TaC, 2 Fe	60	20

* Percent based on TiC content.

Utilization of Thermally Conductive Graphite Foam for Cooling Diesel Engine Blocks

Ronald D. Ott and James W. Klett
Oak Ridge National Laboratory

Objective

The objective of this effort is to determine the feasibility of using the high thermally conductive graphite foam, developed at Oak Ridge National Laboratory, as a cooling medium in a diesel engine block. Cooling problems exist in certain areas of diesel engines that are not adequately cooled by water. There are attempts to cool these areas by the lubricating oil but hot spots around the cylinder block and head still exists. It may be possible to strategically place the graphite foam in these areas to aid in rapidly removing, or redistributing, the heat to the nearest cooling path, be it oil, coolant or air.

In recent years there have been efforts to study the performance of, and methods to improve, the cooling system of diesel engines. For a diesel engine to operate at optimal performance, the thermal stability of the engine is critical. Cooling of the engine block is accomplished by the coolant, lubricating oil, exhaust and losses due to radiation and convection to the surroundings. Approximately 36% of heat removed is achieved by the coolant and the lubricating oil. Almost half of that 36% of the heat removed is accomplished by lubricating oil passages that have been placed in areas where there are high levels of heat, due to inadequate cooling from the coolant. By effective controllable cooling, the life of the engine can be increased as can the fuel economy and performance of the diesel engine.

Technical Highlights

A meeting was held in July with Ron Ott and Dave Stinton from ORNL and Tim Theiss, Robert Wagner, Norberto Domingo, and Jim Conklin from the Advanced Propulsion Technology Center to discuss ways in which the graphite foam could be utilized in cooling diesel engine blocks.

The initial discussion was focused on determining locations within the diesel engine where hot spots commonly occur. One area under consideration was around the edges of the exhaust valves but consensus was that in order to incorporate a cooling device manufactured from graphite foam, considerable alterations to the manufacturing process would have to be undertaken. Another area that could incorporate a device such as a heat pipe would be between siamese cylinder bores where there is no cooling. Such a device could greatly reduce cylinder distortion, thus increasing engine life.

Heat pipe configurations were discussed and it was discovered that this is not a new concept for engine cooling, but was evaluated in the 1980's. There were cracking issues, leading to sodium leaks, and the heat pipes were very expensive. The group did not go into any depth discussing heat pipe configuration utilizing graphite foam. The discussion continued with evaluating other areas in which the graphite foam could be utilized in the engine block. Several ideas came up including oil pans, oil windage trays, transmission coolers and housings, radiator reservoir tanks and torque converters.

Contacts have been made at Thermacore/Modine, Caterpillar and ArvinMeritor. Each of these companies has the ability to contribute to the study considering their diverse areas of expertise. Thermacore is an industry leading company in thermal management with extensive background in heat pipe manufacturing. Caterpillar would be an ideal partner to help in identifying the feasibility of introducing the graphite foam into the diesel engine block for cooling purposes. ArvinMeritor is a world leader in aftermarket products for the automotive and heavy truck industry and could contribute in evaluating add-on cooling components to diesel engines.

In July, a meeting was held with James Klett, April McMillan, Nidia Gallego, and Ron Ott of ORNL and Stephen Memory of Modine and Jon Zuo of Thermacore. Although this meeting was not geared toward evaluating the graphite foam in cooling engine blocks, interest was shown and the topic was discussed. Jon Zuo is to contact Ron Ott with the appropriate person at Thermacore to investigate the feasibility in further detail.

From that meeting a plan of action was laid out to effectively evaluate the performance of the graphite foam in a heat pipe configuration. Thermacore is able to advise ORNL on how to tailor the graphite foam's properties to better suit a heat pipe configuration and manufacturing. A simplified version of a heat pipe utilizing the graphite foam can be manufactured to evaluate its performance. In conjunction, discussions with Caterpillar and Advanced Propulsion Technology Center need to be ongoing in order to evaluate areas within the engine where heat pipes would be advantageous from the cooling aspect, as well as practicable from the manufacturing aspect.

Mike Ready of Caterpillar visited ORNL in July and showed interest in assessing the feasibility of using the graphite foam in cooling diesel engine blocks, other than radiator applications. The appropriate contact at Caterpillar will be identified to further investigate our interaction.

Sam Ciray of ArvinMeritor visited ORNL in June and showed interest in developing the graphite foam for heat pipe applications. ArvinMeritor was excited at the possibilities the graphite foam holds for heat management. An appropriate contact at ArvinMeritor is to be appointed for further communication.

Status of Milestones

The first milestone, evaluating the possibilities of utilizing the graphite foam for cooling diesel engine blocks, has begun. Significant industrial partners have been identified and the proper contacts within each organization are currently being determined.

Communications/Visits

Mark Andrews, who works at Caterpillar Inc. in the Advanced Materials Technology Center, has been in contact expressing interest in the carbon foam for cooling diesel engines, other than radiator designs. He had put together a funding request to Caterpillar's Large Engine Center (LEC) to pursue development of the carbon foam for thermal management applications. This funding was proposed to initiate research to obtain the required data in order to move forward and design a platform for this technology. However, LEC funding has been cut for FY2002, but interest is still strong in carbon foam technologies. If some of the basic research for utilizing the carbon foam in a heat pipe type of device can start in 2002, the likelihood for future funding

would be more probable since the benefits and technical pathways would have already been established.

On that note, James Klett decided whom better to mature the technology of utilizing carbon foam in a heat pipe type of device than Thermacore. Jon Zuo, of Thermacore, was contacted and asked what level of effort would it take to start some basic research in evaluating the carbon foam as the wicking material in a heat pipe type of device. James Klett and Ray Johnson decided it might be possible to support Thermacore initially with approximately $35K to start some basic research. If it is possible to have some technical data generated by mid 2002 that would put the technology in a better situation for future funding from industry.

Publications

No publications to report.

Intermetallic-Bonded Cermets

P. F. Becher, T. N. Tiegs, L. Riester, and S. B. Waters
Oak Ridge National Laboratory

Objective/Scope

The goal of this task is to develop materials for diesel engine applications, specifically for fuel delivery systems and wear components (e.g., valve seats and turbocharger components). This will require materials which have a minimum hardness of 11 GPa and a thermal expansion coefficient of 10 to 15 x 10^{-6}/°C. The material should also have excellent corrosion resistance in a diesel engine environment, flexure strength in excess of 700 MPa, and fracture toughness greater than 10 MPa√m to ensure long-term reliability. The material should also be compatible with steels and not cause excessive wear of the steel counter face. The upper temperature limit for fuel delivery systems applications is 540° C, and for the other wear applications, the limit is 815° C. Finally, the total material processing costs for these advanced materials should be competitive with competing technologies such as TiN or other ceramic coatings on high-speed tool steels.

Technical Highlights

The magnitude of the toughness of the TiC-Ni_3Al cermets depends directly upon the contribution from plastic deformation of the Ni_3Al binder phase. This can be raised by increasing either the Ni_3Al content or the amount of plastic flow within the Ni_3Al. Alloying can raise the yield stress and the strain-hardening coefficient of the Ni_3Al and, thus, limit the contribution of plastic deformation to the cermet toughness. Furthermore in order for the Ni_3Al to plastically deform, the TiC-Ni_3Al interface must debond at local stresses that are equal to or less than those required to initiate plastic deformation. Interface debonding (and cleavage of TiC grains) acts to relieve the triaxial constrains imposed on the Ni_3Al binder phase by the matrix. If this constraint is not relieved, the shape change that must accompany plastic flow cannot occur and plastic flow will be effectively prohibited. In the current cermet processing schemes Mo and Cr_3C_2 additives have been used to fabricate the TiC-Ni_3Al cermets. These additives were selected to attempt to enhance processing and to modify the microstructure. However, such chemical additions can modify the Ni_3Al plastic flow and the TiC-Ni_3Al interface debonding processes.

Molybdenum additions have also been indicated to increase both wetting and provide some interface strength in the Ni–TiC system.[1] As is the case in Ni-TiC cermets, a molybdenum carbide layer forms on the TiC grains in the TiC-Ni_3Al cermets, which apparently improves the interface strength. If this interface is excessively strengthened, interfacial debonding is hindered and the restraint on the Ni_3Al binder phase is not released, which would limit plastic flow in the Ni_3Al. However, *in-situ* observations reveal that interfacial debonding occurs and is accompanied by plastic flow of the Ni_3Al phase during crack propagation in the TiC–Ni_3Al cermets that contain small Mo additions, Fig. 1.[2,3] In addition, some cleavage of large TiC grains is observed, which would also reduce the constraints imposed on the Ni_3Al phase. Plastic flow of the Ni_3Al phase is also enhanced if the grain size is large as weak Ni_3Al grain boundaries are

avoided. Large Ni_3Al grains then can form plastically deforming ligaments that span the crack surfaces in the crack tip wake to toughen the cermet.

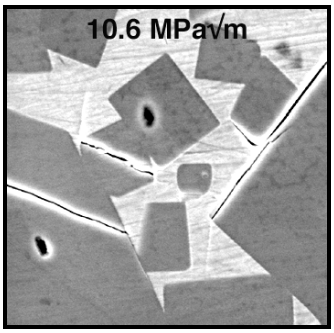

Figure 1. Interface debonding relieves constrain imposed on Ni_3Al (light grey) and allows plastic deformation to be initiated in the Ni_3Al binder phase.

When small additions of Mo, Ta, Cr, V, Zr, or W are added to the TiC-Ni_3Al cermets, a rim structure forms on the TiC grains, which contains the Mo, Ta, Cr, or Zr addition as a carbide [e.g., Mo_2C or (Ti, Mo)C], where Mo and V also accumulate preferentially at the interface between the rim and the TiC grain surface, Fig 2. Note again that for the cermets discussed here, only Ti and Cr have been detected within the Ni_3Al phase and Mo, Cr, and W are found in the rim structure of the TiC grains.[4]

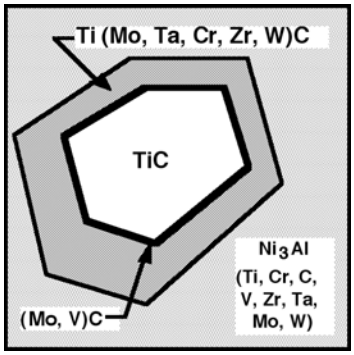

Figure 2. Schematic of <u>potential</u> partitioning of elements in TiC-Ni_3Al cermets.

The phase diagram for simple ternary Ni_3Al-Me alloys (Fig. 1) reveals there are a wide range of Me elements that can go into solution in the Ni_3Al lattice.[5] Among those of interest, Hf, Ti, Zr, W and Mo substitute on Al sites, while Cr and Fe can substitute on either Ni or Al sites. Cu and Co substitute on the nickel sites. In the case of the mechanical properties, Hf, Zr, and W additions significantly raise both the yield stress and the work hardening rate of Ni_3Al at 77K while Ti and Mo have smaller but detectable effects, Figs. 4 and 5.[6] Cr additions are slightly more potent in raising the yield stress than are Ti and Mo but less than that with W, Hf or Zr additions.[7,8] Both B and C take interstitial sites in the Ni_3Al lattice and both were found to raise the room temperature yield stress of ribbons by nearly two-fold at the 1.5 at. % addition level.

Thus B and C are as potent as Hf and Zr in raising the yield stress of Ni_3Al.[7,9] While B is quite effective in improving the ductility of Ni_3Al, C appears to have no effect on ductility.

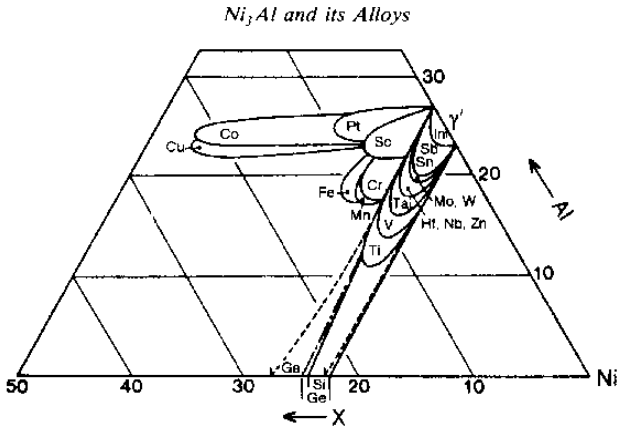

Figure 3. Solubility of elements in Ni_3Al at 1000°C.[5]

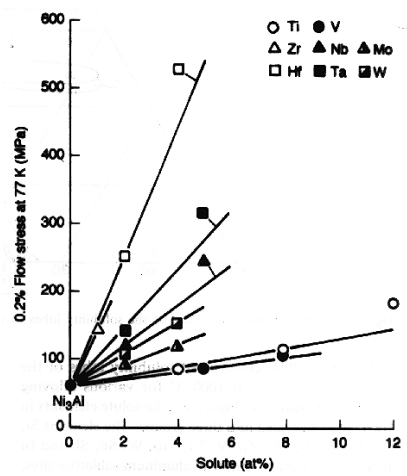

Figure 4. Effect of Me solute elements on the 0.2% yield stress at 77K of Ni_3Al binary alloys.[6]

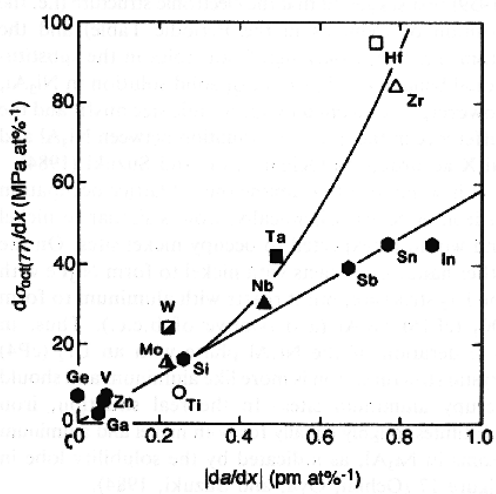

Figure 5. Relationship between solid solution hardening rate of Ni_3Al alloys and the lattice parameter change with solute content.[6]

The mechanical properties have been evaluated for TiC-Ni_3Al cermets containing either Mo and Cr_3C_2 additions and those with no additions. For a given Ni_3Al content, the results indicate that both the flexure strengths and the fracture toughness values are improved with the Mo additions as compared to the Cr_3C_2 additions. In addition, the Cr_3C_2 addition is found to raise the hardness of the Ni_3Al binder phase above that obtained with either Mo or in the absence of such additions (e.g., only Ti and C in solution in the Ni_3Al), Table I. The increase in hardness indicates that the yield stress of the Ni_3Al binder phase is raised by the Cr_3C_2 addition as compared to that for either no or the Mo additions. The slightly greater effect of Cr in raising the yield stress of Ni_3Al as compared to Mo and/or Ti additions may well be a contributing factor in the lower toughness

of the cermets with Cr_3C_2 additions. In the case of the present cermets, only Cr and Ti have been detected in solution in the Ni_3Al binder phase.[4]

It must be also noted that the cermet processing utilizes WC media to attritor mill the powder mixtures and a small amount (< 0.5 wt. %) of WC is introduced due to the wear of the media during milling. As noted earlier, the incorporation of W into the Ni_3Al can raise the yield stress and strain hardening coefficients significantly. However, WC is introduced into all the cermet compositions. Only if the solubility W in Ni_3Al is a function of the specific compound or metal added (e.g., Mo, Ti, or Cr), would one expect there to be a correlation with the variation in Ni_3Al plasticity and the cermet toughening behavior. Considering the solubilities of the various elements in Ni_3Al, as well as the absence of detectional W in the Ni_3Al binder phase, such effects seem unlikely for the WC and additive levels involved here.

It appears that the Cr_3C_2 addition effects are mostly due to the incorporation of additional C into the Ni_3Al binder phase. As shown earlier, interstitial C is among the most potent in raising the yield stress of Ni_3Al, rivaling the effects of Zr and Hf additions. Raising the C content through the dissolution of Cr_3C_2 in the Ni_3Al phase during sintering would substantially limit the contribution of plastic deformation. Very small increases in C (e.g., at 1.5 at. % C) have been shown to double the yield stress. Thus, the increased hardness of the Ni_3Al phase is seen to be due to increases in interstitial C content with only a very minor effect due to Cr substitution into the Ni_3Al. The resultant increase in yield stress of the Ni_3Al alloy, which the increased hardness reflects, would then diminish the contribution of plasticity and result in lowering the toughness of the cermet as is observed.

Table I. Characteristics of TiC-Ni_3Al Cermets

Ni_3Al content vol. %	Added to TiC wt. %	Oxygen content after milling mixture wt.%	Hardness of Ni_3Al regions GPa	Elastic modulus of Ni_3Al region GPa	Cermet Flexure Strength MPa	Cermet Fracture Toughness MPa√m
40	None	0.58			1181	17.5
40	1 Mo	0.63	5.98	249	892	
40	1 Mo	0.36	5.75	229	1111	
40	2 Cr_3C_2	0.87	6.55	270	641	
50	2 Cr_3C_2	0.39	6.37	265	998	17.4
50	2 Mo	0.92	5.93	236	1247	21.6

Status of Milestones

On Schedule

Communication/Visits/Travel

Meeting held at ORNL on Nov. 14, 2001 to discuss progress on processing and evaluation of cermets for engine applications with R. Stafford and M. Naylor of Cummins Engine, J. Stephan of AMT/CoorsTek, D. Wittmer of Southern Illinois University, and R. Johnson, T. Tiegs and P. Becher of ORNL.

Publications

None

Reference

1. P. Ettmayer, "Hardmetals and Cermets," pp. 145-64, Annual Review of Materials Science, Vol. 19, Annual Reviews Inc., Palo Alto, CA, 1989.
2. P. F. Becher, K. P. Plucknett,* and C.-H. Hsueh, "Toughening and Strengthening Response in Ni_3Al–Bonded Titanium Carbide Cermets," *Zietschrift für Metallkunde*, 92(8) 995-99 (2001).
3. K. P. Plucknett, P. F. Becher, and K. B. Alexander, "In–Situ SEM Observations of Fracture Behavior of Titanium Carbide/Nickel Aluminide Composites," *J. Microscopy*, 185 (2) 206-16 (1997).
4. T. N. Tiegs, J. L. Schroeder, F. C. Montgomery, and D. L. Barker, "Sintering and Evolution of Microstructure in TiC-Ni_3Al Cermets," *Int'l J. Powder Metall*., 36 (7) 46-57 (2000).
5. S. Ochiai, Y. Oya, and T. Suzuki, "Alloying Behavior of Ni_3Al, Ni_3Ga, Ni_3Si and Ni_3Ge," *Acta Met*. 32:289-98 (1984).
6. Y. Mishima, S. Ochiai, N. Hamao, M. Yodogawa, and T. Suzuki, "Solid Solution Hardening of Nickel-Role of Transition Metal and B-subgroup Solutes," *Trans. Jpn Inst. Metals*, 27(9) 656-64 (1986).
7. S. C. Huang, C. L. Briant, K.-M. Chang, A. I. Taub, and E. L. Hall, "Carbon Effects in Rapidly Solidified Ni_3Al," *J. Mater. Res*. 1(1) 60-7 (1986).
8. R. D. Rawlings and A. E. Staton-Bevan, "The Alloying Behavior and Mechanical Properties of Polycrystalline Ni_3Al (γ' Phase) with Ternary Additions," *J. Mater. Sci*. 10: 505 (1975).
9. S. C. Huang, A. I. Taub, and K. M. Chang, "Boron Extended Solubility and Strengthening Potency in Rapidly Solidified Ni_3Al," *Acta Metall*. 32(10) 1703-07 (1984).

Low-Cost Manufacturing of Precision Diesel Engine Components

S.B. McSpadden, Jr.
Oak Ridge National Laboratory

Objective/Scope

To develop and demonstrate optimized, cost-effective fabrication processes for the production of precision components for use in diesel engines. To develop and demonstrate optimized, cost-effective, non-destructive testing methods for the detection and prevention of machining-induced damage in engine components.

Technical Highlights

New Creep Feed Surface Grinder Procurement – The K.O. Lee creep feed surface grinder has been installed at the High Temperature Materials Laboratory and is fully operational. Instrumentation has been added to measure grinding forces, spindle power, vibration, acoustic emission, coolant pressure, coolant flow, and coolant temperature. The grinder will be used in a wide range of machining studies aimed at improving grinding technology and reducing the cost of manufacture of diesel engine components.

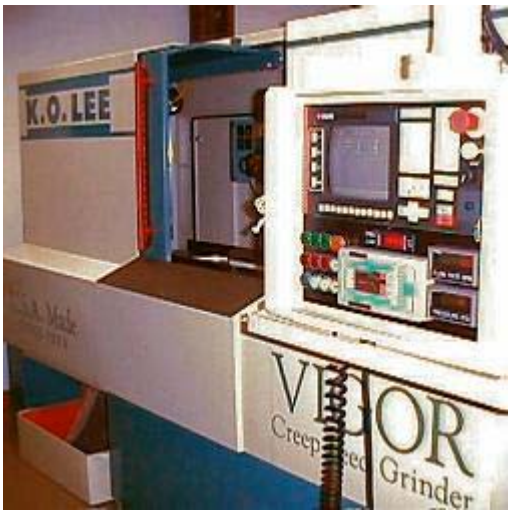

Investigation of Non-Destructive Detection of Flaws in Ceramic Diesel Engine Fuel System Components – Work is continuing on this State Partnership Program funded project. Zirconia specimens that were ground under aggressive and conservative grinding conditions were examined using the ELSAM acoustic microscope. Transverse cracks indicative of machining damage were clearly visible on the surface of the aggressively ground sample. These cracks extended beneath the surface for a depth of several microns and their 3-dimensional structure could be seen in images obtained with the microscope. Although evidence of grinding could be seen in the surface topography of the conservatively ground specimen, transverse cracks were not present. The acoustic microscope has demonstrated its potential as a tool for detecting both obvious and hidden machining damage.

Despite the extremely promising results obtained on the acoustic microscope, it will require refurbishment and an upgrade of existing software in order to make it a useful diagnostic and research tool. Currently, the computer system that controls the instrument is obsolete. The computer hardware is approximately 10 years old and replacement parts are no longer readily available. The operating system is no longer supported and only means of extracting stored information is through a printout or on a floppy diskette. Unfortunately, the format of the floppy diskette is not compatible with any modern operating system (PC, Linux, or Macintosh). Because of these limitations, the excellent acoustic images (similar in appearance to those obtained with an SEM) cannot be exported from the instrument and analyzed with imaging software.

An upgrade is available for approximately $37,000 that will replace the antiquated computer and control hardware. The upgrade included Windows-based software that will greatly simplify the operation of the instrument and enable the acoustic images to be stored in a format that is compatible with a large number of analysis programs. Current plans are to procure this upgrade in the near future.

Communications/Visits/Travel

None.

Publications

None.

Cylindrical Wire Electrical Discharge Machining (EDM) and Temperature Measurement

Albert Shih
North Carolina State University

Objective/Scope

To develop precise, efficient, and cost-effective cylindrical Wire Electrical Discharge Machining (WEDM) process for cermet and other electrically conductive advanced engineering materials, and temperature measurement methods for grinding and diesel exhaust aftertreatment devices.

Technical Highlights

Two highlights in this quarter are the abrasive waterjet machining of Ti-6Al-4V and the temperature measurement of diesel engine exhaust aftertreatment filters.

1. Abrasive Waterjet Machining of titanium

The Abrasive WaterJet (AWJ) machining process was developed in 1983 for glass cutting. Since then, the AWJ has been applied for machining a wide range of materials [1]. Although not as precise as the wire EDM, the AWJ offers a productive alternative with high material removal rate and flexibility. Based on the study of Arola and Ramulu [2], the material removal and surface integrity are highly dependent on the mechanical properties of the work-material. The AWJ cutting of various metals and ceramics have been reported in the literature. However, the machinability and surface properties of AWJ cut Ti alloys are not available. In this study, the AWJ experiments have been conducted on machining of a stationary 58 mm thick block and a 12.7 mm diameter rod driven by a rotary spindle. The work-material is Ti-6Al-4V. The gap width, jet divergence and convergence, and surface finish were studied at different cutting feed rates. For comparison, the wire Electrical Discharge Machining (EDM) is applied to machine the same Ti alloy.

1.1 Machine setup and process parameters

The AWJ experiments were conducted in an AWJ machine at the ADR Hydro-Cut, Inc. at Morrisville, NC. The machine setup and process parameters of AWJ machining and wire EDM are listed in Table 1.

Table 1. Machine setup for the abrasive waterjet and wire EDM experiments.

Abrasive Waterjet		Wire EDM	
Waterjet machine	Flow International Integrated Fine Bridge	Wire EDM machine	Brother HS-5100
Nozzle diameter (mm)	1.0	Spark cycle (μs)	18
Water pressure (ksi)	50	On-time (μs)	14
Abrasive metering orifice diameter (mm)	6.0	Axial wire speed (mm/s)	15
Abrasive average size (mm)	0.32	Gap voltage (V)	60
Feed rate (mm/s)	7.2 -- 36	Feed rate (mm/s)	1.5

1.2 Experimental results and discussion

Nine AWJ cuts on a 58 mm thick Ti-6Al-4V workpiece were conducted. All the other process parameters remains the sane except the feed rate is increased from 7.2 to 36 mm/s with 3.6 mm/s increment. The gap width was measured at eight positions for each slot to identify the change in gap width and the convergence and divergence of waterjet. Pictures of the top, front, and back view of the nine grooves machined by AWJ are illustrated in Fig. 1. Measurements of the gap width, ranging from 0.7 to 1.7 mm, are shown in Fig. 2. Two trends can be observed from Figs. 1 and 2:

- The gap width decreased when the feed rate increased. As shown in Fig. 1(a), the difference in gap width was not significant on the top surface, where the abrasive waterjet first hits the workpiece surface.
- Deeper from the top of cut surface, as shown in Fig. 1(b), the gap width for most grooves becomes narrower. The two cuts at low feed rates (7.2 and 10.8 mm/s) are the exceptions. In the upper section of the grooves in these two cuts, because of the divergence of waterjet, the gap of width slightly increases before the convergence of AWJ to produce narrower gap width.

For the wire EDM process, the gap width is much smaller, about 0.35 mm, and consistent.

The surfaces of abrasive waterjet machined Ti workpiece at different feed rates are shown in Fig. 3. The surface machined by AWJ can be categorized into three regions [2]:

- Initial Damage Region (IDR). The IDR is at the top of the machined surface where the AWJ first impinges the surface. It is the result from the jet expansion prior to impingement.
- Smooth Cutting Region (SCR). The SCR is below IDR. The surface texture in SCR is determined by the abrasive particle size.
- Rough Cutting Region (RCR). The RCR is below the SCR and has the waviness pattern, as shown in Fig. 3, governed by the cutting parameters, such as the feed rate.

It can be observed in Fig. 3 that the IDR and SCR areas shrink and RCR area expands when the feed rate is increased. The surface roughness and waviness were measured at eight positions on the AWJ machined surfaces. Results of the measured roughness and waviness are shown in Fig. 4. These results are compared to the roughness and waviness of the wire EDMed surface. Some observations can be made:

- Lower feed rate generated lower surface roughness and waviness. The lowest roughness (R_a) and waviness (W_a) of the surface machined at 7.2 mm/s (20%) feed rate are about 2 and 3 μm, respectively. The highest roughness (R_a) and waviness (W_a) of the surface machined at the 36 mm/s (100%) feed rate are as high as 13 and 85 μm, respectively.
- The surface roughness and waviness are not sensitive to the cutting depth for low feed rate (20% and 30% or 7.2 and 10.8 mm/s) cuts. Both surface roughness and waviness increase rapidly at 30 mm from the top surface for high feed rate (60%, 80%, and 100%) cuts. That is partially because the low feed rate surfaces have larger SCR and, in contrast, the low feed rate surfaces consist of larger RCR.

- The surface roughness and waviness values are at same level for surfaces cut at low feed rate, while the waviness dominates the surface feature for high feed rate cut surfaces.
- The surface roughness and waviness of the wire EDM processed surface are comparable to that of the low feed rate AWJ cut surface. According to our previous study [7], the surface finish could be improved significantly by skim cut in wire EDM. The drawback of wire EDM process is the much lower feed rate, 1.5 mm/s. It is much slower than the 7.2 mm/s or 20% of maximum feed rate.

1.3 Future work

Experiments of AWJ of rotating Ti workpiece to generate cylindrical shape have been conducted. This feasibility of this concept has been demonstrated. Parts are currently under examination and results will be presented in the next quarterly report.

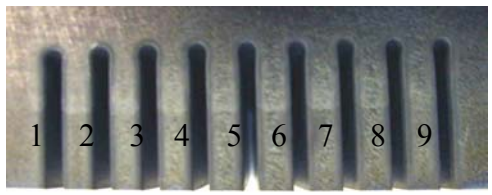

(a) Top view

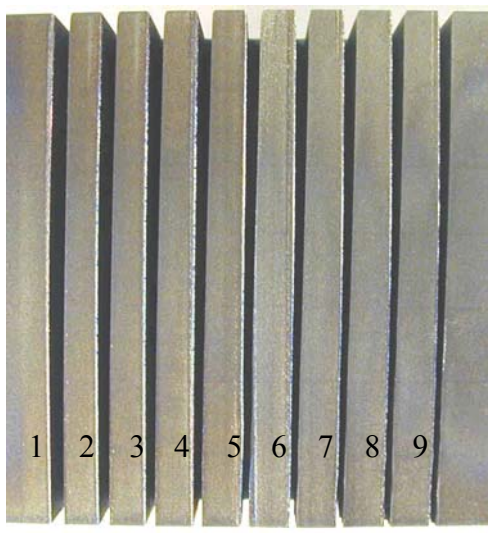

(b) Front view

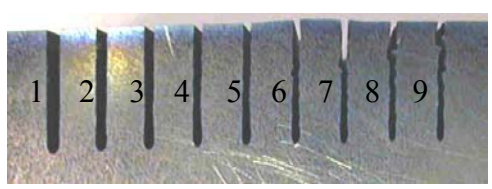

(c) Bottom view

Fig. 1. Waterjet machining of Ti-6Al-4V at nine feed rates (1: 20%, 7.2 mm/s; 2: 30%, 10.8 mm/s; 3. 40%, 14.4 mm/s; 4. 50%, 18 mm/s; 5. 60%, 21.6 mm/s; 6. 70%, 25.2 mm/s; 7. 80%, 28.8 mm/s; 8. 90%, 32.5 mm/s; and 9. 100%, 36 mm/s).

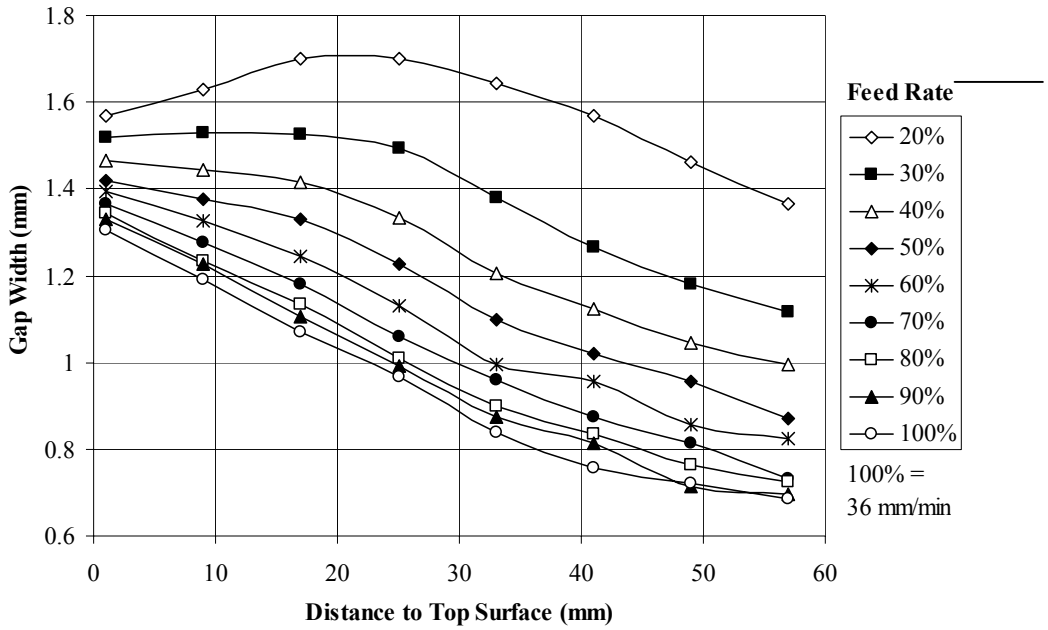

Fig. 2. Gap width at different feed rates and cutting depths in AWJ machining.

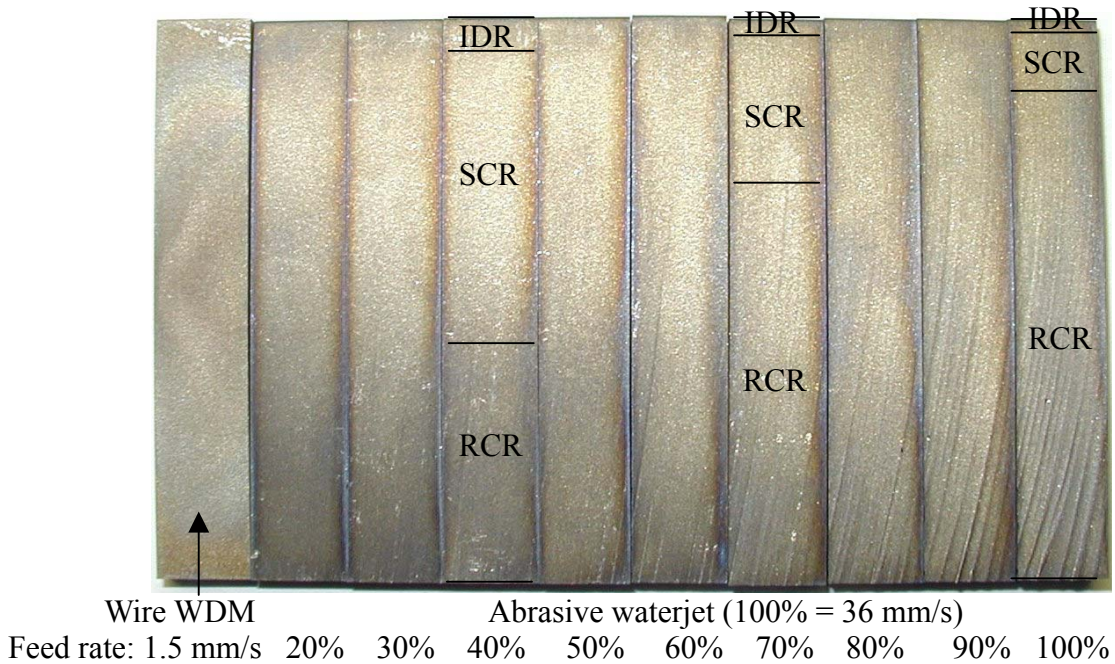

Fig. 3. Surfaces machined by AWJ and wire EDM.

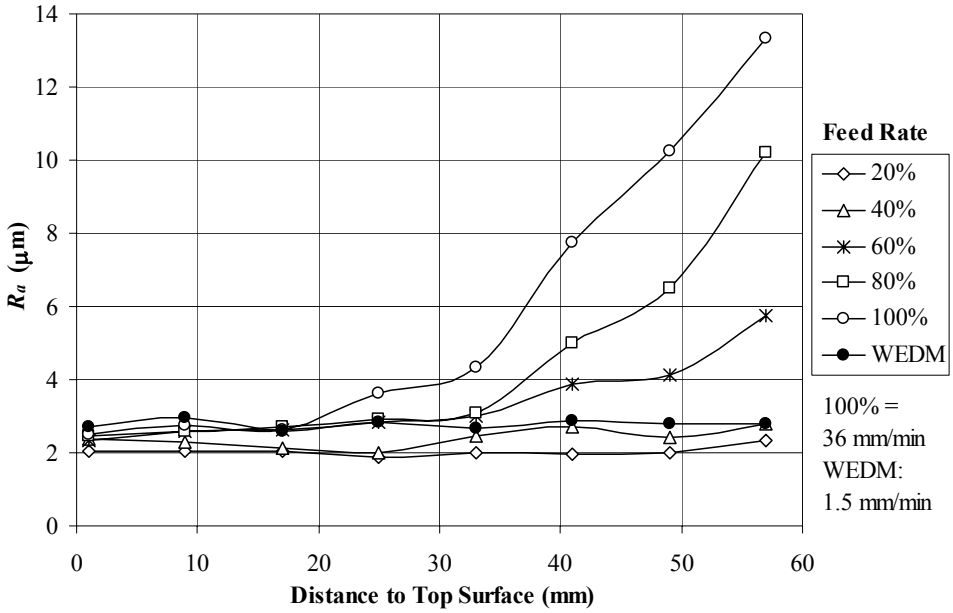

(a)

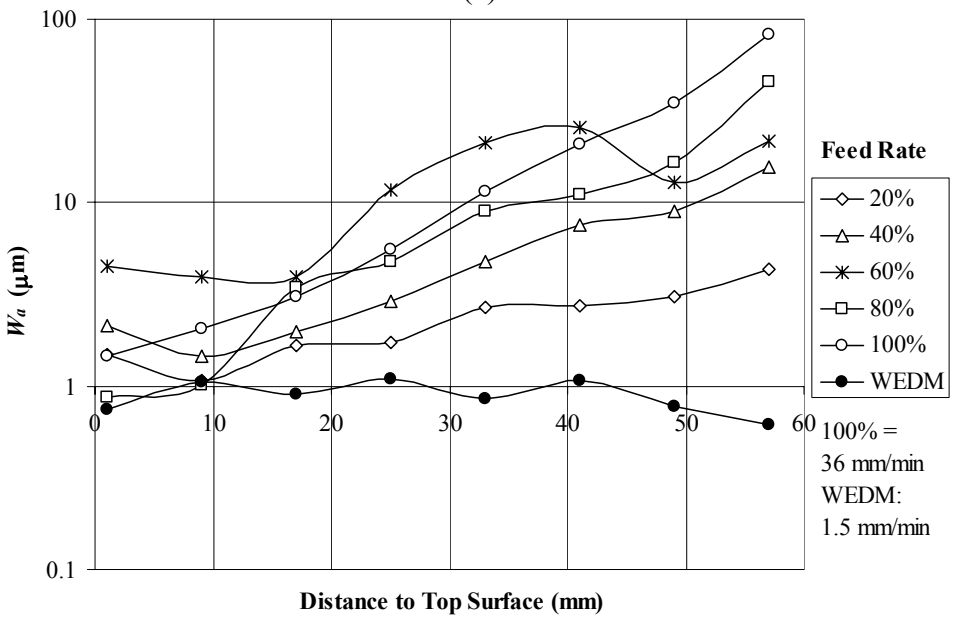

(b)

Fig. 4. Surface roughness and waviness of AWJ and wire EDM.

2. Temperature Measurement in Diesel Engine Exhaust Aftertreatment Filters

As mentioned in the last quarterly report, during regeneration, the temperature in diesel engine exhaust aftertreatment filters varies from 673 to 1073 K. This temperature is much lower than the 3000 K observed in SiC grinding of zirconia. As shown in Fig. 5, the peak of radiation spectrum has moved away from the 0.75 to 0.95 μm near-infrared region at 3000 K to the 3 to 5 μm mid-infrared region for radiation at 673 to 1073 K. The Si-based Ocean Optics USB2000 infrared spectrometer used to measure the temperature in SiC grinding of zirconia is unable to acquire strong enough signal in the 3 to 5 μm region. A market survey of suitable infrared

sensors for temperature measurement has been conducted. A PbS and PbSe two-color infrared sensor is selected in this study. A single crystal sapphire optical fiber is used to harness the infrared signal from the filter to the sensor. The proposed temperature measurement system for the diesel engine exhaust aftertreatment filters is presented.

2.1 Description of Proposed Temperature Measurement System

The layout of the temperature measurement system is shown in Figure 6. It consists of five components: 1. two-color infrared detector, 2. sapphire optical fiber, 3. microwave oven (for heating), 4. ceramic filter, and 5. data acquisition and signal processing unit.

2.1.1 Two-Color Infrared Detector

A survey of more than 20 infrared detector manufacturers resulted in the selection of the two-color near-infrared detector made by Electro-Optical Systems Inc. (EOS) at Phoenixville, PA. The performance and cost are two selection criteria. The detector [3] consists of two sandwiched Lead Sulfur (PbS) and Lead Selenium (PbSe) photoconductors, both 2 mm diameter. As shown in Figs. 6 and 7, the front PbS and back PbSe photoconductor receive infrared radiation in the 1.0 to 3.2 μm and 1.0 to 4.7 μm wavelength range, respectively. The front PbS acts as a long wave pass spectral filter for the back PbSe. The detector is housed in a thermal electric cooled dewar. The detector temperature is maintained at 243 K to enhance the detectability and stability. A dual gain amplifier is used to condition two signals from sensors to two DC voltage outputs.

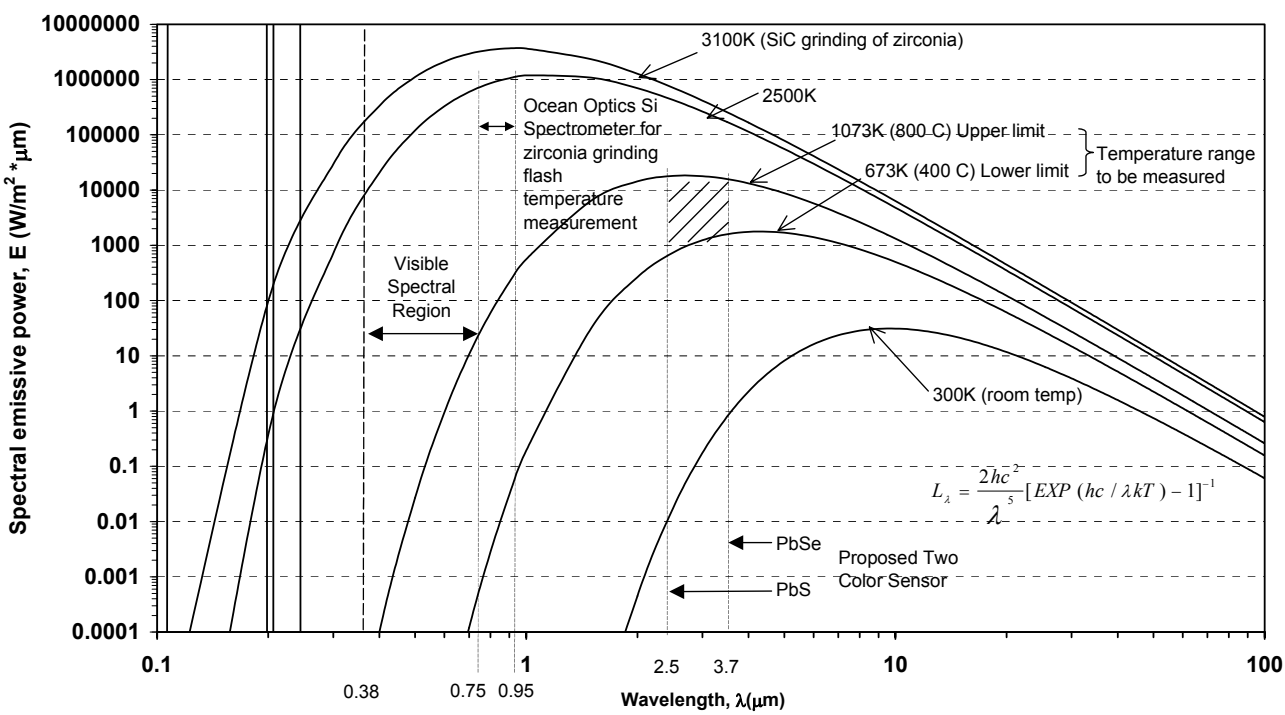

Fig. 5. Spectral blackbody emissive power.

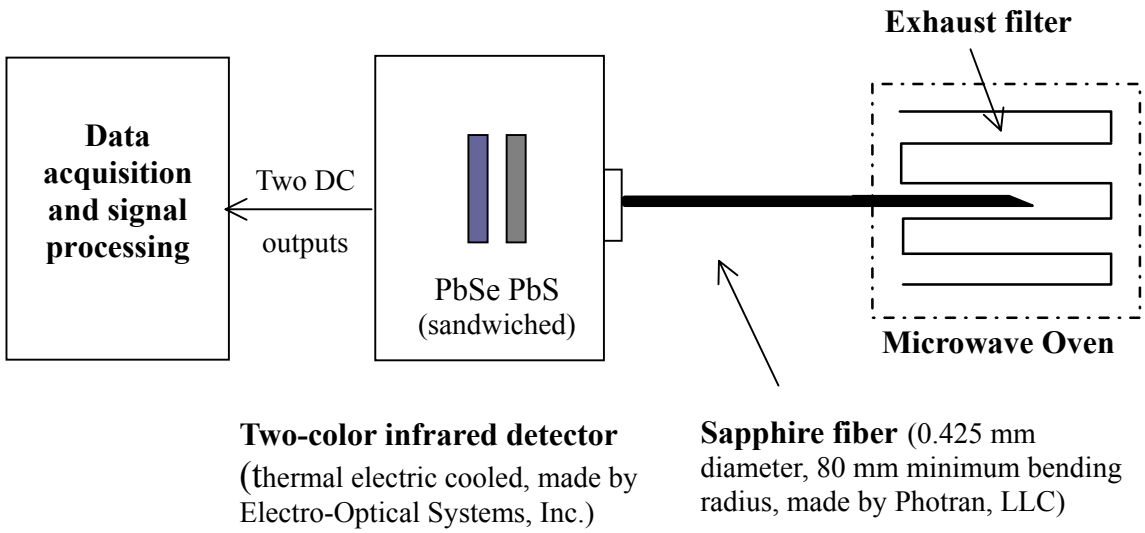

(a)

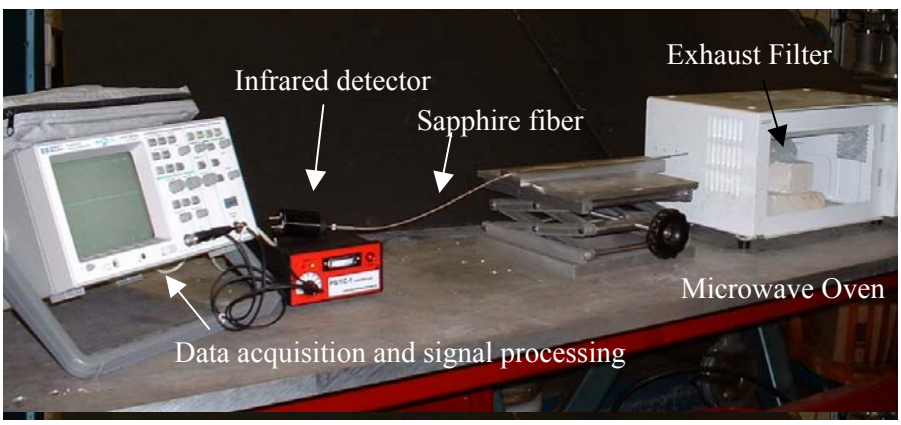

(b)

(c) (d)

Fig. 6. (a) System schematic drawing (b) temperature measurement setup (c) infrared detector and thermal electric cooling controller (d) filter in microwave oven with fiber.

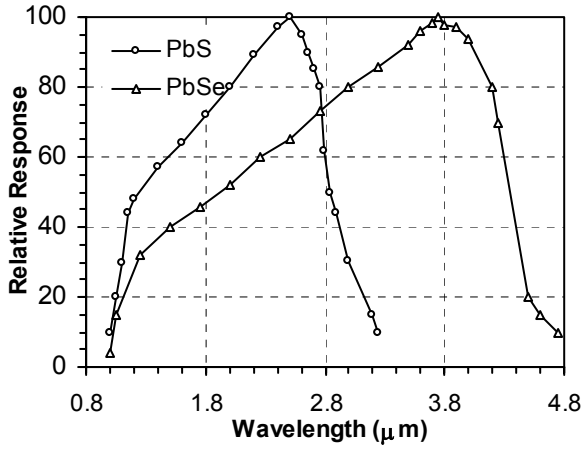

Fig. 7. PbS/PbSe spectral response [3]

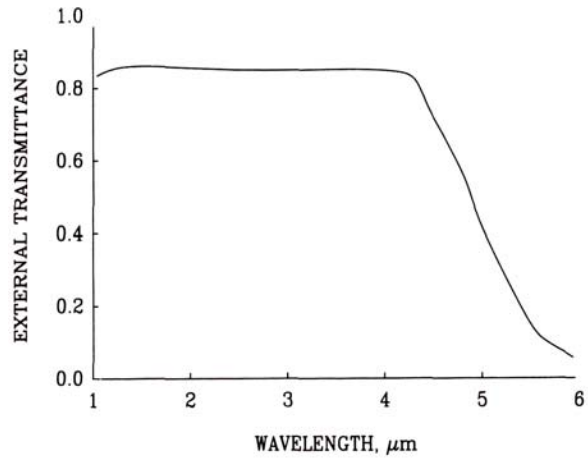

Fig. 8. Sapphire infrared transmittance [5]

2.1.2 Sapphire Optical Fiber

The optical fiber, manufactured by Photran LLC at Amherst, NH, is made of single crystal sapphire [4]. The sapphire material can withstand high temperature (over 2300 K) and does not interfere with the microwave during regeneration. This has made the real-time, in-situ temperature measurement during filter regeneration possible. As shown in Fig. 8 [5], the sapphire also has high transmission in the 1 to 4.7 μm wavelength range for the two-color detector. It has superior stiffness, 345 GPa at room temperature, for minimal flexural deflection. The sapphire fiber used in this study is 0.425 mm in diameter and 1 m long. It has a 0.66 m long stainless steel flexible armoring from the SMA coupling proximal end.

Fig. 9. The filter heated by microwave

2.1.3 The Ceramic Filter

Two ceramic filters made by Industrial Ceramic Solutions of Oak Ridge, TN, and Fleetguard of Cooksville, TN, are used in this study. Both filters contain either the SiC fiber or infiltrated SiC particles. SiC reacts promptly and efficiently under microwave to generate heat. Figure 9 shows a ceramic filter heated using the microwave. The difference in color indicates the non-uniformity of temperature distribution during the microwave heating. The goal of this study is to quantify the local temperatures in the microwave-heated filter and be able to map the temperature distribution to compare to the modeling results.

2.1.4 The Microwave Heater

A household microwave oven was modified to heat the ceramic filter and to adopt the insertion of sapphire fiber for temperature measurement. As shown in Fig. 10(a), several 2.8 mm diameter holes were drilled on the outside wall of the microwave oven. The 0.425 mm diameter fiber passed through the outer wall (Fig. 10 (a)) and a ventilation hole of the inner wall (Fig. 10 (b)) of the microwave oven into one of the cavities in the filter (Fig. 6(d)). A 2.8 mm OD and 2.1 mm ID metal tube was used as a support. A lab jack and a V-shaped groove were also used to support the thin fiber.

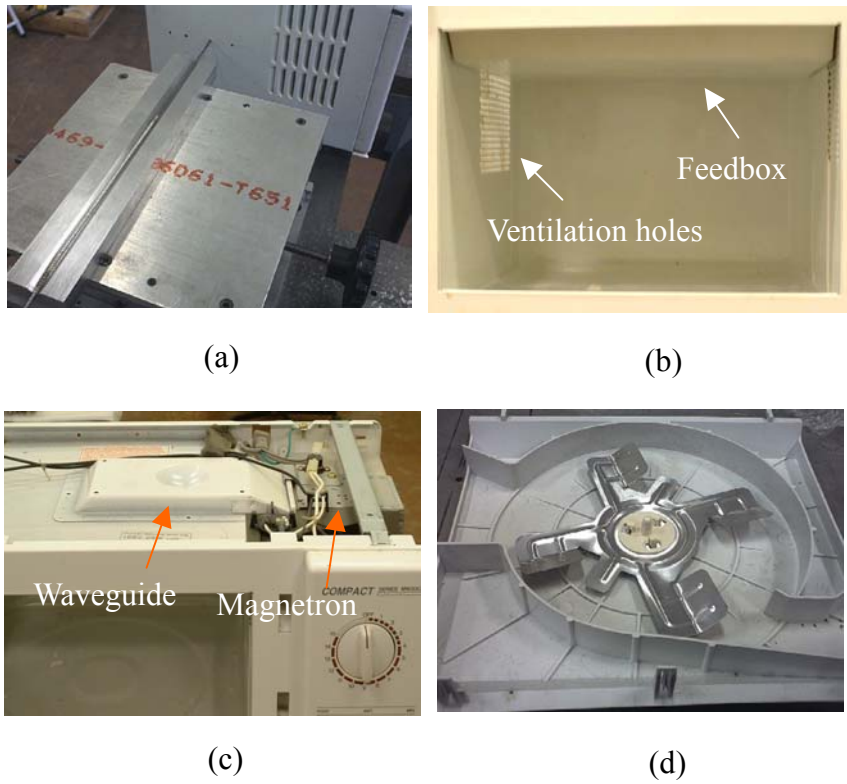

Fig. 10. (a) Holes for fiber insertion. (b) Magnetron and waveguide. (c) Ventilation holes and feedbox. (d) Feedbox and stirrer.

As shown in Fig. 10(c), the microwave energy is generated by a magnetron. The microwave travels through a waveguide (Fig. 10(c)) to a plastic feedbox (Fig. 10(b)), which is located on the top of the chamber in the oven. The microwave inside the feedbox is mixed by a rotating stirrer with four metal blades in the feedbox (Fig. 10 (d)) and transmitted through the plastic plate in the bottom of the feedbox into the top of chamber.

2.1.5 Data Acquisition and Signal Processing

A HP 54645A digital oscilloscope is used to acquire the two DC signals from two-color detector. The Matlab software will be used for signal processing.

2.2. Technical Challenges

Several technical challenges are expected during the development of such temperature measurement method:

- It is hard to observe the local area temperature variation with the fiber piercing through and parallel to the filter cavity wall as shown in Fig. 6(d). In order to collect the local area infrared signal, it is under consideration that either bending the fiber tip or designing some tip attachment to narrow the incident light in smaller area.

- When going through the narrow filter cavities, the fiber is often touched on the hot filter surface. In this case, the parasitic radiation could enter the fiber via its side wall and may be scattered at crystal defects or refracted at surface imperfections at an angle where the fiber transmits light to the detector. This effect is expected to be much larger for the thin flexible optical fiber thermometry, because the defect rate of the flexible fiber increases with a decreasing diameter. The influence of the scattered light is therefore of great interest since it might lead to a reduction of the local resolution or a falsification of the "true" temperature signal [6].

Status of Milestones

Milestone 1: Develop process technology to achieve high material removal rate in cylindrical WEDM of advanced engineering materials.

Status: Two journal and two conference papers have been published or accepted on this research.

Milestone 2: Determine the level of form tolerances and surface finish achievable by the cylindrical WEDM.

Status: Nothing to report. The surface finish was as low as 0.68 μm Ra, comparable to rough grinding, for the carbide materials.

Milestone 3: Prototype needles, armature pins, and plungers for diesel engine fuel injectors.

Status: Several prototype diesel injector plungers were manufactured. Exploratory experiments to machine miniature shafts in the size under 0.1 mm diameter were conducted.

Milestone 4: Develop mathematical models for material removal rate and surface finish of the cylindrical WEDM.

Status: Noting to report. The mathematical models for material removal rate and surface finish have been derived. These results have been summarized in a technical paper.

Milestone 5: Characteristics of the recast layer after WEDM and cylindrical WEDM and the surface condition after abrasive blasting.

Status: The recast layer was removed by micro abrasive blasting. The surface finish has been improved by 40%~60%.

Milestone 6: Development of optical fiber based temperature measurement method, with applications for grinding process and diesel exhaust aftertreatment filters.

Status: A system for infrared-based temperature measurement of diesel exhaust aftertreatment filters was designed. The system setup is undergoing and some initial experiments can be expected in the next quarter.

Communications/Visit/Travel

- Albert Shih, Jun Qu and John Kong visited Cummins Engine Company and Oak Ridge National Lab on Oct. 15 – 16, 2001
- Jun Qu and William Clark visited Oak Ridge National Lab on Nov. 12 – 14, 2001.
- Jun Qu visited Oak Ridge National Lab. on Nov. 26 – 27, 2001.
- Albert Shih and Scott Miller visited Porvair and Oak Ridge National Lab on Dec. 19 – 20, 2001.

Publications

1. Qu, J., Shih, A.J., and Scattergood, R., 2001, "Development of the Cylindrical Wire Electrical Discharge Machining Process," *Symposium on Nontraditional Manufacturing Research and Applications*, *Proceedings of 2001 ASME International Mechanical Engineering Congress and Exposition*, Vol. 3, Nov. 11-16, New York.
2. Qu, J., Shih, A. J., Scattergood, R. and McSpadden, S. B., 2001, "Cylindrical Wire Electrical Discharge Machining Process Development," *Proceedings of the ASPE 2001 Annual Meeting*, Vol. 25, Nov. 10-15, pp. 501-504.

References

[1] Kovacevic, R., Hashish, M, Mohan, R., Kim, T.J., and Geksin, E.S., 1997, "State of the Art of Research and Development in Abrasive Waterjet Machining," Journal of Manufacturing Science and Engineering, Vol. 119, pp. 776-785.

[2] Arola, D. and Ramulu, M., 1997, "Material Removal in Abrasive Waterjet Machining of Metals Surface Integrity and Texture," *Wear*, Vol. 210, pp. 50-58.

[3] *Electro-Optical Systems, Inc*., Phoenixville, PA.

[4] *Photran, LLC*., Amherst, NH.

[5] Klocek, P., 1991, *Handbook of Infrared Optical Material*, Marcel Dekker, New York, 1991, pp. 198.

[6] Stenzel, C., Vavoulidis, G., 2000, "Application of flexible sapphire fibers as temperature control sensors in high-temperature multi-zone furnaces," in *Applications of Optical Fiber Sensors, Alan J. Rogers, Editor, Proceedings of SPIE,* Vol. 4074, 2000, pp. 202–213.

[7] Qu, J., Shih, A.J., and Scattergood, R., "Development of the Cylindrical Wire Electrical Discharge Machining Process, Part II: Surface Integrity and Roundness," *ASME Journal of Manufacturing Science and Engineering* (Accepted).

NDE Development for Ceramic Valves for Diesel Engines

J. G. Sun, W. A. Ellingson,
Argonne National Laboratory

and M. J. Andrews
Caterpillar, Inc.

Objective/Scope

Emission reduction in diesel engines designated to burn fuels from several sources has lead to the need to assess ceramic valves to reduce corrosion and emission. The objective of this work is to evaluate several nondestructive evaluation (NDE) methods to detect defect/damage in structural ceramic valves for diesel engines. One primary NDE method to be addressed is elastic optical scattering. The end target is to demonstrate that NDE data can be correlated to material damage as well as used to predict material microstructural and mechanical properties. There are three tasks to be carried out: (1) Characterize subsurface defects and machining damage in flexure-bar specimens of NT551 and SN235 silicon nitrides to be used as valve materials. Laser-scattering studies will be conducted at various wavelengths using a He-Ne laser and a tunable-wavelength solid-state laser to optimize detection sensitivity. NDE studies will be coupled with examination of surface/subsurface microstructure and fracture surface to determine defect/damage depth and fracture origin. NDE data will also be correlated with mechanical properties. (2) Assess and evaluate subsurface damage in ceramic valves to be run in bench test and in a single-cylinder-engine test. All valves will be examined at ANL prior to test, during periodic scheduled shut downs, and at the end of the planned test runs. (3) Evaluate healing of subsurface damage by laser glazing on machined surfaces of GS44 ceramics. ANL will perform laser-scattering characterization on machining surfaces at before and after glazing treatment. NDE data will be correlated with glazing parameters and mechanical properties.

Technical Highlights

Work during this period (October-December 2001) focused on preparing step-wedge samples for optical transmission property measurement of new Si_3N_4 ceramics and on developing laser scatter system for valve scans.

1. Elastic Optical Scattering NDE for Machining Damage

During this period we received from Caterpillar Inc. three flexure-bar specimens in each of GS44, SN235P, NT551, and L-M C99091-3 Si_3N_4 ceramics. These specimens are used to make step-wedge samples for measuring their optical transmission properties at various wavelengths. This property is essential when selecting an optimum optical wavelength for each ceramic in laser scatter test that is most sensitive to the defects within the transmission depth of interest. Figure 1 is a photograph of these flexure-bar specimens (exclude GS44 specimens). To determine if there is pre-existing defect, they were scanned within the middle 20-mm section on both front and back surfaces at wavelength 633 nm. Figures 2a-c show the laser scatter sum images for the front surfaces of SN235P, L-M C99091-3, and NT551 specimens, respectively. The scatter images for the SN235P and L-M C99091-3 specimens appear normal, with observable subsurface material variations and some surface markings. However, the scatter image for NT551 specimens shows some interesting features: a dark band at all edges and some

brighter (high scattering) features near the edges. The cause for these features is not clear at present.

Step-wedge specimens were machined for the SN235P, L-M C99091-3, and NT551 Si_3N_4 ceramics. Figure 3 shows the machining diagram and Fig. 4 is a photograph of the step-wedge specimens. It is apparent that the thickness at each step is not uniform, especially within the thin steps. Tests are underway to measure the thickness and transmission property of these specimens.

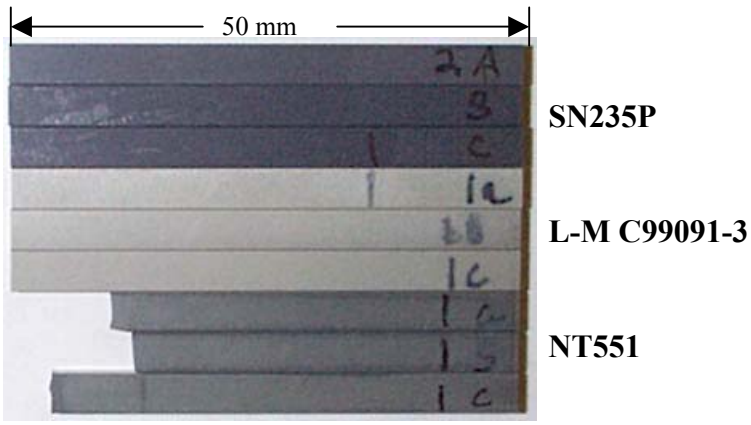

Fig. 1. Photograph of SN235P, L-M C99091-3, and NT551 flexure-bar specimens.

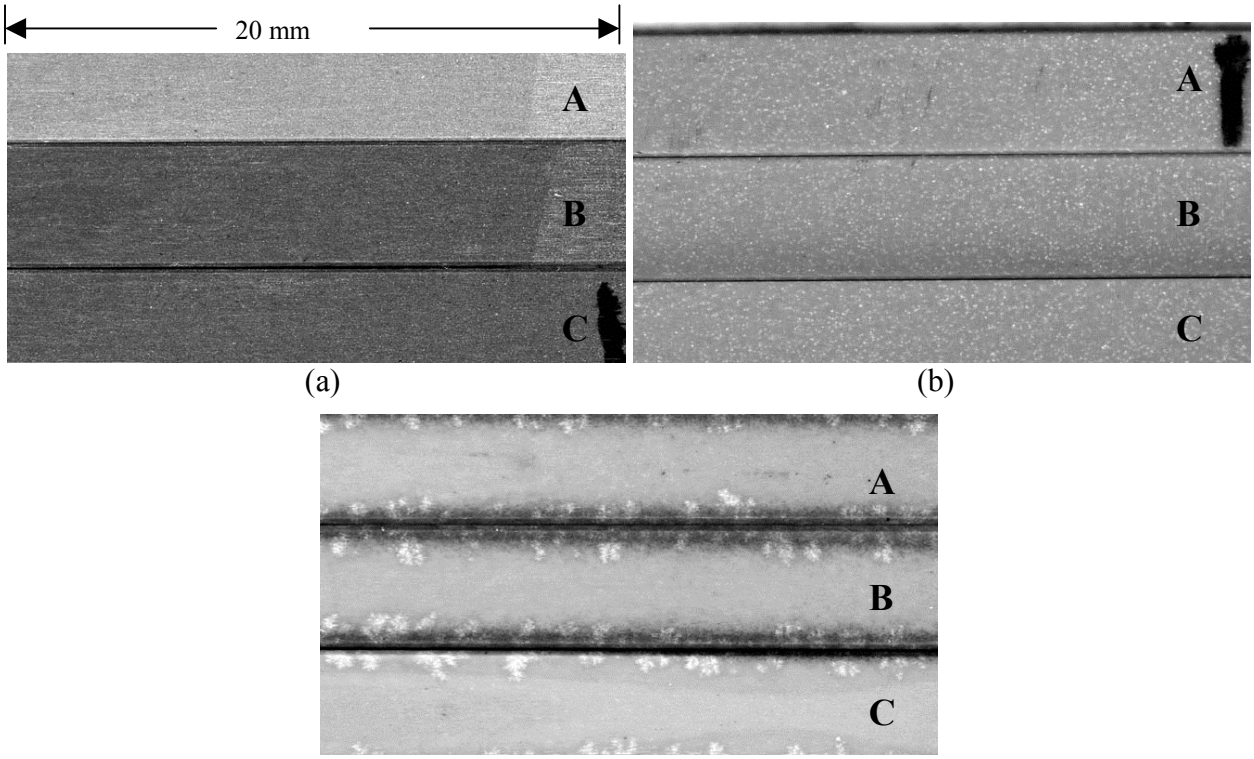

Fig. 2. Laser-scattering sum images on front surfaces of (a) SN235P, (b) L-M C99091-3, and (c) NT551 Si_3N_4 flexure-bar specimens.

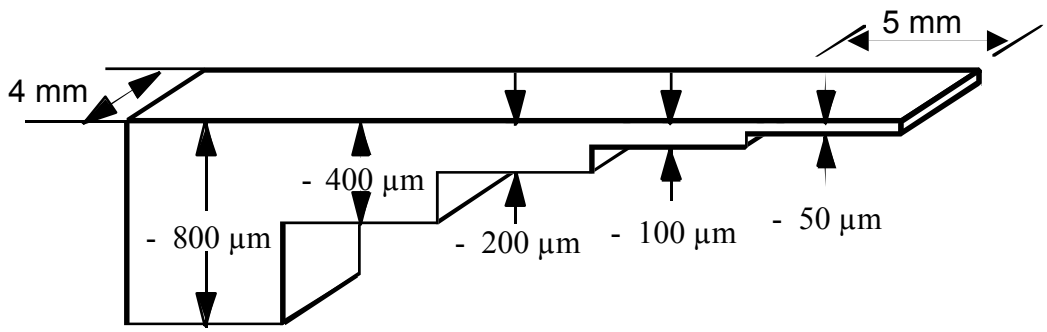

Fig. 3 Step-wedge diagram for determining optical tramsnission propterties of Si_3N_4 ceramics.

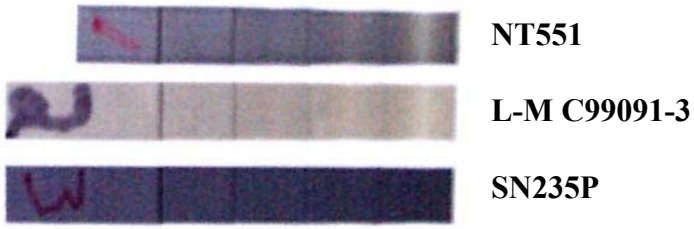

Fig. 4 Photograph of step-wedge specimens of NT551, L-M C99091-3, and SN235P ceramics.

2. Laser-Scattering System Development for Si_3N_4 Valves

During this period we received a NT551 valve from Caterpillar Inc. Figure 5 is a photograph of the valve. Work is being conducted to configur the laser scattering system so an entire valve can be tested in one scan. The hardware modification includes to deliver the laser light by a fiber optics and set the detetor train on stages that can follow the contour of the valve. The fiber optics has been purchased in this period. The sofeware is accordingly being modified.

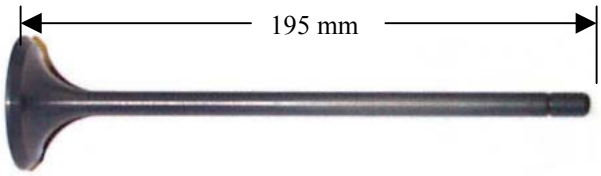

Fig 5. Photograph of a NT551 valve.

Status of Milestones

Current ANL milestones are on or ahead of schedule.

Communications/Visits/Travel

None this period.

Problems Encountered

None this period.

Publications

An abstract entitled "Laser Scattering Detection of Subsurface Defects as Fracture Origins in Silicon-Nitride Ceramics" was submitted for a presentation at the American Ceramic Society 104th Annual Meeting & Exposition in St. Louis, MO, April 28-May 1, 2002.

Processing and Characterization of Structural and Functional Materials for Heavy Vehicle Applications

J. Sankar, Z. Xu, and S. Yarmolenko
North Carolina A & T State University

Objective/Scope

Continue to investigate the combustion chemical vapor deposition technique of fully stabilized zirconia (YSZ) thin films for solid oxide fuel cells.

Task

Investigate the effects of controlling parameters on the growth of the YSZ thin films.

Technical Highlights

The properties and applications of zirconia vary with its forms of phases. In its partially stabilized form, it is a very good high-temperature structural material, owing to its good strength, toughness and superior resistance to wear. It has been widely used in tribological applications. In its fully stabilized form (cubic phase), on the other hand, it has high oxygen-ion conductivity over a wide range of temperature and oxygen pressure. It is the first material that was demonstrated as an effective electrolyte in solid oxide fuel cells (SOFCs), as well as oxygen sensors for combustion control. Yttria stabilized zirconia (YSZ) is one of the successful solution to obtain fully stabilized cubic phase. Moreover, to minimize the electrical path of fuel cell, thin film (less than 40 μm) of the electrolyte is preferred. It is very hard to produce such a dense thin film using the present industrial techniques such as screen printing, tape casting, slurry spray, etc. On the other hand, the chemical vapor deposition (CVD) technique can provide thin film coating with very high density.

Combustion chemical vapor deposition (CCVD) has some overwhelming advantages such as, but not limited to, low setup, minimal running cost and conformal coatings on irregular or large objects over other CVD techniques. We have developed a CCVD system in our center and at present investigations on the main controlling parameters of the coating processing are being carried out. The quality of the deposited samples was characterized with scanning microscopy and X-ray diffraction.

Results and Discussion

As stated in the previous report, a liquid fuel CCVD system has been developed. Zirconium 2-ethylhexanoate (2-ETH) and yttrium 2-ethylhexanoate (2-ETH) was used as reagents. They were dissolved in toluene. Thin films are deposited on Si(100) and Mgo(100) substrates.

The main controlling parameters of the CCVD thin film processing investigated are mixing ratio of the oxidant (i.e. oxygen) to the fuel (toluene solutions) and substrate temperature. The effects of these parameters on the films are briefly reported below.

Effect of the mixing ratio of oxygen to fuel

The mixing ratio of oxygen to liquid fuel determines the oxidation condition of the aerosol flame. Different ratio results in different temperature distribution along the axis of the flame.

Temperature profiles of flames at different mixing ratios, as shown in Fig. 1, were measured with an infrared thermometer. Generally, the higher mixing ratio results in higher maximum temperature in the flame and lower temperature at the end of the flame. However, as can be seen from the graph, redundant oxygen will cool down the flame.

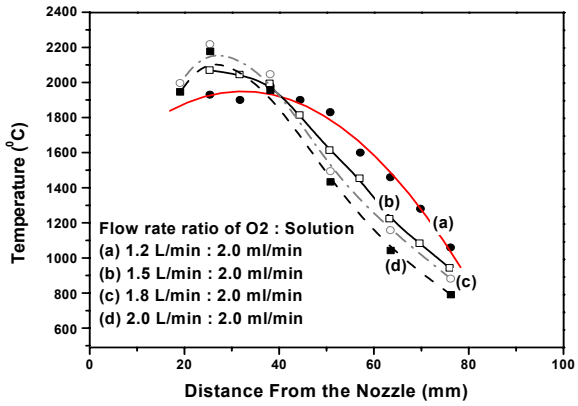

Figure 1. Temperature profiles of flames at different ratios of oxygen to liquid fuel.

To confirm the effect of the amount of oxygen, the film deposition was performed at various oxygen to liquid fuel mixing ratios, while all the other parameters were kept unchanged. The SEM images, as shown in Fig. 2, were taken from the as-grown samples. The pictures manifest that with a higher mixing ratio of oxygen to liquid fuel, the crystallinity of the film is improved.

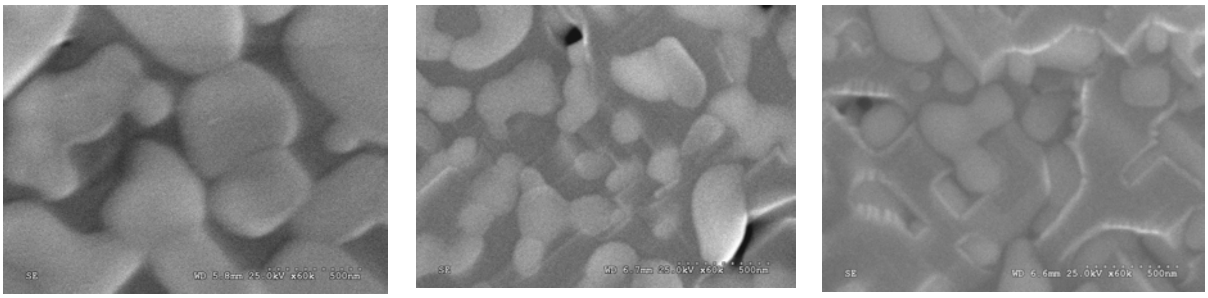

(a) (b) (c)

Figure 2. SEM images taken from the as-grown films deposited at the following conditions: substrate temperature, at about 1300^0C, nozzle-to-substrate distance, 75mm, solution concentration, $5x10^{-4}$ M, liquid fuel flow rate, 2 cm^3/min, and the flow rate of oxygen, (a) 1200 cm^3/min, (b) 1600 cm^3/min, (c) 2000 cm^3/min.

Effect of substrate temperature

The temperature of the substrate is another important factor that controls the film growth modes and its quality in chemical vapor deposition. It usually affects the absorption/desorption, the reactivity and diffusivity of adatoms or clusters on the substrate surface, and then to the quality of the films. The effect of the substrate temperature on the film's morphology is shown in Fig. 3.

At lower substrate temperatures, the films have grainy particles. Increasing of the substrate temperatures leads to films with better faceted crystals. Moreover, X-ray diffraction, as shown in Fig. 4, manifests that within the range of temperature employed in the experiments, higher substrate temperature deposition produces films with stronger characteristic peaks and faceted at one predominant orientation.

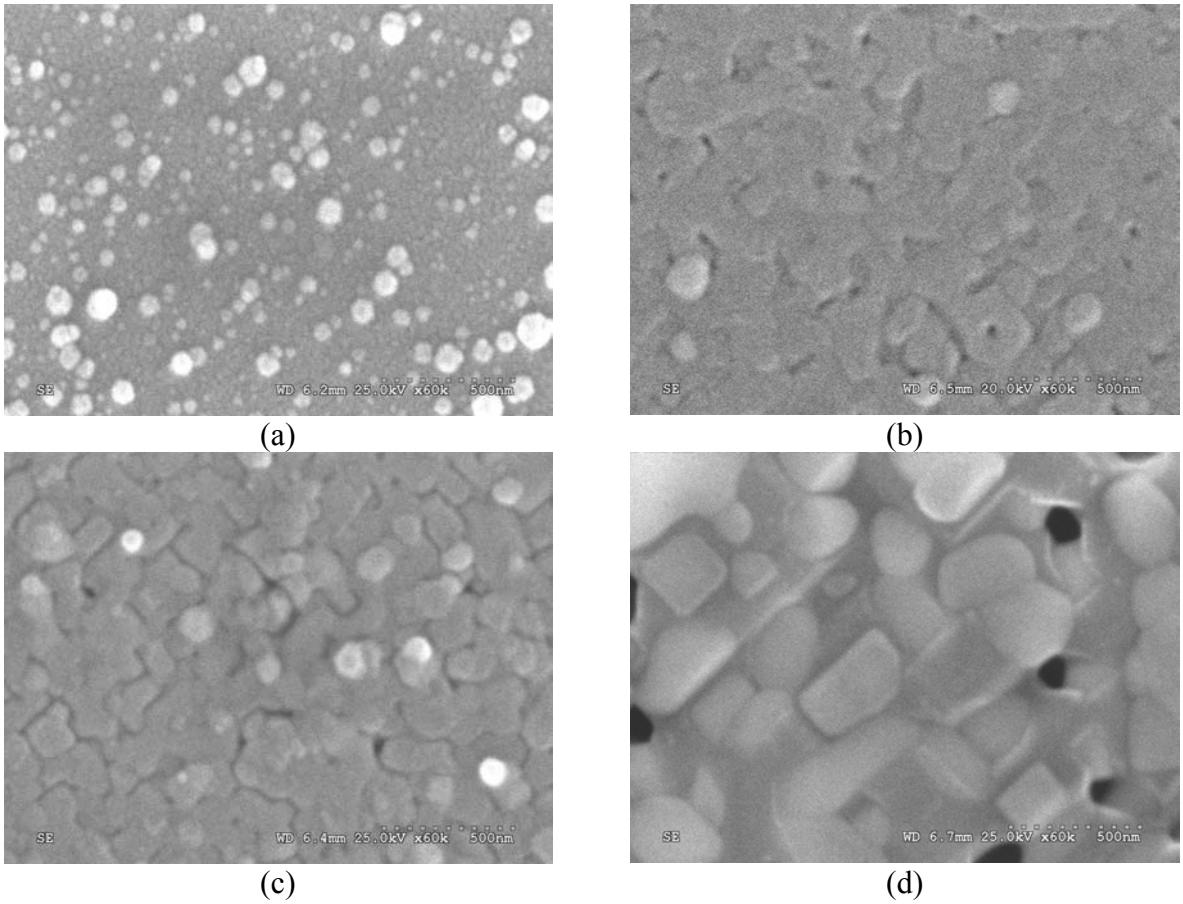

Figure 3. Morphology of films grown at different substrate temperatures. (a) 950^0C, (b) 1150^0C, (c) 1230^0C and (d) 1340^0C. Other parameters are as follows. O_2: solution = 1600: 2.0 cm^3/min, nozzle-to-substrate distance = 75 mm, total metal concentration in solution = 5×10^{-4} M, ratio of Y/Zr = 10 %.

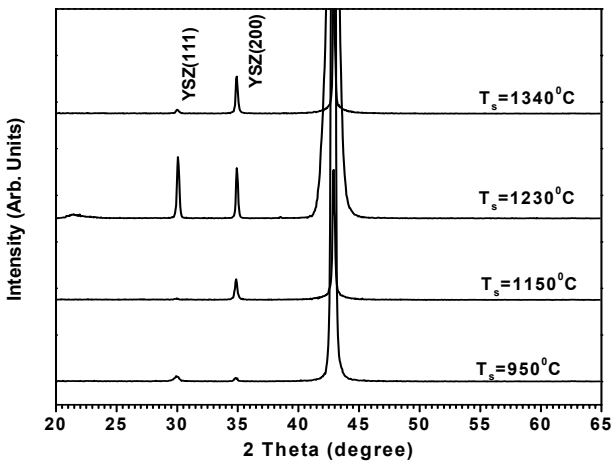

Figure 4. XRD of films grown at different substrate temperatures.

Status of Milestones

On Schedule

Communications/Visitors/Travel

None

Problems Encountered

None

Publications

1. "Preparation And Properties of YSZ Electrolyte Thin Films Via Liquid Fuel Combustion Chemical Vapor Deposition", to be published in Proceedings of The 26th Annual International Conference On Advanced Ceramics & composites, Jan. 18-18, 2002, Cocoa Beach, FL.
2."Combustion Chemical Vapor Deposition of YSZ Thin Films for Fuel Cell Applications," published in proceedings of ASME 2001 Congress, New York (Peer reviewed).

Life Prediction of Diesel Engine Components

H. T. Lin, T. P. Kirkland, M. K. Ferber
Oak Ridge National Laboratory
and
M. J. Andrews
Caterpillar, Inc.

Objective/Scope

The valid prediction of mechanical reliability and service life is a prerequisite for the successful implementation of structural ceramics as internal combustion engine components. There are three primary goals of this research project which contribute toward that implementation: the generation of mechanical engineering data from ambient to high temperatures of candidate structural ceramics; the microstructural characterization of failure phenomena in these ceramics and components fabricated from them; and the application and verification of probabilistic life prediction methods using diesel engine components as test cases. For all three stages, results are provided to both the material suppliers and component end-users.

The systematic study of candidate structural ceramics (primarily silicon nitride) for internal combustion engine components is undertaken as a function of temperature (< 900°C), environment, time, and machining conditions. Properties such as strength and fatigue will be characterized via flexure and rotary bend testing.

The second goal of the program is to characterize the evolution and role of damage mechanisms, and changes in microstructure linked to the ceramic's mechanical performance, at representative engine component service conditions. These will be examined using several analytical techniques including optical and scanning electron microscopy. Specifically, several microstructural aspects of failure will be characterized:

(1) strength-limiting flaw-type identification;
(2) edge, surface, and volume effects on strength and fatigue size-scaling
(3) changes in failure mechanism as a function of temperature;
(4) the nature of slow crack growth; and
(5) what role residual stresses may have in these processes.

Lastly, numerical probabilistic models (*i.e.*, life prediction codes) will be used in conjunction with the generated strength and fatigue data to predict the failure probability and reliability of complex-shaped components subjected to mechanical loading, such as a silicon nitride diesel engine valve. The predicted results will then be compared to actual component performance measured experimentally or from field service data. As a consequence of these efforts, the data generated in this program will not only provide a critically needed base for component utilization in internal combustion engines, but will also facilitate the maturation of candidate ceramic materials and a design algorithm for ceramic components subjected to mechanical loading in general.

Technical Highlights

Evaluation of mechanical properties of NGK SN84 silicon nitride bend bars after 1000 h exposure in an oil ash environment was completed during this reporting period. Mechanical testing was conducted in four-point-bending using 20mm/40mm, α-SiC, semi-articulating fixtures at 850°C at 0.003 MPa/s in air. Load was continuously measured as a function of time, and flexure strength was calculated using ASTM C1161. Results showed that the strength of SN84 silicon nitride after 1000 h oil ash exposure was comparable to the as-received material (746 MPa versus 761 MPa), as shown in Fig. 1 and Table 1. Also, it was noted that the exposed material exhibited a similar Weibull modulus (m = 11.07) to that obtained for the as-received material (m = 10.27). The obtained results suggest that the SN84 silicon nitride exhibits an excellent corrosion resistance to the simulated diesel engine environment. Note that no apparent effect of long-term oil ash exposure on the mechanical properties of both SN235 and GS44 silicon nitride materials was also observed and reported previously. Both optical and SEM analysis on fracture surface and polished cross section of selected SN84 bend bars will be carried out to understand the extent of inward diffusion of oil ash elements into the silicon nitride and/or secondary phase at grain boundary and triple grain junctions.

Dynamic fatigue tests on SN84 silicon nitride bend bars, which were transversely machined per ASTM C116 standard, were also initiated during this reporting period to provide an understanding on the effect of grinding orientation on the mechanical properties. Mechanical tests for transversely machined bend bars would be more representative of strength obtained for the ceramic valves, which would be transversely machined in the component production lines. Test results showed that transversely machined SN84 bend bars exhibited strength, which was ~ 13% lower than those obtained for bend bars longitudinally machined, as shown in Table 1 and Figs. 2-3. Similar strength difference between transversely and longitudinally machined specimens has also been previously reported for candidate silicon nitride materials evaluated under this subtask. Flexure strength versus stressing rates curve revealed a high fatigue exponent of SN84 silicon nitride at 20°C, indicative of no fatigue effect (Fig. 4). Tests at temperatures up to 1200°C will be carried out to elucidate the temperature-dependence on the characteristic mechanical strength, Weibull modulus, and fatigue exponents. The temperature limit at which the SCG and/creep process would initiate and govern the lifetime of candidate silicon nitride will be evaluated as well.

Status of Milestones

All milestones are on schedule.

Communications / Visitors / Travel

Dynamic fatigue results at 850°C of SN84 after 1000 h oil ash exposure were communicated with M. J. Andrews at Caterpillar.

Dynamic fatigue results of transversely machined SN84 bend bars at 20°C at 30 and 0.003 MPa/s were communicated with M. J. Andrews at Caterpillar.

Update of the status of initial bench test on Norton NT551 exhaust valves was held with M. J. Andrews at Caterpillar.

Communication with M. J. Andrews at Caterpillar on SN84 silicon nitride designed for use as a mechanical load pin for a thermal-mechanical test apparatus

Problems Encountered

None.

Publications

None.

References

[1] A. A. Wereszczak, M. J. Andrews, M. K. Ferber, and T. P. Kirkland, "Life Prediction Verification," *Heavy Vehicle Propulsion System Materials Program Semiannual Technical Progress Report to DOE Office of Transportation Technologies*, Apr. 1997 - Sep. 1997.

[2] A. A. Wereszczak, and T. P. Kirkland, M. J. Andrews, M. K. Ferber, and R. Tandonl, "Life Prediction of Ceramic Diesel Engine Components," *Heavy Vehicle Propulsion System Materials Program Semiannual Technical Progress Report to DOE Office of Transportation Technologies*, Oct. 1998 - Mar. 1999.

[3] H. T. Lin, T. P. Kirkland, M. K. Ferber, and M. J. Andrews, "Life Prediction of Diesel Engine Components," *Heavy Vehicle Propulsion System Materials Program Bimonthly Technical Progress Report to DOE Office of Transportation Technologies*, Apr. 2001 - June 2001.

Table 1. Summary of uncensored Weibull strength distributions for NGK SN84 (longitudinally and transversely machined) specimens per ASTM C1161.

Material	# of Spmns. Tested	Stressing Rate (MPa/s)	Temp. (°C)	Uncens. Weibull Modulus	± 95% Uncens. Weibull Modulus	Uncens. Chrctstic Strength (MPa)	± 95% Uncens. Chrctstic Strength (MPa)
SN84 (Long.)	20	30	20	10.59	7.06, 15.00	858	818, 898
SN84 (Long.)	20	0.003	20	9.61	6.52, 13.80	754	716, 792
SN84 (Tran.)	15	30	20	12.52	7.59, 18.24	758	723, 793
SN84 (Tran.)	15	0.003	20	10.10	6.67, 14.02	659	662, 697
SN84 (1000h oil ash exposure)*	15	0.003	850	11.07	6.71, 16.84	746	708, 786
SN84 (Long.)	15	0.003	850	10.27	6.51 15.06	761	718, 803

*Note that the 1000 h oil immersion test was carried out at 850°C in air.

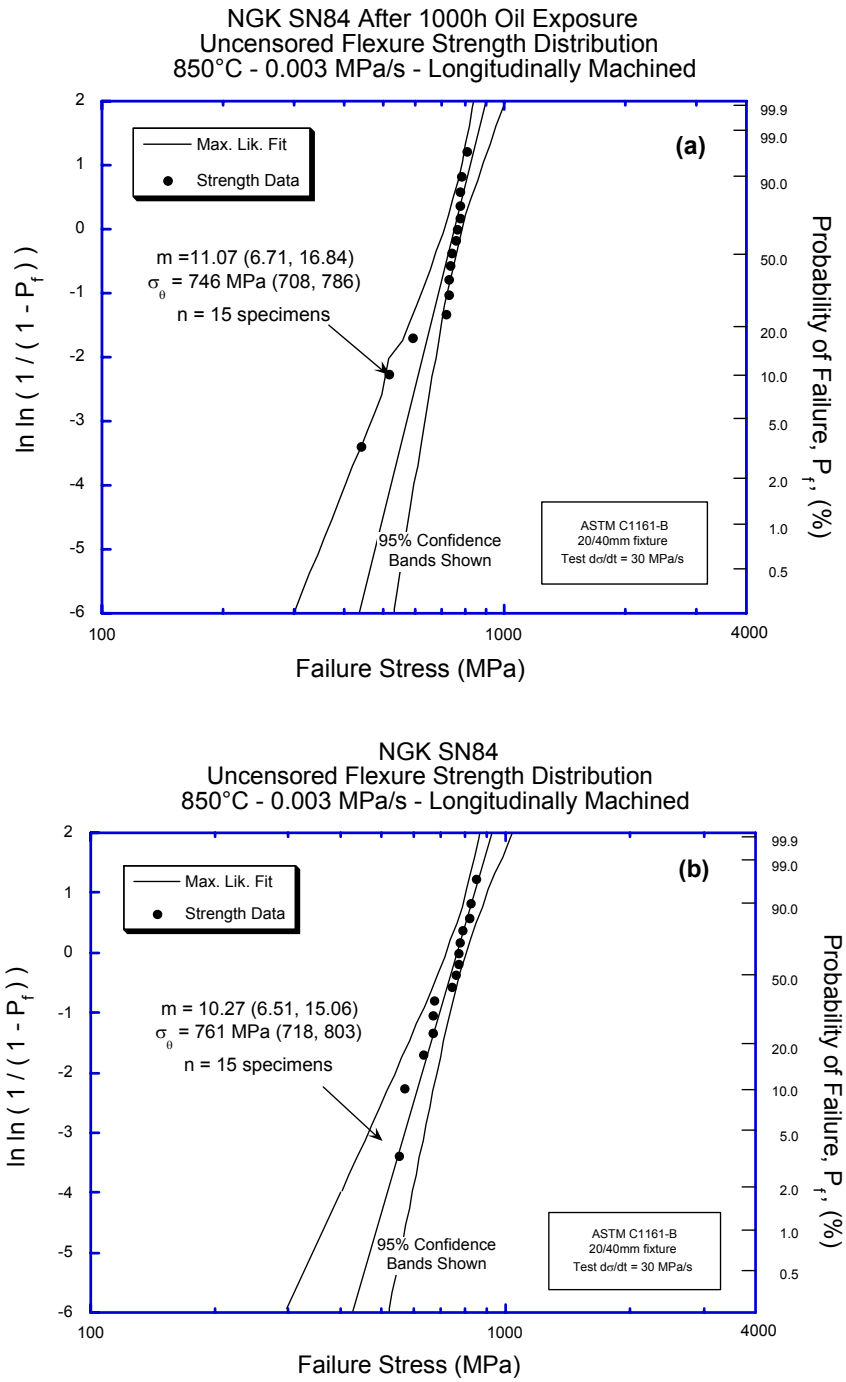

Figure 1. Characteristic strength of NGK SN84 silicon nitride tested at 850°C and 0.003 MPa/s after 1000h oil ash exposure (a) and in the as-received condition (b). Note that the dimension of bend bar has been scaled down to unit size in the analysis.

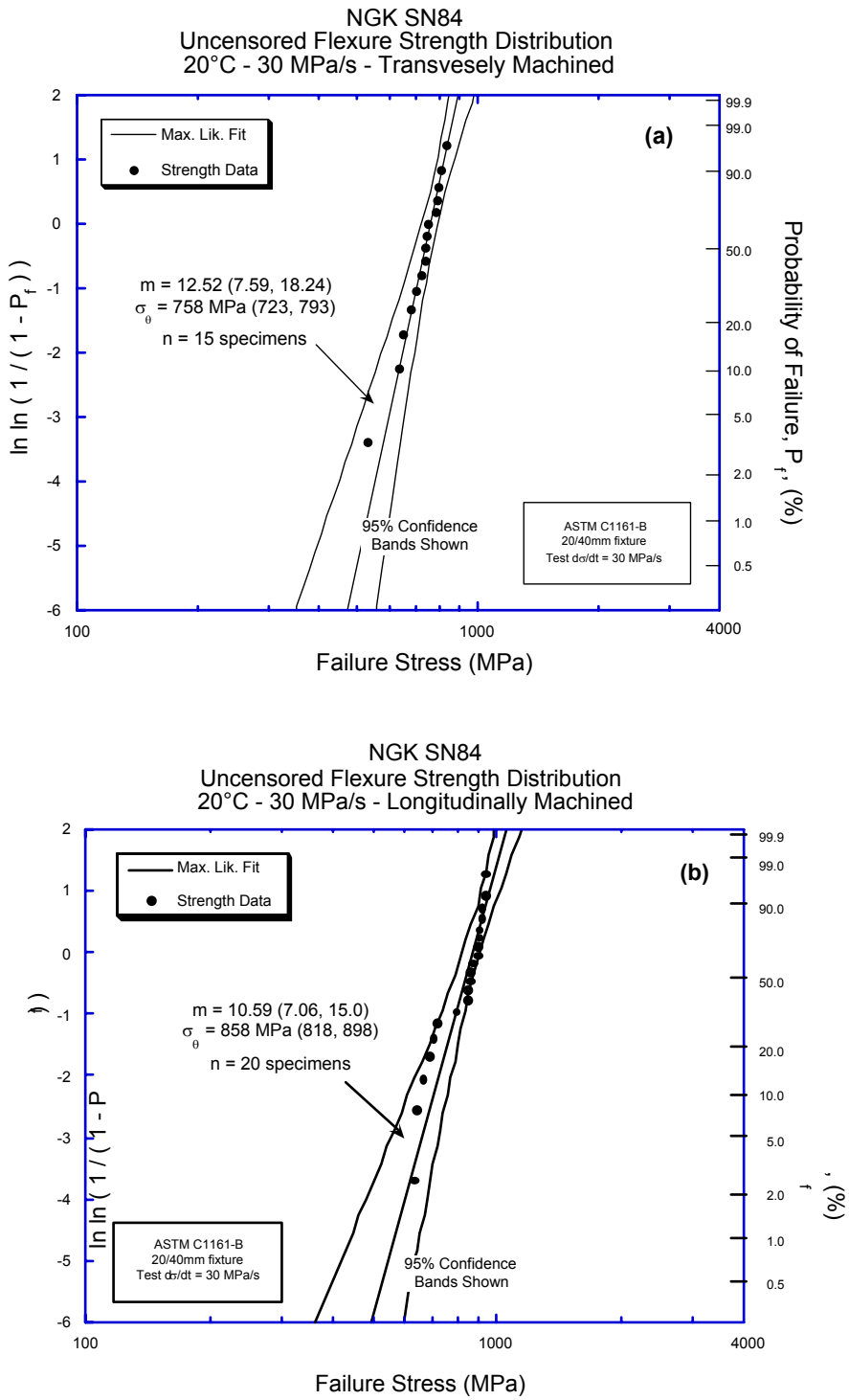

Figure 2. Characteristic strength of NGK SN84 silicon nitride machined transversely (a) and longitudinally (b) tested at 20°C and 30 MPa/s. Note that the dimension of bend bar has been scaled down to unit size in the analysis.

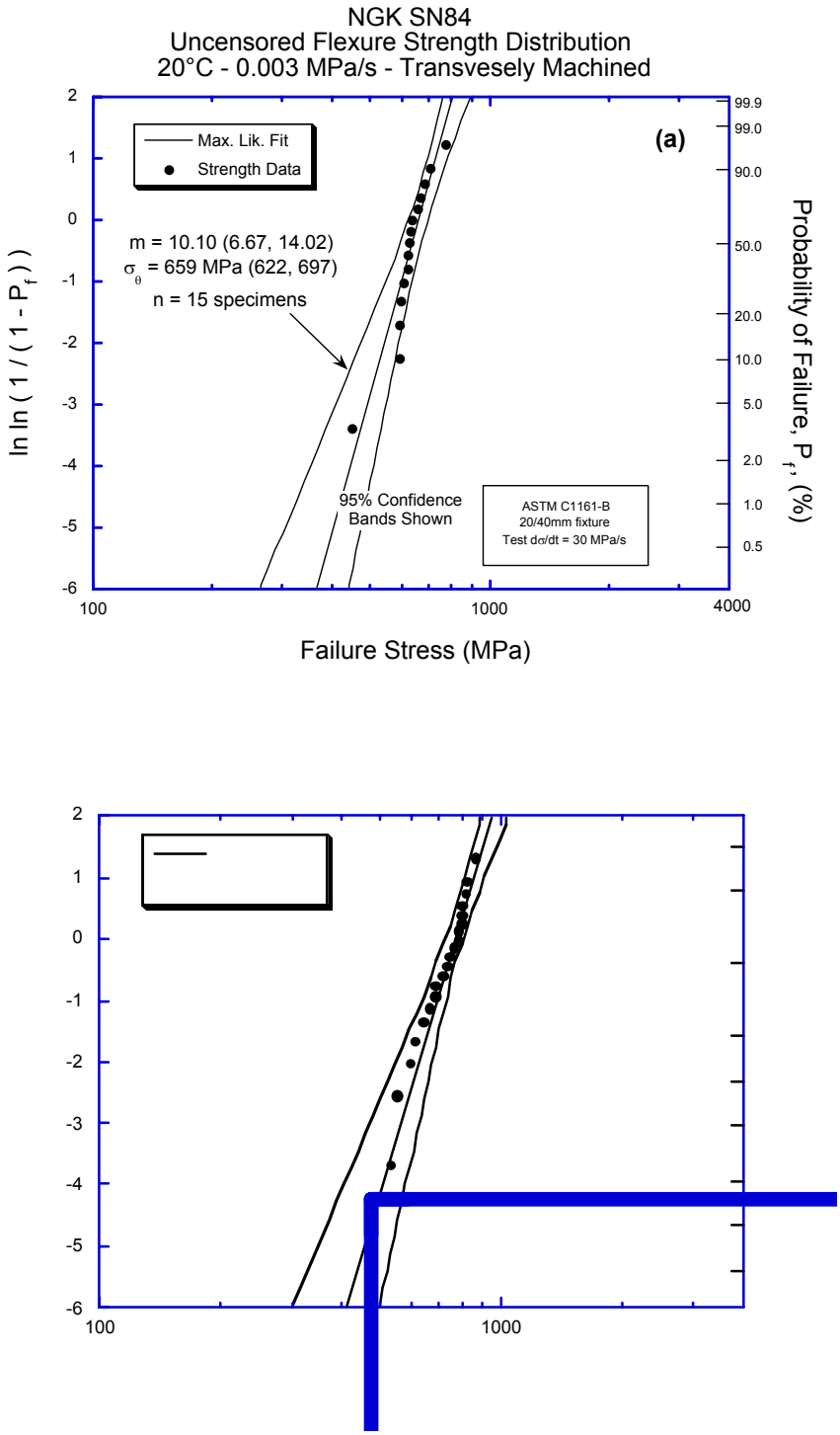

Figure 3. Characteristic strength of NGK SN84 silicon nitride machined transversely (a) and longitudinally (b) tested at 20°C and 0.003 MPa/s. Note that the dimension of bend bar has been scaled down to unit size in the analysis.

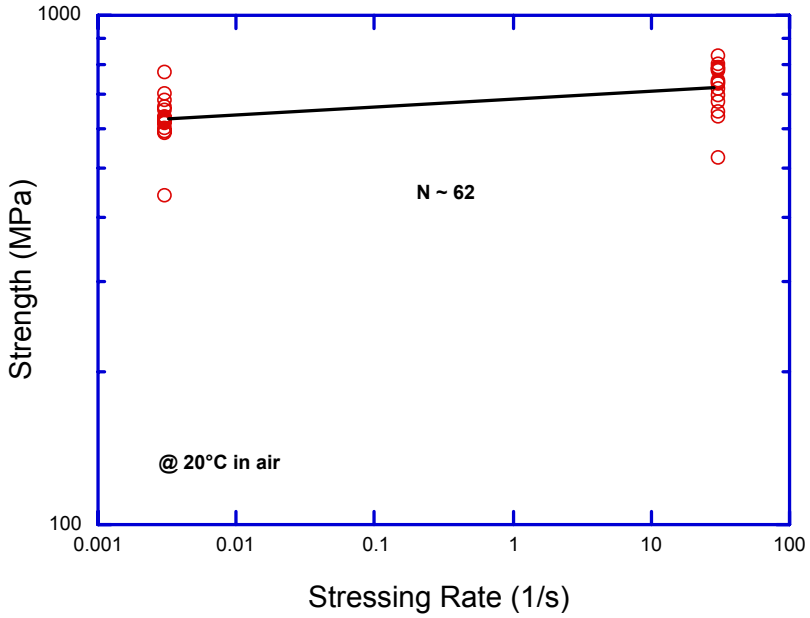

Figure 4. Fatigue exponent of NGK SN84 silicon nitride transversely machined tested at 20°C.

Field Emission Analytical Electron Microscopy for Characterization of Catalyst Microstructures

L. F. Allard, D. A. Blom, and T. A. Nolan

Objective/Scope

The objective of the research is to use analytical and high resolution transmission electron microscopy (TEM) to characterize the microstructures of emission control catalysts. Emphasis is placed on relating microstructural changes to performance of diesel NOx reduction catalysts. The research is focussed on understanding these changes through TEM studies of experimental catalysts materials reacted in an ex-situ catalyst reactor system especially constructed to allow appropriate control of the reaction conditions and the transfer of the sample between reactor and microscope.

Technical Progress

Work has begun on a new series of catalyst samples with colleagues at Caterpillar Co. The experimental catalysts for NOx emission reduction are composed of Ag clusters and particles supported on alumina, which were provided to us for characterization of the microstructure as a function of preparation and reaction conditions. Fresh samples comprised 1,2,4 and 8% by weight of Ag on Al_2O_3, calcined in air at 600°C. The same samples were also bench-tested (BT) under nominal reaction conditions, with SO_2 in the feedstock. A final set of samples comprising 2 and 8% Ag were exposed to SO_2 feedstock for ~5h and ~40h, to obtain information on the progress of formation of sulfur compounds. Some initial interesting results on these samples are presented in this report.

Samples of all the catalysts were prepared for TEM observation by grinding aggregates of the material in isopropanol, and depositing a droplet of the suspension onto copper specimen grids supporting holey carbon films. The 1% and 2% Fresh Ag samples showed Ag particles, confirmed by EDS spectra, in the range of 10-40nm that were widely distributed. When the electron beam was placed over areas of alumina support material that contained no apparent Ag particles, in the 1% sample no Ag peaks were observed, but in the 2% sample, small Ag peaks were observed, suggesting that there was also a dispersion of Ag at the near atomic level throughout the support aggregates at 2% by weight loading. The 2% sample which was treated with SO_2 for 5 hours showed no noticeable difference in the distribution of Ag species, but also did not show significant sulfur concentration, either associated with the Ag particles or with the alumina support. Figure 1 is an example of the typical Ag particle with its EDS spectrum showing no S in the 2% sulfur-treated sample. Figure 2 shows a 10-minute EDS spectrum from a nearby area of alumina; no S peak is noted also in this sample. To

obtain a better idea of the sulfur reaction on the samples, the 8% Ag specimen exposed to SO_2 for 40h was examined. Figure 3 shows a typical Ag particle in this specimen, which appears to be clean (i.e. shows no reaction layer on its surface), and the EDS spectrum from the particle. Note the lack of S peak in this spectrum. A 10-minute spectrum from the adjacent area shows a small S peak, again suggesting that the S is adsorbed onto the surface of the alumina particles, and does not react specifically with the Ag particles.

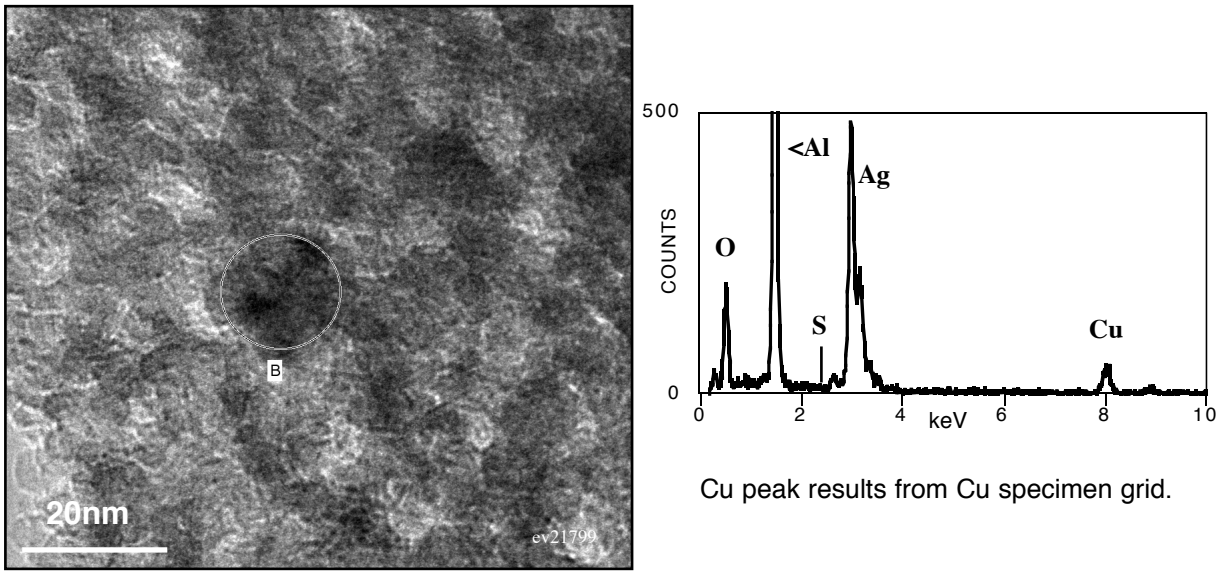

Fig. 1. Small clump of Ag particles (area B) on Al_2O_3 support material, in 2% Ag sample treated 5h in SO_2. The EDS spectrum confirms Ag, but shows no evidence of S.

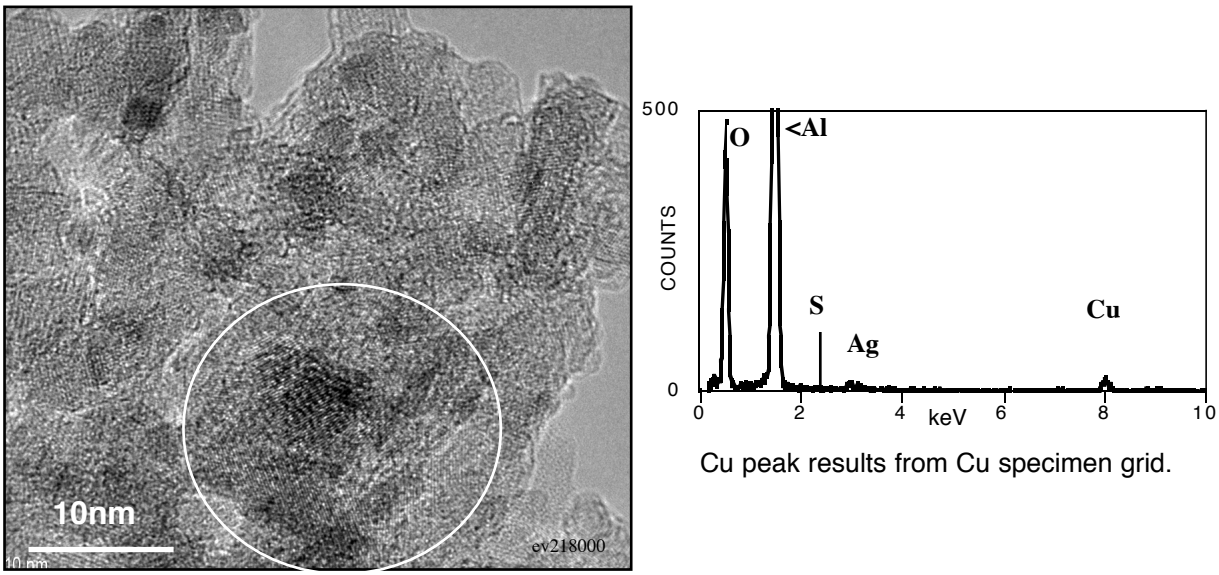

Fig. 2. Area adjacent to Fig. 1, but containing no evident Ag particles. The EDS spectrum shows a residual Ag peak, suggesting a near-atomic dispersion of Ag, but no apparent S also.

In order to get an initial feel for the reaction of SO_2 with the Ag samples, the 8% Ag specimen treated in SO_2 for 40h was examined. The Ag particles were in a similar size range to the lower Ag concentration samples, but were much more evident and easy to find due to the higher loading. Figure 3 shows a typical isolated particle, and its EDS spectrum. The particle appears clean (i.e. no apparent surface film), and the spectrum shows no S present. However, the EDS spectrum from a nearby area that included no evident Ag showed a clear S peak, as seen in Fig. 4. The small Ag peak in this sample again suggest that the Ag may also be dispersed at the near-atomic level in addition to the larger particulates seen. The conclusion is that the SO_2 in these treated specimens is adsorbed on the surface of, or reacts with, the alumina support particles. Future work will clarify this question, especially when the "bench-tested" specimens are examined.

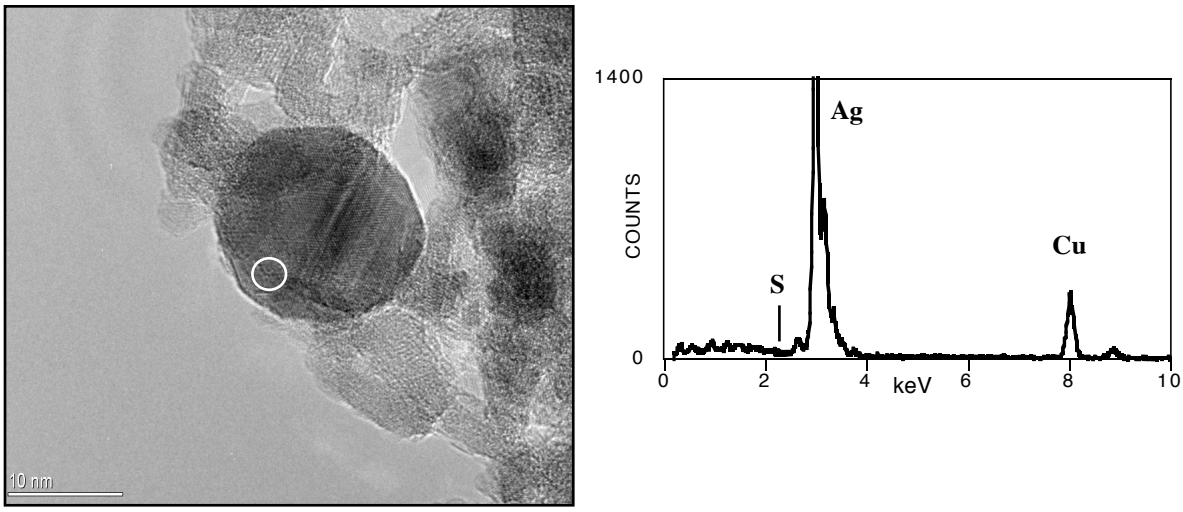

Fig. 3 Nearly isolated Ag particle in 8% Ag sample treated 40 hours. EDS spectrum from area (circled) apparently clear of alumina particles shows Ag with no apparent S evident.

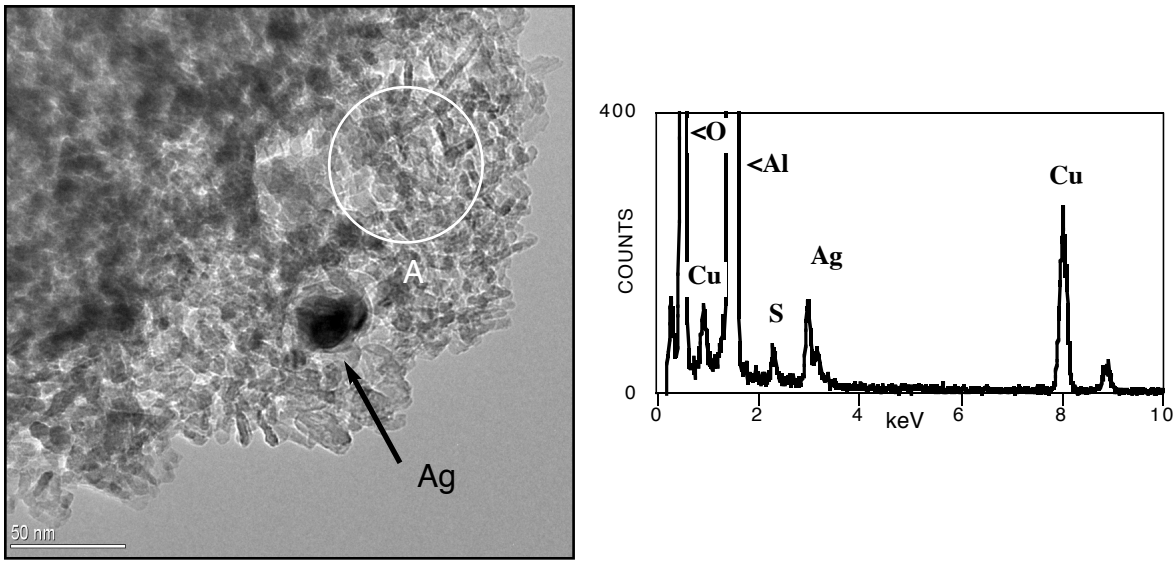

Fig. 4 Lower magnification image from nearby area showing EDS spectrum from area A, having no discernable Ag particles. A peak from S is clearly evident, as is an Ag peak, which suggests a near-atomic dispersion of Ag species as well as discrete Ag particles (arrowed).

Status of Milestones

On schedule.

Communications/Visits/Travel

None

Publications and Presentations

1. “Direct Imaging of Nearly Uniform Os5C Clusters Dispersed on MgO Powder,” L. F. Allard,G. A. Panjabi,S. N. Salvi and B. C. Gates, *Nano Letters*, in press.

Durability of Diesel Engine Component Materials

Peter J. Blau and Ronald D. Ott
Oak Ridge National Laboratory

Objective/Scope

The objective of this effort is to enable the development of more durable, low-friction moving parts in diesel engines for heavy vehicle propulsion systems by conducting friction, lubrication, and wear analyses of advanced materials, surface treatments, and coatings. The scope of materials and coatings is broad and includes any metallic alloy, intermetallic compound, ceramic, or composite material which is likely to be best-suited for the given application. Parts of current interest include scuffing-critical components, like fuel injector plungers and EGR waste gate components. Hot scuffing is a primary surface damage mode of interest. Bench-scale simulations of the rubbing conditions in diesel engine environments are used to study the accumulation of surface damage, and to correlate this behavior with the properties and compositions of the surface species. The effects of mechanical, thermal, and chemical factors on scuffing and reciprocating sliding wear are being determined. Results will be used to refine material selection strategies and suggest materials for durability-critical engine components.

Technical Highlights

Development of a Wear Test for Fuel Injector Components. An oscillating, cylinder-on-twin-cylinder (COTC) design was selected for initial studies. The rationale and description of this test was described in the previous quarterly report. A series of unlubricated tests was conducted to establish a baseline for tests in diesel fuels. The following conditions were used for these tests:

Load	100 N	Lubrication	none
Frequency	10 cycles/sec	Test duration	300 s (6 m sliding distance)
Stroke length	10 mm	Atmosphere	air (~ 40-60%RH)

Two tests were conducted per material combination. Kinetic friction coefficients were obtained from chart recordings of the rectified, root-mean-square tangential force. Wear was measured using the mass loss of the specimens. The following material combinations were used in baseline testing:

Upper Cylinder	Lower Cylinders (twin)
52100 bearing steel	52100 bearing steel
440C stainless steel	440C stainless steel
Nitronic 50	Nitronic 50
Co-based alloy 625	Co-based alloy 625
zirconia	zirconia
440C stainless steel	zirconia
zirconia	440C stainless steel

The three steels (Nitronic 50 is a high-nitrogen stainless steel) are currently used in bearing applications. The Co-based alloy 625 is used of high-temperature wear applications. Figure 1 shows the sizes and shapes of the wear scars produced on self-mated 52100 steel specimens, and Figure 2 shows the total system wear for the baseline material pairs.

Figure 1. Significant wear indications on the 52100 steel specimens.

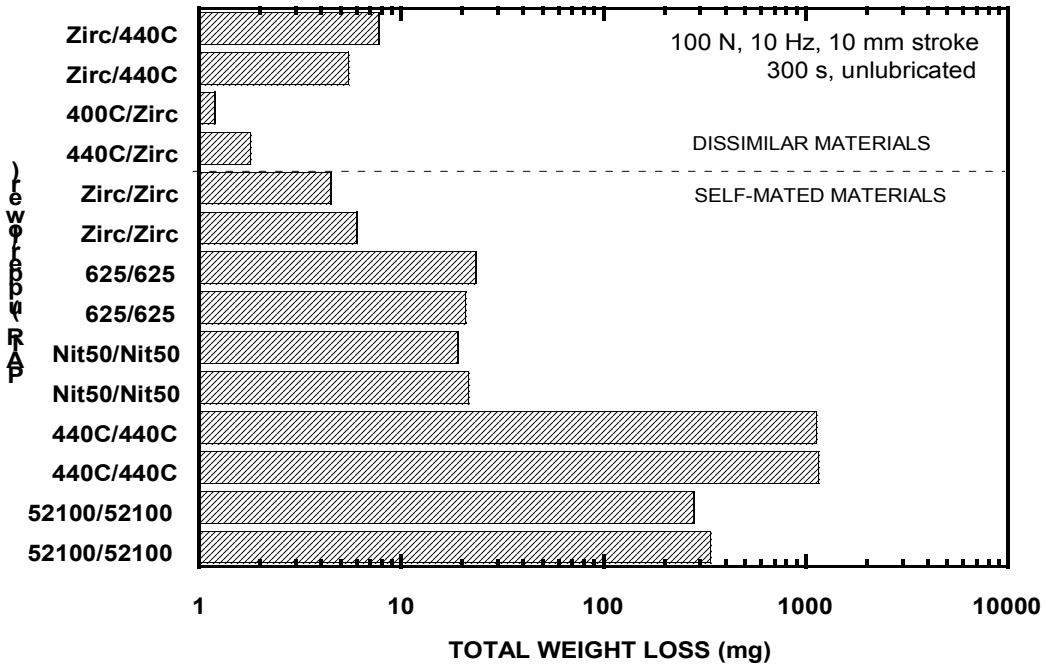

Figure 2. Baseline wear-testing results for self-mated and dissimilar sliding couples.

Highest total wear was for the 440C steel couple, followed by the high-Cr bearing steel. The other two metallic alloys had similar total wear losses. The couple with an upper 440C stainless steel cylinder reciprocating against zirconia had the lowest overall wear.

Since the upper cylinder specimen sees relatively constant contact pressure, but the lower specimens experience contact fatigue in addition to reversed sliding, the position of a given

material as the top or bottom specimen can product different results. Figure 3 shows the wear (mass loss) of the upper specimen relative to the total wear for the two lower specimens.

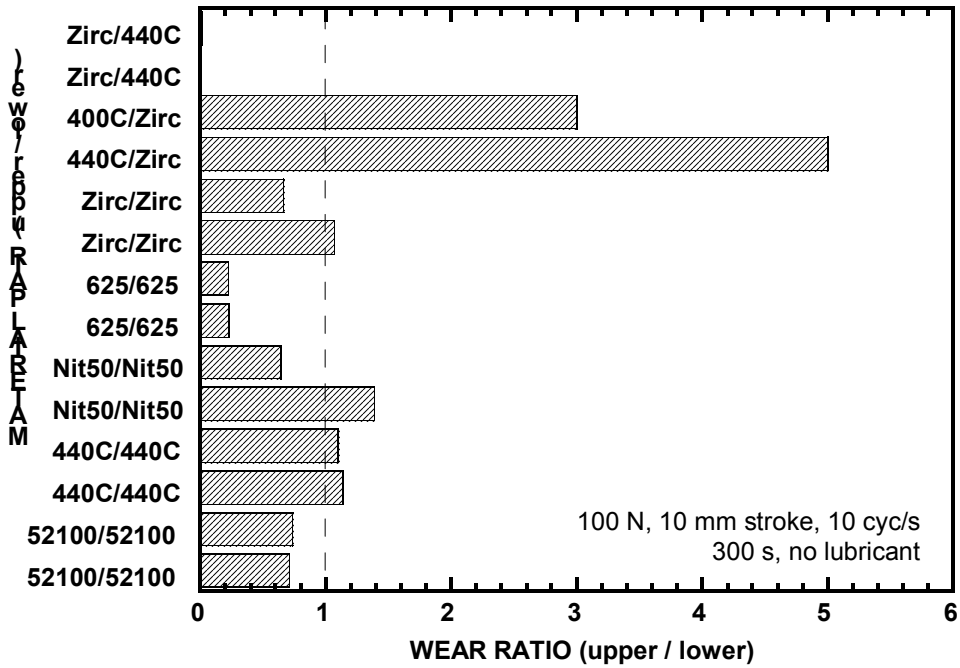

Figure 3. Relative mass losses of the upper and lower specimens.

For the self-mated steel couples, the 440C stainless steel upper specimen tended to wear slightly more than the lower, but the reverse was true for 52100 steel and alloy 625. This suggests a difference in the relative importance of fatigue and shearing processes for these alloys. The Nitronic 50 did not show a consistent preference for upper or lower specimen wear.

Diesel fuel has been obtained for use in conducting lubricated tests during the next period.

Future Plans

1. Continue metallurgical studies of scuff-tested specimens, and conduct additional tests to examine the effects of intermittent operation on the durability and frictional torque behavior of the four leading material pairs. Two new materials will be evaluated, following a suggestion from Carpenter Technology Corporation: Custom 465™ and Pyromet 80™.

2. The potential for improving high-temperature scuffing behavior still further using coated or modified surfaces will be investigated.

3. Conduct cylinder-on-twin cylinder tests on fuel injector plunger materials under diesel fuel-lubricated conditions.

Travel

None.

Status of FY 2002 Milestones

1) Complete design and construction of fixtures to adapt existing ORNL friction and wear testing machine for fuel injector plunger materials. (December 15, 2001 – completed.)

2) Complete elevated temperature scuffing tests of leading candidate materials and coatings under transient conditions. Submit report. (March 31, 2002)

3) Complete tests of candidate ceramics and cermets for fuel injector applications. Submit report. (September 30, 2002)

Publications

(none this period)

Implementing Agreement For A Programme Of Research And Development On Advanced Materials For Transportation Applications

M. K. Ferber
Oak Ridge National Laboratory

Objective/Scope

The International Energy Agency (IEA) was formed via an international treaty of oil consuming countries in response to the energy crisis of the 1970s. A major objective of the IEA is to promote secure energy supplies on reasonable and equitable terms. The governing board of the IEA, which is composed of energy officials from each member country, regularly reviews the world energy situation. To facilitate this activity, each member country provides energy experts who serve temporary staff assignments at IEA headquarters. These staff or secretariat support the governing board by collecting and analyzing energy data, making projections in energy usage, and undertaking studies on specialized energy topics. The governing board is also assisted by several standing groups – one being the committee on energy research and technology (CERT), which encourages international cooperation on energy technology. Implementing agreements (IAs) are the legal instruments used to define the general scope of the collaborative projects. There are currently 40 active implementing agreements covering research topics such as advanced fuel cells, coal combustion science, district heating and cooling, enhanced oil recovery, fluidized bed conversion, fusion materials, solar heating and cooling, pulp and paper, hydropower, heat pumping technologies, hybrid and electric vehicles, high temperature super conductivity, wind turbines, and high temperature materials. A complete listing can be found at the IEA website, www.iea.org.

This progress report summarizes recent activities in the implementing agreement entitled, "Implementing Agreement For A Programme Of Research And Development On Advanced Materials For Transportation Applications." This implementing agreement currently consists of one active annex entitled," Annex II: Co-Operative Program on Ceramics for Advanced Engines and Other Conservation Applications". The motivation for this IA is the development of new and improved ceramic materials, brittle material design methods, and life prediction methodology. The objective of Annex II is coordinated R&D on advanced ceramics leading to standardized methods for testing and characterization.

The Executive Committee for the IA on Advanced Materials is also exploring the possibility of adding a new effort (Annex III) focusing on the characterization of materials for diesel engines. Possible topics include characterization of contact damage (fatigue) and novel methods for the assessment of the mechanical reliability of coatings.

Technical Highlights

The United States hosted the annual executive committee meeting held in conjunction with the PAC RIM IV meeting on 4-8 November 2001 in Wailea, Maui, Hawaii, at the Outrigger Wailea Resort. The following persons were in attendance:

- Sidney Diamond – Department of Energy (DOE) Office of Transportation Technologies (United States Executive Committee Chairman),

- Matt Ferber – Oak Ridge National Laboratory (ORNL) (Operating Agent Technical Representative, United States Alternate Committee Member, and Working Group Coordinator of Subtask 11),
- Rolf Wäsche – Bundesanstalt für Materialforschung und-Prüfung (BAM) (German Executive Committee Member),
- Mikio Iwasa – National Institute of Advanced Industrial Science and Technology (AIST) (representing Japan),
- Jenny Jackman – Natural Resources Canada (NRC) (invited to discuss activities in Canada that could be relevant to our Implementing Agreement {IA}),
- Kevin Ewsak – Sandia National Laboratories (SNL) (Working Group Coordinator of Subtask 12 and US Coordinator of Subtask 12),
- Steve Freiman – National Institute of Standards and Technology (NIST) (invited to discuss NIST's proposal on contact damage assessment), and
- Steve Gonzy – Gateway Materials (under contract to ORNL to assess coating characterization activities relevant to our IA).

The major objectives of this meeting were to (1) conduct a technical information exchange between the participating countries, (2) review the status of the active subtasks (11 and 12), and (3) discuss the future activities of the group. Concerning future activities, the possibility of focusing on diesel engine materials was discussed in detail. Dr. Ferber suggested that the development and verification of advanced characterization methods for these materials would be an appropriate topic.

Status of Milestones

All milestones are on track.

Communications/Visits/Travel

Matt Ferber represented the DOE, the current Operating Agent for Annex II, by chairing the annual executive committee meeting held in conjunction with the PAC RIM IV meeting on 4-8 November 2001.

Matt Ferber visited NIST to attend the Contact Reliability Working Group Meeting.

Publications

A preliminary draft of the Annual Report for the implementing agreement has been prepared.

References

None

Standards For Reliability Testing Of Heavy Vehicle Propulsion Materials

Said Jahanmir and William Luecke
Ceramics Division
National Institute of Standards and Technology

Objective/Scope

The objective of this project is to develop international standard test methods for assessing the reliability of ceramic components used in diesel engines and other heavy vehicle propulsion systems. Advanced ceramics such as silicon nitride offer a unique combination of properties that include light weight, excellent high-temperature strength, and resistance to wear and corrosion. These properties make them particularly attractive for diesel engines, where their use as key engine components will allow the higher operating temperatures that lead to higher thermal efficiencies and environmentally cleaner propulsion systems. Reliability and cost-effectiveness are critical issues in implementing ceramics in the valve train of diesel engines. Ceramic valve train components are subjected to demanding conditions that include high contact loading, elevated temperatures, and corrosive environments. To ensure a reliable service life, standard test methods are needed to evaluate the performance of potential ceramics in highly loaded rolling and sliding contacts. This project will develop test methods for evaluating the contact damage behavior of ceramics under rolling and sliding conditions that simulate the cam roller followers, valves and valve seats. In support of this goal we will pursue four research thrusts: 1) fundamental issues in the relation between ceramic microstructure and performance reliability, 2) basic mechanisms that lead to formation and propagation of contact damage and the effect on reliability of residual stresses developed during machining and by contact, 3) effect of machining damage on contact reliability as well as the interactions between machining and contact damage that may lead to premature failure, 4) development of international standards for assessing contact damage.

Technical Highlights

Pre-Standards Research for Rolling Contact Fatigue

Although early grades of silicon nitride exhibited rolling contact fatigue failures by spalling, similar to bearing steels in various laboratory tests[1,2], modern grades typically do not fail by RCF[3,4,5] in laboratory testing. Effectively, the newer materials have outstripped the ability of the test method. Although several test geometries exist for evaluating RCF in the laboratory (thrust washer, ball-on-3-balls, twin-disc-on-rod), the 3-ball-on-rod (Federal Mogul test) is the most common in the United States. We are conducting research into extending this test method to once again yield RCF data on modern grades of silicon nitride, as well as examining the potential of the test for ASTM standardization.

The 3-ball-on-rod test[1], see Figure 1, uses a 9.52 mm diameter rod approximately 75 mm long, held in a precision chuck and driven at 3600 rpm. A special test head clamps 3 (or 5) specially prepared M50 steel balls against the rod at a known, fixed load. An accelerometer mounted on the test head detects the vibration produced as the balls drop into a developing spall, and shuts the test down when that vibration reaches a prescribed level.

During this reporting period research focused on two areas of the 3-ball-on-rod test using Ceradyne Ceralloy 147-31N test rods. The first area of research is in replacing the special M50 steel test balls normally used in the test with Si_3N_4 balls. Research in other laboratories has demonstrated [6,7] that during the test, even with M50 balls on M50 rods, the stress drops, from an initial 5.4 GPa -6.3 GPa to 4 GPa or less due to wear and deformation of the M50 ball. Although previous research at NTN[7] demonstrated that test stresses of 5.4 GPa or 3.4 GPa produce the same ranking for RCF life for many bearing steels in the 3-ball test, this relation has not been demonstrated for Si_3N_4. Furthermore, this stress drop complicates any fundamental analysis of the RCF life.

Preliminary testing, summarized in Table I, using both Si_3N_4 and M50 steel balls, has revealed two important phenomena. The standard test load using Si_3N_4 balls on Si_3N_4 rods produces an initial contact stress of 7.3 GPa. At this stress, commercially finished (CF) rods ($R_a \approx 0.08$ µm) CF rods fail by mechanism that might be described as spalling, in which a 25 µm-50 µm deep track encompassing 1/4 to 1/3 of the circumference forms nearly after 250 000-1 000 000 stress cycles (0.5 h-2 h). The remainder of the test track has a minimal (0.2 µm deep) wear track. Figure 2 is an example of such a failure. The formation of this "spall" triggers the test machine to shutdown. In contrast, rods prepared by hand-polishing (HP) the commercially finished (CF) test rods never show excessive vibration, but have deep, highly polished wear tracks up to 50 µm deep. Figure 3 illustrates the wear track left by testing for 449 h. In contrast to this behavior, testing with the special M50 steel balls never produces spalls large enough to stop the test. Instead, most tests end by the spalling of one of the M50 balls. Work is underway to test the rods at the same contact stress (6.3 GPa) for both M50 and Si_3N_4 loading balls. The effect of machining damage will be probed with specially prepared test rods.

Report from Contact Damage Working Group Meeting

The Contact Damage Working Group held its second meeting, at NIST on December 5, 2001 with participants from Norton-St. Gobain, Caterpillar, Ceradyne, Chand Associates, ORNL, and NIST. During the meeting Said Jahanmir reviewed the NIST Advanced Engine Materials Program with a focus on ceramics for diesels and thermal barrier coatings for turbines. The program has recently formed an external review panel consisting of Dr. Robert Katz (WPI), Dr. Curtis Johnson (General Electric CRD), Dr. Gregg P. Wagner (Siemens-Westinghouse), Dr. Nabil Hakim (Detroit Diesel) and Richard Allor (Ford). The panel met with the NIST scientists involved in the program on Dec. 7. Jahanmir also reviewed his proposal to the Executive Committee of the IEA Advanced Materials For Transportation Applications Annex II (Ceramics For Advanced Engines) during their November 2001 in Maui, Hawaii. At that meeting he proposed to establish a new subtask on Contact Damage in Advanced Engine Materials. The Contact Damage Working Group endorsed the plan for the development of international standards and felt that there would be minimal barriers to their participation in such an activity. Matt Ferber (ORNL) made a brief presentation on the structure of IEA, especially the Implementing Agreement on Advanced materials for Transportation Applications. He proposed that the proposed subtask on Contact Damage in Advanced Engine Materials be a separate annex, rather than a subtask. He agreed to develop the first draft of Annex III for review by the Executive Committee.

During the afternoon discussion session, the group resolved to pursue two research areas in 2002. The first will be a small scale round robin (5 participants) on the 3-ball-on-rod test machine, using two types of Si_3N_4 rods. The second will be to compare the results of the 3-ball test with actual roller follower tests in collaboration with Caterpillar. Both the round-robin and the simulation tests will employ several types of commercially available silicon nitrides.

Status of Milestones

1. Propose to the IEA Executive committee the formation of a new subtask under Annex III to study contact damage (December 2001): complete.
2. Compare the nature of failure mechanisms in single-cycle ball-on-flat contact damage to those in rolling contact fatigue for silicon nitride. (March 2002) on schedule
3. Compare the nature of failure mechanisms in multi-cycle contact damage to those in rolling contact fatigue for silicon nitride. (July 2002) on schedule
4. Explore the feasibility of standardizing the 3-ball-on-rod rolling contact fatigue (RCF) test and assemble a team of users of the 3-ball-on-rod RCF test to conduct an interlaboratory study of RCF of engine ceramics. (September 2002) on schedule.

Communication/Visits/Travel

The Contact Damage Working Group held its second meeting at NIST on December 5, 2001. Steve Freiman attended the Executive Committee meeting of the IEA Advanced Materials For Transportation Applications Annex II (Ceramics For Advanced Engines) during November 2001 in Maui, Hawaii and presented a proposal to establish a new subtask on Contact Damage in Advanced Engine Materials.

Publications

None this period

References

[1] Douglas Glover, "A Ball-rod Rolling Contact Fatigue Tester," pp 107—124 in *Rolling Contact Fatigue Testing of Bearing Steels*, J. J. C. Hoo, ed. ASTM STP 771, American Society for Testing and Materials, Philadelphia, Pa, (1982)

[2] Harold L. Burrier Jr. "Optimizing the Structure and Properties of Silicon Nitride for Rolling Contact Bearing Performance," *Trib. Trans.*, **39**[2], 276—285 (1996)

[3] L.-Y Chao, R. Lakshminarayanan, N. Iyer, G.-Y. Lin, and D. K. Shetty, "Transient Wear of Silicon Nitride in Lubricated Rolling Contact," *Wear*, **223**, 58-65, (1998).

[4] Vimal Pujari and William Collins, "All Ceramic Bearing", United States Patent 6158894,December 12, 2000.

[5] Deborah L. Allen, "Effect of Composition and Physical Properties of Silicon Nitride on Rolling Wear and Fatigue Performance," *Trib. Trans.*, **37**[2], 410—414, (1994)

[6] John W. Lucek, "Rolling Wear of Silicon Nitride Bearing Materials," Paper 90-GT-165, 1990, American Society of Mechanical Engineers ``Presented at the Gas Turbine and Aeroengine Congress and Exposition, June 11--14, 1990 Brussels, Belgium.

[7] Mary-Jo Liston, "RCF Life Comparision of Bearing Steels at Two Stress Levels," Lub. Eng., **55**[6], 12-19, (1999).

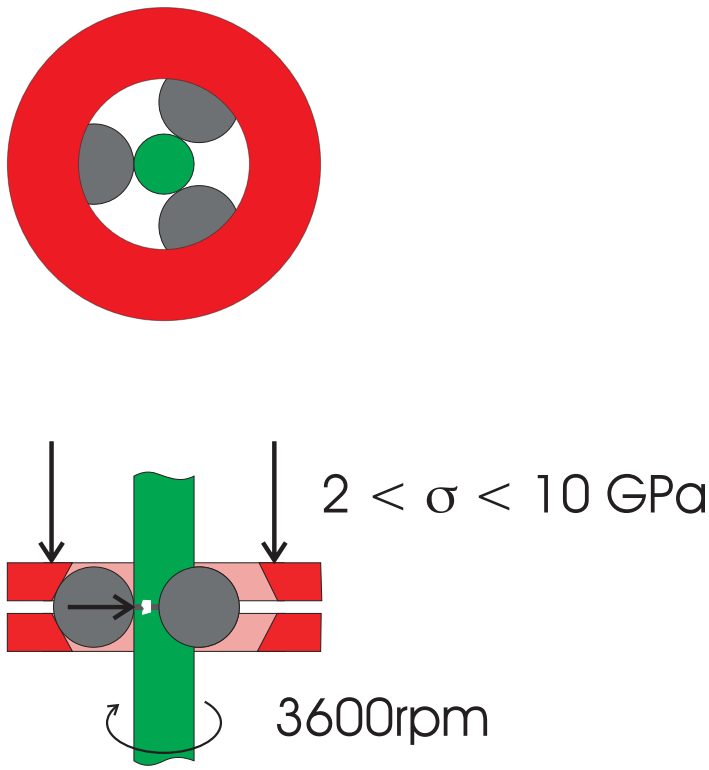

Figure 1. Geometry of the 3-ball-on-rod RCF test.

Table 1 Summary of RCF Tests

Rod-Track	Initial Stress (GPa)	Ball Mat'l	# Cycles	Wear track depth (μm)	Spall size	Notes; why shutdown
HP1-0	6.3	M50	1.3E7	0.2	no spall	M50 ball spall
HP1-4	6.3	M50	5.8E6	0.4	no spall	M50 ball spall
HP1-5	6.3	M50	5.2E7	3.0	no spall	3 restarts, all M50 ball spalls
HP5-1	6.3	M50	3.1E7	0	no spall	suspended test
HP1-1a	6.3	M50	2.3E7	0.4	no spall	
CF6-1	6.3	M50	<3.5E7	0	19.3 μm deep	suspended test
CF6-2	6.3	M50	6.27E7	0	2 μm deep	M50 ball spall
CF6-14	6.3	M50	5.8E7	0	no spall	suspended test
CF6-3	7.3	Si_3N_4	3.6e5	0	19.6 μm ¼ circumference	rod spall
CF6-4	7.3	Si_3N_4	3.1E5	0s	27.9 μm ¼ circumference	rod spall
CF4-1	7.3	Si_3N_4	4.6E5	2.2	16.5 μm 1/3 circumference	rod spall
HP5-2	7.3	Si_3N_4	2.3E8	58.6	no spall	uniform, deep wear; suspended test
HP5-4	7.3	Si_3N_4	4.1E5	0.7	no spall	wear rate test, suspended
HP5-5	7.3	Si_3N_4	9.8E5	5.6	no spall	wear rate test, suspended

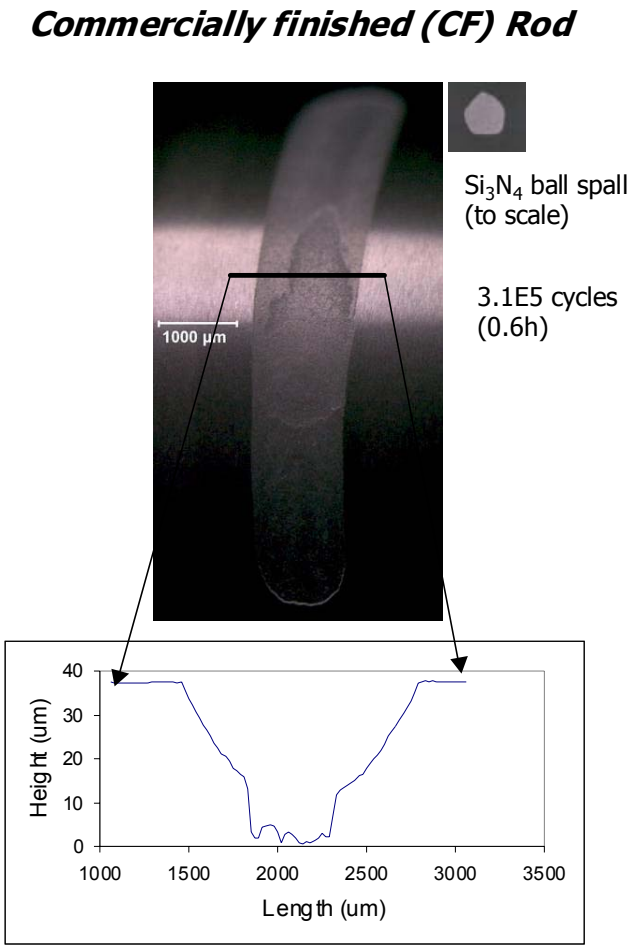

Figure 2. Failure by spalling of commercially finished test rod 6 (CF6-2). The track extends only about 1 /4 of the circumference of the rod.

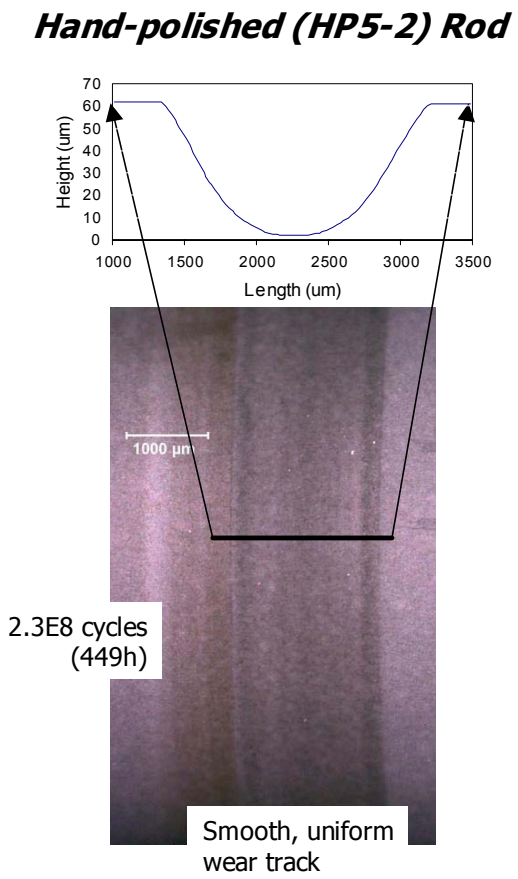

Figure 3. Extreme wear of hand-polished RCF test rod HP5-2. Note that the bottom of the wear track is much less rough than that of the spall in test rod CF6-4 in Figure 2 .

Mechanical Property Test Development

George Quinn
Ceramics Division
NIST

Objective/Scope

This task is to develop mechanical test method standards in support of the Propulsion Systems Materials Program. Test method development should meet the needs of the DOE engine community but should also consider the general USA structural ceramics community as well as foreign laboratories and companies. Draft recommendations for practices or procedures shall be developed based upon the needs identified above and circulated within the DOE engine community for review and modification. Round robins will be conducted as necessary. Procedures will be standardized by ASTM and/or ISO.

Technical Highlights.

1. General

Work on flexure testing of cylindrical rods specimens resumed this quarter. Ground silicon nitride and silicon carbide specimens were tested. Previously tested glass rods were reexamined for evidence of contact damage. Revisions were made to several ASTM and ISO standards including room temperature flexural strength, elevated temperature flexural strength, fractographic analysis, and fracture toughness. Last minute SCF fracture toughness testing was done to support the ISO fracture toughness standard.

2. Fracture Toughness

a. ASTM standard C 1421 revisions approved.

A series of 19 corrections or refinements to C 1421 were balloted in the September of 2001 and all passed without comment or negative in the fall 2001 ASTM ballot.

b. ISO SCF method

The ISO draft standard for fracture toughness testing had been balloted for elevation to Draft International Standard Stage. Input from the Korean delegation indicated that they were still concerned that slow crack growth could occur in many ceramics when tested at room temperature under lab ambient conditions. They felt that inert testing conditions should be mandatory. To prove their point, they had performed experiments on **Coors AD 995 alumina** under a variety of testing conditions including lab ambient; lab ambient with extra humidity; inert-oil coated; and inert in dry nitrogen atmosphere. They concluded that the only safe way to test was under totally inert conditions with specimens coated with paraffin wax *and* in dry nitrogen gas environment. We felt this was too restrictive and excessively

conservative. There are many ceramics that have no slow crack growth at room temperature (silicon carbides and many silicon nitrides) and it would be a nuisance to have to test these materials with wax coatings and in inert nitrogen gas or vacuum chambers.

To double-check the Korean results, we obtained some spare specimens from the Koreans. The specimens were tested at NIST by the SCF method without wax coatings. We tested them in our normal bend fixtures with a simple plastic sleeve that slides up and down to seal the testing environment. The top of the chamber was sealed with a plastic bag. Dry nitrogen gas was passed into the chamber to purge it for a few minutes. The test was then conducted in a normal fashion. Five specimens tested in this manner showed no trace of slow crack growth. The fracture toughness outcomes were high and matched the best results the Korean delegates furnished. We conclude that our simple gas chamber around our normal bend fixtures is adequate. The ASTM standard C 1421 already recommends a simple procedure like this if the user is concerned about possible slow crack growth interferences.

Why then did the Korean delegation have problems with their inert dry nitrogen testing? Their data and specimens did show evidence of slow crack growth. We learned that their method of introducing the nitrogen gas was to aim a jet of nitrogen gas from a nozzle onto the bottom of the specimen during the test. Obviously this does not ensure the test piece is protected from the humidity in the air, since swirling flow and turbulence will cause the nitrogen gas to mix with lab ambient air.

In September we also tested some **Alsimag 614 alumina** specimens furnished by Dr. Jon Salem at NASA-Glenn. We wanted to "complete the trifecta" and compare SCF data to chevron notch and single-edged precracked beam results on the same material. The average fracture toughness for four specimens by the SCF method in dry nitrogen was 3.47 ± 0.12 MPa√m. These results were in excellent agreement with Salem's chevron notch data collected in oil and in air. The small SCF precracks were very hard to detect with normal optical microscopy, but became clear when a green felt tip pen was used to paint the fracture surface. Figure 1 on the next page illustrates this trick.

We used to have difficulty detecting precracks in both the Coors AD 995 and the Alsimag 614 aluminas, yet not anymore. A 98 N (10kgf) indentation precrack load makes precracks that are much easier to find than the precracks made with the C 1421 recommended load of 49N (5 kgf). The larger precracks were easier to see. We will recommend C 1421 be revised again to encourage 98 N indentation precracks.

(a)

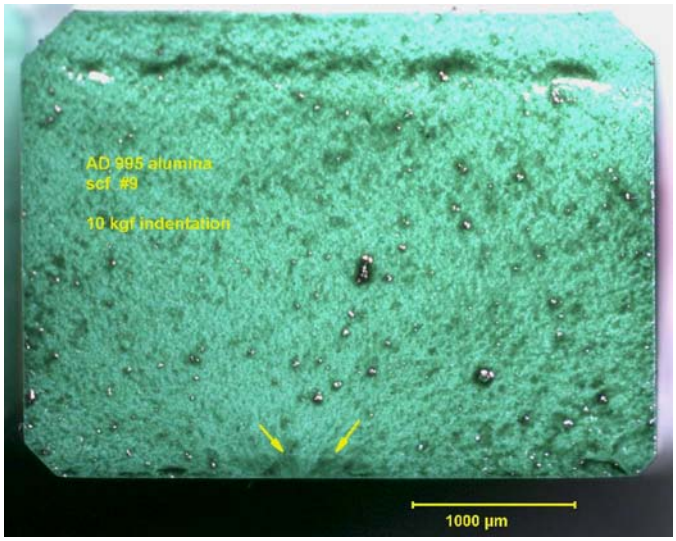

(b)

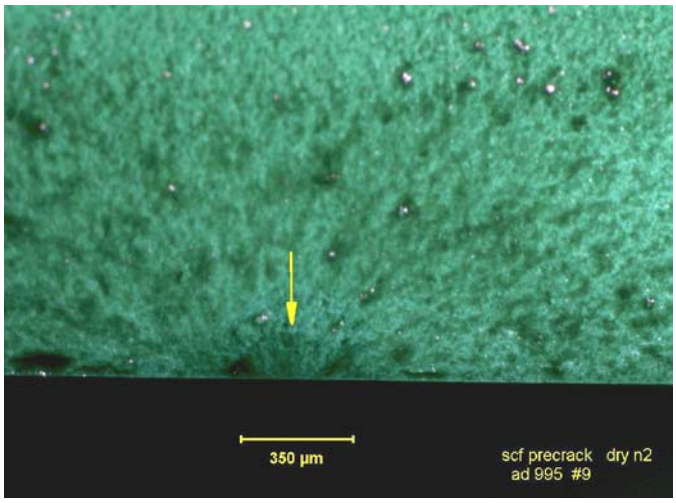

Figure 1. Fracture surface of a Coors AD 995 fracture toughness specimen. The small SCF precrack is marked by the yellow arrows. (b) is close-up and shows the slightly darker color of the SCF precrack. The SCF precrack and other fracture features in translucent ceramics are much easier to detect. The tint helps cut down the internal reflections that blur the fracture surface. The dye also runs into crevices and valleys and accentuates the fracture surface features. The fanlike pattern radiating from and draws one's attention to the Knoop precrack. Simple tricks like this should enable materials engineers to detect SCF precracks or fracture origins in white ceramics.

3. Flexural Strength of Advanced Ceramics – Rectangular Specimens

a. ASTM C 1161 Revisions

After 11 years on the books, ASTM standard C 1161 was overhauled in the fall of 2001 when twenty-six revisions were approved. In addition to many minor clarifications or refinements, some major changes were made. The old 1/8" x ¼" x 2" specimen on 0.75" x 1.5" fixtures (Configuration "D") was deleted. A major change to the "standard" machining procedure was approved. This latter revision is important and we must follow it up with announcements and articles in trade journals. Letters to key machine shops must also be sent. We hope that the new engineering drawing of a standard bend bar (shown in the last DOE Quarterly progress report) will aid the transition.

A handful of affirmative with comment ASTM ballots were received from Jeff Swab, Sung Choi, Jonathan Salem, and Vic Tennery. Additional minor revision will be made to ASTM C 1161 to settle their concerns. ASTM will post a follow-on ballot of 4 items in early January 2002. For example, Ceradyne requested that we tighten our scratch examination protocol. In their experience, well-machined specimens were prone to scratch damage. These scratches could become strength limiting flaws, thereby negating the value of the bend test. The earlier versions of C 1161 had generalized cautionary remarks about handling damage. They were sufficient for specimens with a general duty 320 grit final finish. As grinding has gravitated to finer finishes, specimens seemed to become more susceptible to scratch damage. Thus, Ceradyne felt that more specific precautions and warnings should be in C 1161. We concur. The following revision will be balloted in ASTM Committee C 28 in January:

Revise paragraph 7.2.5:

7.2.5 Handling Precautions **and Scratch Inspection** — Care should be exercised in storing and handling of specimens to avoid the introduction of random and severe flaws, such as might occur if specimens were allowed to impact or scratch each other**. If required by the user, inspect some or all of the surfaces as required for evidence of grinding chatter, scratches, or other extraneous damage. A 5X – 10X hand loupe or a low power stereo binocular microscope may be used to aid the examination. Mark the scratched surface with a pencil or permanent marker if scratches or extraneous damage are detected. If such damage is detected, then the damaged surface should not be placed in tension, but instead on the compression mode of loading when the specimen is inserted into the test fixtures.**

Note: Damage or scratches may be introduced by handling or mounting problems. Scratches are sometimes caused by loose abrasive grit.

Revise Paragraph 8.2.

8.2 Carefully place each specimen into the test fixture to preclude possible damage and to ensure alignment of the specimen in the fixture. In particular, there should be an equal amount of overhang of the specimen beyond the outer bearings and the specimens should be directly centered below the axis of the applied load**. If the one of the wide specimen surfaces has been marked for the presence of a scratch or extraneous damage, then place the damaged surface so that it is loaded in compression. If a side surface is marked as damaged, then the specimen may be tested, but shall be inspected after the test to confirm that the scratch or damage did not cause fracture.**

Add a new paragraph 8.11

8.11 Reject all specimens that fracture from scratches or other extraneous damage.

The original version C 1161 was a good standard when adopted, but years of new experience by the ceramics and engineering community especially at ORNL and NIST warrant the major overhaul.

b. ASTM C 1211, Elevated Temperature Flexural Strength Revisions

This standard, the elevated temperature version of C1161, is also due for an overhaul. The changes will be much less extensive since C 1211 was already revised in 1997. We will propose that this standard be shortened considerably and the users referred back to C 1161. When this standard was created in 1994, the ASTM committee wanted it to be a stand-alone document. Unfortunately this led to a lot of unnecessary redundancy with C 1161. A list of proposed changes and the proposal to shorten C 1211 will be prepared for the April 2002 meeting of Committee C-28 in St. Louis.

c. ISO 17565, Elevated Temperature Flexural Strength

Fourteen editorial revisions were recommended for this standard. It began its 5-month worldwide balloting period at the end of October 2001.

4. ASTM Standard C 1322, Fractographic Analysis of Advanced Ceramics

This ground breaking standard is also due for renewal. It was the first standard in the world to set a course of action for normal fractographic analysis and interpretation of fractured strength-test specimens. In late December, the author in cooperation with Mr. J. Swab of the U.S. Army Research Laboratory, compiled a group of 19 revisions to C 1322. They will be balloted by ASTM in late January 2002.

Many of the revisions are intended to shorten the document and make it easier for users to understand. For example, the tables comparing the merits and drawbacks of various specimen-cleaning solvents will be deleted since most users are already familiar with the cleaning agents. The extensive bibliography will also be eliminated. It was originally included to steer users to additional sources of information, but the bibliography would be better placed in a textbook or guide.

C 1322 will be expanded in some areas. More guidance will be furnished on component failure analysis rather than merely lab test specimen analysis. A simple flowchart will illustrate the logical order of the common fractographic analysis, putting into an illustration what previously had been pages of text only.

The revision will also include a new, vastly expanded appendix of fracture mirror constants. Fracture mirrors, which surround the fracture origin in brittle ceramics, are very useful indicators of the stress in the part at the instant of fracture. The fracture mirror constant (A) in conjunction with the mirror size, R, may be used to directly calculate the stress in the part at fracture (σ):

$$\sigma = \frac{A}{\sqrt{R}}$$

Fracture mirror shape distortion is also a key indicator of stress gradients and even the stress state. Branches and mirrors in biaxially loaded specimens manifest themselves differently that in uniaxially loaded specimens. Table 1 is a portion of a large new table that will be included in the revised ASTM standard. The new table will be the largest compilation of fracture mirror constants ever published. Review of the data shows consistency for constants in some cases, but wide divergences in other cases. This underscores a need for some guidance or a standard for the determination and interpretation of fracture mirror sizes. We will leave this matter for the time being, but may revisit it in the future.

Table 1 Fracture Mirror Constants for a variety of Ceramic Materials. The full table with citations will be published in a revision to the ASTM Advanced Ceramic Fractography standard C 1322 in 2002.

Material	Technique	*Mirror-Mist* A_i (MPa·$\sqrt{m}$)	*Mist-Hackle* A_o (MPa·$\sqrt{m}$)	Branching A_b (MPa·$\sqrt{m}$)
Silicon Carbide:				
Sintered SiC (Hexoloy SA)	Flexure (Bars)		5.39	
Sintered SiC (Hexoloy SA)	Flexure (Biaxial ring-on-ring plates)			6.30 ± 0.54
Sintered SiC (Hexoloy SA)	Flexure (Biaxial ring-on-ring plates)			5.45 ± 0.30
Sintered SiC toughened (Hexoloy SX)	Tension (Rods) and Flexure (Bars)		7.0?	7.0?
Sintered (Carolt S)	Flexure (Bars, optical, SEM)		6.1, 6.8	
Hot-pressed SiC (NC-203)	Flexure (Rods) Flexure-Delayed Fracture (Rods)		11.4 11.9	
Hot-pressed SiC (NC-203)	Flexure (Rods)		11.5	
Hot-pressed SiC (ACE)	Flexure (Rods)		10.8	
Siliconized SiC (KT)	Flexure		10.7	
Zirconia:				
Ytttria stabilized (Y-TZP)	Flexure (Bars)		9.95	
Ytttria stabilized (Y-TZP)	Flexure (Biaxial ring-on-ring disks)			11.48 ± 1.46
Zircar (Alfred-Union Carbide, 0.4 μm)	Flexure (Bars)		15.2	
Zyttrite (AFML, 10 μm)	Flexure (Bars)		7.4	
Silicon Nitride:				
Sintered Reaction Bonded (Ceraloy 147-31N)	Flexure (Rods) Flexure (Bars)		8.47 ± 0.07 7.79 ± 0.02	
Sintered (SSN-500 yttria/alumina)	Flexure (Bars)		5.81	
Sintered (SN 220)	Flexure (Biaxial ring-on-ring disks)			8.13 ± 2.36
Sintered (AS 44)	Flexure (Biaxial ring-on-ring disks)			10.85 ± 2.71
Hot-pressed (Ceraloy 147A)	Flexure (Bars)		7.83	
Hot-pressed (NC-132)	Flexure (Rods)		9.2	
Hot pressed (NC-132)	Flexure (Rods) Flexure-Delayed Fracture (Rods)		8.9 9.2	
Hot-pressed (NC-132)	Flexure (Rods)		14.3	
Hot-pressed (NC-132)	Flexure (Bars) Flexure (Biaxial ring-on-ring)		9.40 ± 1.19	 7.92 ± 2.08
Hot-pressed (HS-130)	Flexure		18.1	
Hot-pressed (HS-130)	Flexure (Rods)		9.1	
Hot-isopressed (NT 154)	Flexure (Bars)		5.88 ± 0.14	
Hot-isopressed + 30vol% SiC whiskers	Flexure (Bars)		6.63 ± 0.11	
Hot-isopressed (GN-10)	Flexure (biaxial ring-on-ring) Tension (Rods)		 11.78 ± 1.41	10.32
Reaction Bonded (NC 350)	Flexure (Bars)		3.89	
Reaction Bonded (NC 350)	Flexure (Bars)		3.19	
Reaction Bonded (AME A25B)	Flexure (Rods)		4.2	

Another major change to the ASTM fractography standard will be inclusion of more examples and illustrations of machining damage cracks, based on the lessons we have learned in this program in the last few years. Figure 2 shows some of these.

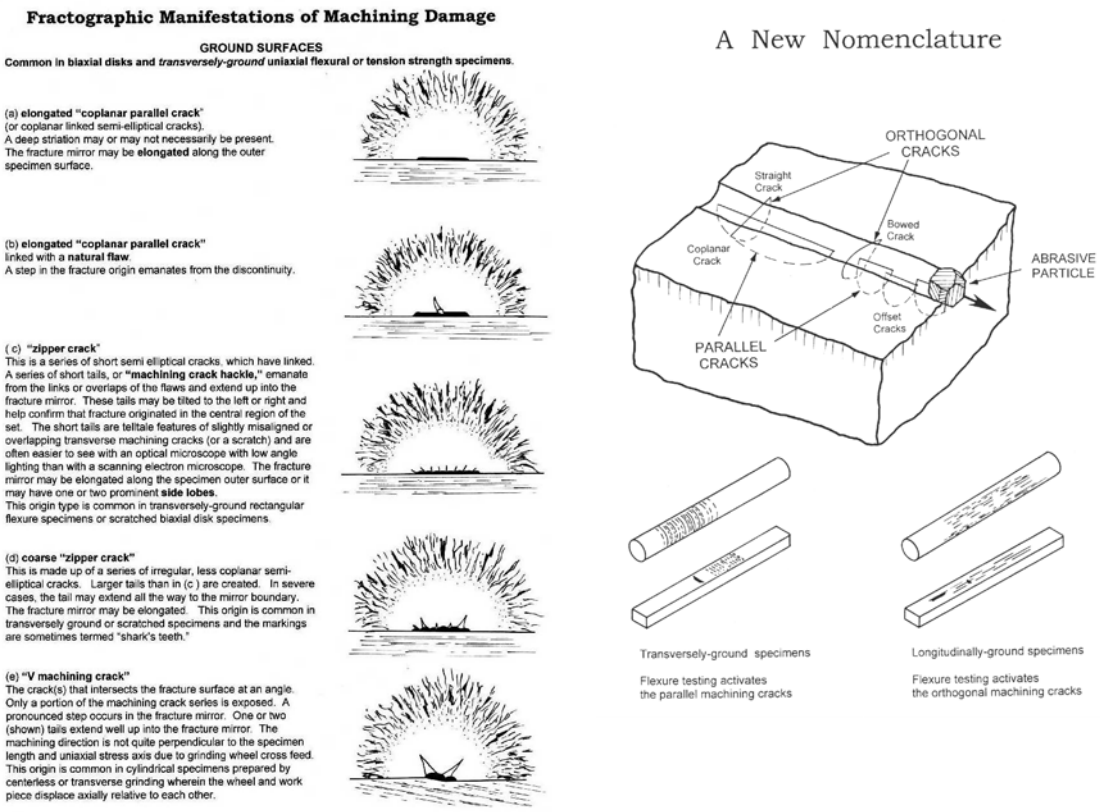

Figure 2. Schematics of Machining damage that will be incorporated into the revised ASTM C 1322.

5. Flexural Strength Testing of Cylindrical Ceramic Specimens

As the NIST Ceramic Machining Consortium program wound its way to completion, an additional set of Ceradyne sintered reaction bonded silicon nitride specimens was tested. Centerless 220 grit ground rods were fractured and compared to prior test data as shown in Figure 3. As expected, the 220 grit specimens had severer machining damage cracks than the 320 and 600 grit ground specimens. Our experience in detecting machining cracks in this material was helpful and the new machining cracks were easy to detect. Analysis of these results is still underway and time must be found to write a comprehensive paper on the findings of this study.

A batch of Hexaloy sintered alpha Silicon carbide was also machined transversely with a 220-grit wheel. Machining crack fracture origins were easy to discern as illustrated in Figure 4.

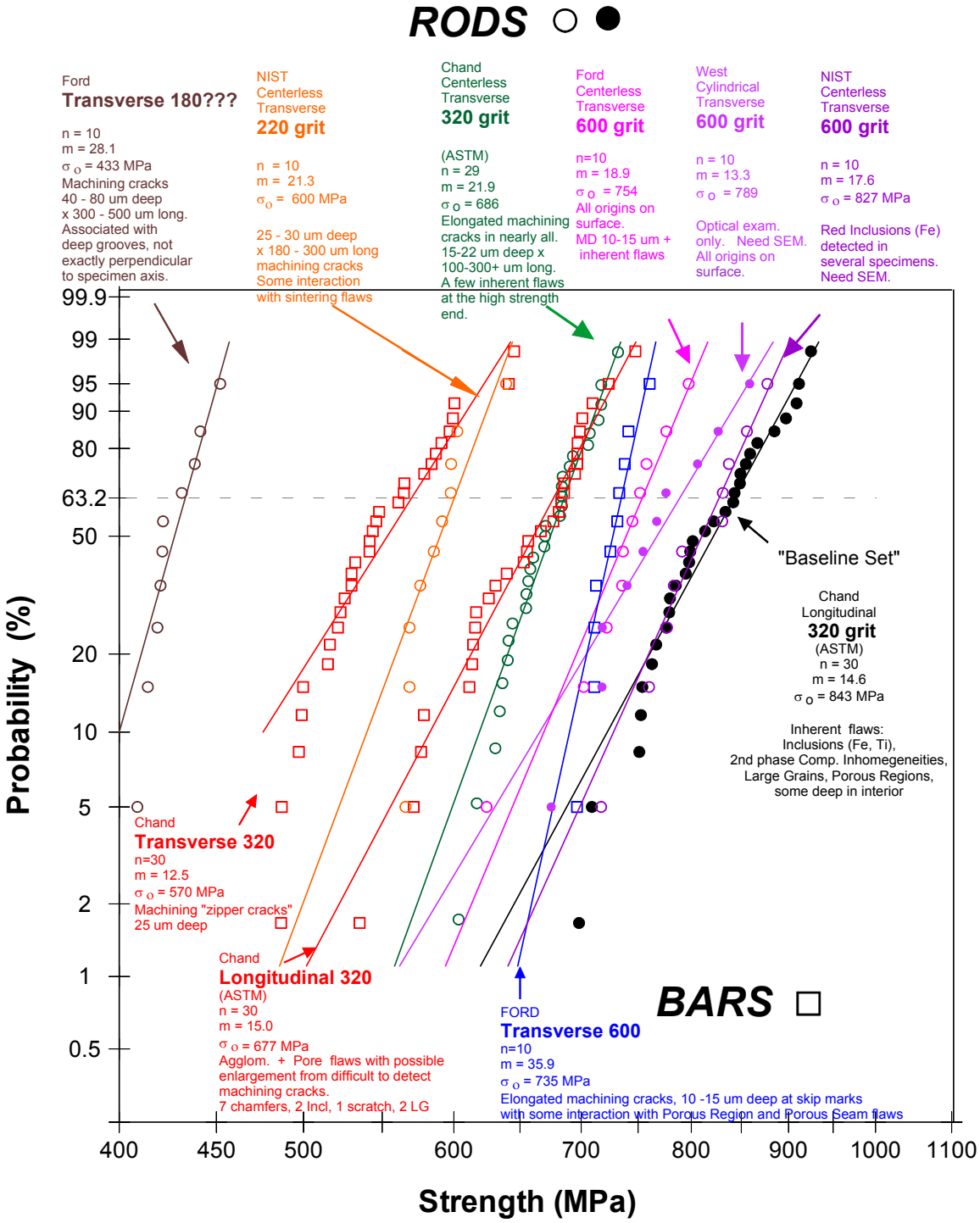

Figure 3 Weibull strength distribution plot of ground, sintered reaction-bonded silicon nitride rods and bars.

(a)
Matching fracture halves

(b) Fracture surface close-ups

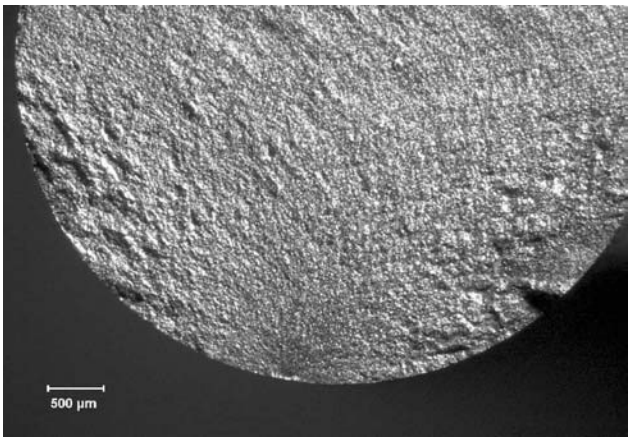

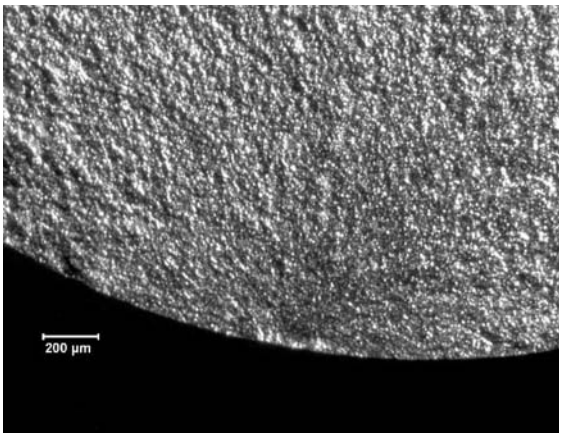

(c) View of outer ground surface at the origin.
The pores did not initiate fracture in this specimen.

The origin is exactly opposite the arrow.

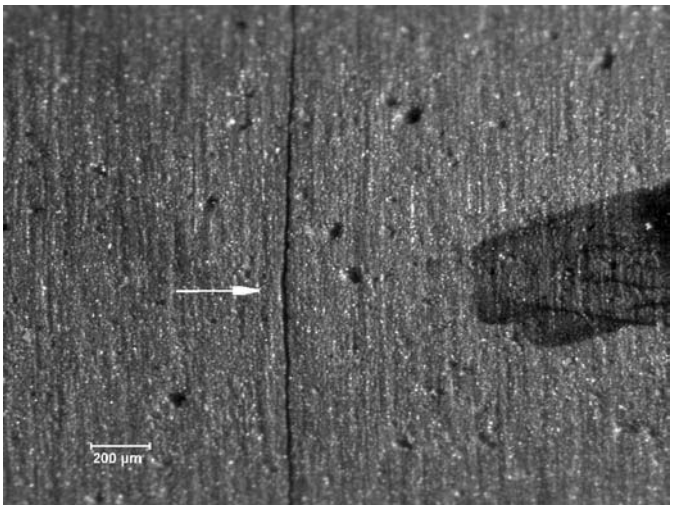

Figure 4 Matching fracture surfaces of a Hexaloy silicon carbide rod that fractured at 198 MPa. The rod was centerless ground with 220 grit wheel. The origin is a machining crack that is readily discernable (with the right lighting) with a stereo binocular optical microscope.

In the meantime, we reexamined some old glass specimens that we had tested in a conventional rectangular bar bend fixture. Contact damage cracks were detected in all specimens, underscoring some of the hazards associated with testing rod shaped specimens on fixtures with loading rollers. Figure 5 shows some examples.

Common fixture for testing Rectangular bars.
Right side photo shows a portion of a glass rod tested in the fixtures. Multiple fractures occurred, often from contact cracks created by the loading rollers.

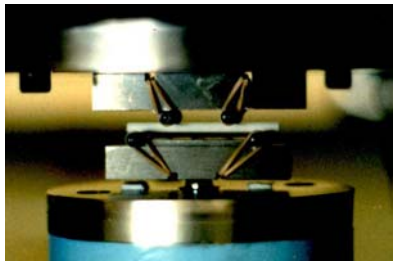

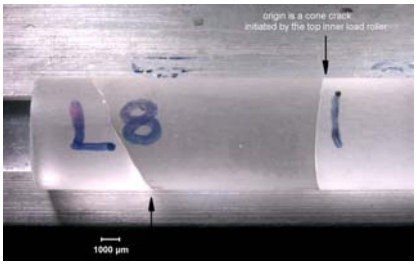

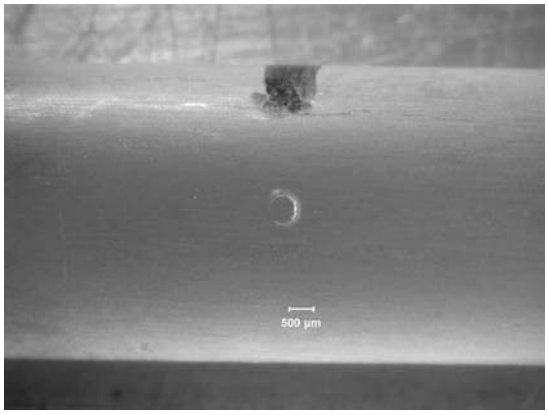

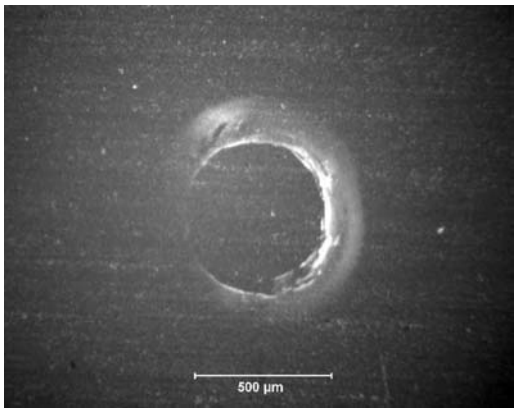

Surface of glass rod after flexural strength testing showing a contact damage crack. The primary fracture occurred elsewhere.

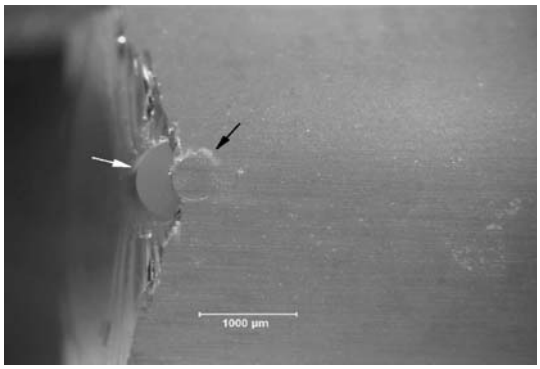

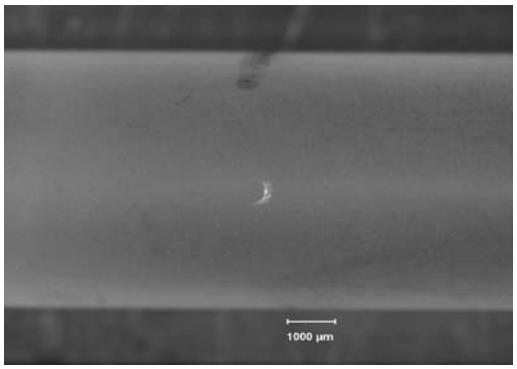

In some instances, the contact crack was the strength limiting flaw as shown in the left view. The white arrow shows the fracture surface. The right hand view shows a partial cone crack in another specimen that fractured from a different location. Notice that the cone cracks are elliptical in shape, a consequence of the different elastic properties of the glass specimen and the steel contact roller.

Figure 5. Contact damage Hertzian cone cracks in glass rods tested in flexure with a common four-point bend fixture designed for rectangular bend bars.

6. Compare SCF Knoop artificial cracks to machining cracks in Ceradyne SRBSN

We completed a careful fractographic study of artificial Knoop cracks and compared them to machining cracks. The apparent fracture toughness of the material could be calculated from the size of the machining cracks and the strengths of the test bars (or rods) via fracture mechanics analysis. We assumed there were no residual stresses as a first approximation. Figure 6 shows these results. Quite amazingly, the apparent fracture toughness calculated from the machining flaws matches the results obtained from the three ASTM fracture toughness methods (SCF-Knoop, chevron notch, and single-edge precracked beam). The toughness of this material over a broad crack size range is 5.6 MPa√m. Some machining cracks showed evidence of stable crack extension (presumably from R-curve behavior) and the critical crack size was used in the calculation. SCF precracks made at 98 N (10kgf) or greater were easy to detect and measure. Those made at 49N (5kgf) were very hard to measure since they blended into the background microstructure. Precracks made at smaller loads were undetectable. The machining cracks were easy to detect since, although they were very shallow, they were much longer (up to 300 –500 μm on the surface) and exhibited many tell tale features that we are now able to recognize.

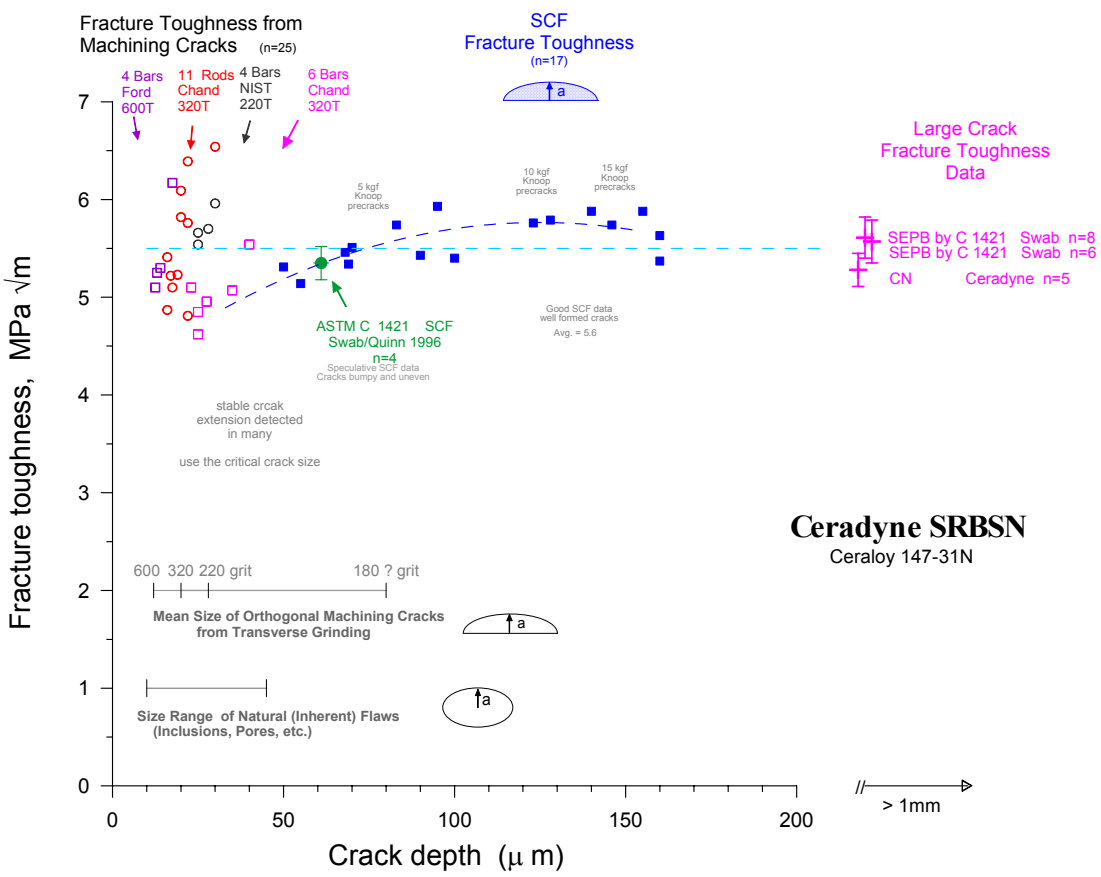

Figure 6. Fracture toughness versus crack size using data from a variety of methods. Analysis of the shallow (10 – 30 μm deep) machining cracks in strength specimens gave fracture toughness values in good agreement with the data from fracture toughness experiments.

Status of Milestones

412146	Ballot major revisions to ASTM C 1161 flexural strength	September 2001, **Completed, October 2002✓**
412147	Prepare ballot revisions for ASTM C 1322, Fractographic Analysis	April 2002, **Completed, January 2002✓**
412148	Prepare follow on specimen machining revisions to ASTM C 1161 flexural strength if needed	April 2002
412149	Prepare ballot-ready first ASTM draft of cylindrical rod flexure strength test	April 2002
412150	Prepare paper on effect of machining on strength of SRBSN rods.	May 2002
412151	Prepare review paper on flexural testing of cylindrical rods.	October 2002

Communications/Visits/Travel

G. Quinn attended the ASTM Committee C-28 meeting in November 2001. A paper on the strength testing of the Ceradyne silicon nitride rods and bars was given at the PAC RIM IV conference in November. Jim Klett at ORNL was contacted in connection with procedures for ASTM standards development. Biljana Mikjelj of Ceradyne, Sam McSpadden of ORNL, Dick Allor of Ford, and Ron Chand of Chand Associates meet with Mr. Quinn at NIST in December to review the ceramic machining results in the Ceramic Machining Consortium.

Publications

1. G. D. Quinn and J. A. Salem, "Effect of Lateral Cracks Upon Fracture Toughness Determined by the Surface Crack in Flexure Method," accepted by J. Am. Ceram. Soc. July 2001.
2. S. W. Freiman and G. D. Quinn, "How Property Test Standards Help Bring New Materials to the Market," ASTM Standardization News, Oct. 2001, pp. 26-31.
3. G. D. Quinn, P. Green, and K. Xu, "Cracking and the Indentation Size Effect for Knoop Hardness of Glasses," subm. to J. Amer. Ceram. Soc., Oct. 2001.
4. G. D. Quinn, S. Jahanmir, and L. Ives, "Flexural Strength Testing of Cylindrical Rods and Rectangular Bars," presented at the PAC RIM IV Conference, Maui, Hawaii, Nov. 8, 2001.